Cyst reduction in a first-in-kind *Drosophila* model of polycystic kidney disease

Cassandra Millet-Boureima

A
Thesis
in the Department
of
Biology

Presented in Partial Fulfillment of the Requirements
For the Degree of Master of Science (Biology) at
Concordia University
Montreal, Quebec, Canada

December 2019

CONCORDIA UNIVERSITY
School of Graduate Studies

This is to certify that the thesis prepared

By: Cassandra Millet-Boureima

Entitled: Cyst reduction in a first-in-kind *Drosophila* model of PKD

and submitted in partial fulfillment of the requirements for the degree of

Master of Science (Biology)

complies with the regulations of the University and meets the accepted standards with respect to originality and quality.

Signed by the final Examining Committee:

Dr. Michael Sacher _____ Chair
Dr. Michael Sacher

Dr. Vladimir Titorenko _____ External Examiner
Dr. Vladimir Titorenko

Dr. Alisa Piekny _____ Examiner
Dr. Alisa Piekny

Dr. Michael Sacher _____ Examiner
Dr. Michael Sacher

Dr. Chiara Gamberi _____ Supervisor
Dr. Chiara Gamberi

Dr. William Zerges _____ Co-supervisor
Dr. William Zerges

Approved by Dr. Robert Weladji
Dr. Robert Weladji, Graduate Program Director

Fall 2019 Dr. Patrick Gulick
Dean of Faculty

Abstract

Cyst reduction in a first-in-kind *Drosophila* model of polycystic kidney disease

Cassandra Millet-Boureima

Polycystic kidney disease (PKD) is an incurable degenerative disease affecting 12.5 million people worldwide. Numerous cysts form in the renal tubules, which progressively enlarge and damage the surrounding kidney tissues, severely reducing quality of life and leading most patients to kidney failure with the need for dialysis or transplant. Partly due to lack of knowledge of the precise PKD pathological mechanisms, therapeutic options are limited. The complex anatomy of the human and vertebrate kidney makes it difficult to define the PKD mechanisms and perform drug discovery. In contrast, the fruit fly *Drosophila melanogaster* shares high genetic conservation with humans and features anatomically isolated Malpighian (renal) tubules with physiologically diversified regions, making it an ideal model for studying renal cystogenesis and performing rapid drug discovery *in vivo*. One mimic of the second mitochondria-derived activator of caspases (Smac), a class of pro-apoptotic molecules being developed for cancer therapy, was found to reduce renal cysts in a murine ADPKD model. Here, we used our first-in-kind *Drosophila* PKD model, the *Bicaudal C* mutant, to test the cyst-reducing properties of four novel Smac mimics. Smac mimicry was found to decrease the overall incidence of tubular cysts. Intriguingly, cysts were reduced at different rates along the Malpighian tubules, underscoring functional differences in the tubular regions. Thus, this study suggests novel hypotheses on the conservation of renal cystic mechanisms and the function of RNA-binding protein Bicaudal C in the renal tubule.

Acknowledgements

I would like to sincerely thank my supervisor, Dr. Chiara Gamberi, for trusting me with this project and for her continuous guidance since I have started the lab. The past years were sometimes challenging but these challenges are what made me learn a great deal from Dr. Gamberi. She is admirably 100% dedicated to her students reaching their full potential.

I would also like to thank my administrative supervisor, Dr. William Zerges, and my committee members, Dr. Alisa Piekny and Dr. Michael Sacher, for their support and advice during committee meetings. I could not have improved without them.

Moreover, I would like to thank past lab trainees Josh Oliver, Stephanie He and Candice Le for their help with general *Drosophila* work that contributed to my project.

Additionally, I would like to thank Christian Charbonneau from the Institute for Research in Immunology and Cancer (IRIC, University of Montreal) and Dr. Chris Law from the Centre for Microscopy and Cellular Imaging (CMCI, Concordia University), for their help in microscopy and data analyses, respectively.

This research was funded in part by a Mitacs Accelerate Grant and a Concordia University Part-time Faculty Association (CUPFA) grant.

Lastly, I want to thank my family and friends for their constant words of encouragement. I would like to dedicate this thesis to my parents Nicole Millet and Abdallah Boureima who have always pushed me to seek higher education and who have supported me throughout my university years, as well as my boyfriend Christophe Pisarski for his never-ending love and support.

Contribution of Authors

Millet-Boureima, C., Chingle, R., Lubell, W.D., and Gamberi, C. 2019. Cyst reduction in a polycystic kidney disease *Drosophila* model using Smac mimics, *Biomedicines* 7(4), 82 :

Dr. Ramesh Chingle and Dr. William D. Lubell synthesized the Smac mimics (sections 3.2.3 and 3.3.1, Figure 3.1 and Scheme 3.1).

I performed all the *in vivo* assays and data analyses, wrote the manuscript first draft and contributed extensively to the final text.

Dr. Chiara Gamberi coordinated research and contributed to the text. All authors edited the manuscript.

Table of Contents

List of Figures

List of Tables

Abbreviations

ADPKD – Autosomal dominant polycystic kidney disease

ARPKD – Autosomal recessive polycystic kidney disease

Ca^{2+} – Calcium

cAMP – Cyclic adenosine monophosphate

cIAP – Cellular inhibitor of apoptosis protein

EGFR – Epidermal growth factor receptor

GPCR – G-protein-coupled receptor

FADD – Fas-associated protein with death domain

Fas – TNF superfamily receptor 6

JAK-STAT – Janus-family tyrosine kinase-signal transducer and activator of transcription

mTOR – mechanistic target of rapamycin

PC1 – Polycystin 1

PC2 – Polycystin 2

PKD – Polycystic kidney disease

RIPK – Receptor interacting protein kinase

Smac – Second mitochondria-derived activator of caspases

TNF – Tumor necrosis factor

TRAF – Tumor necrosis factor (TNF) receptor-associated factor

Chapter 1: Introduction

My thesis describes the use of the fruit fly *Drosophila melanogaster* to model renal disease. Specifically, I tested *in vivo* the anti-cystic effects of novel antineoplastic mimics of the *N*-terminal of the pro-apoptotic protein Second mitochondria-derived activator of caspases (Smac). Using our first-in-kind *Drosophila* model of Polycystic Kidney Disease (PKD), we have found that Smac mimic administration significantly reduced cysts in the Malpighian (renal) tubules of *Drosophila*. Intriguingly, the Smac mimics appeared to affect distinct sections of the Malpighian tubules differentially.

1.1 Polycystic Kidney Disease

Polycystic kidney disease is one of the most common renal degenerative diseases, affecting 12.5 million people worldwide with occurrence between 1 in 400 and 1 in 2500 individuals (1). There is no cure for PKD, with dialysis and kidney transplant being the only effective treatments. Although the stages of disease progression and general pathophysiology of PKD are well characterized, the mechanisms leading to renal cystogenesis are complex and still a mystery. PKD is a renal neoplasia causing the formation of numerous fluid-filled cysts in the kidneys and impaired function of the renal tubule, the nephron (Figure 1.1). Cysts only occur in about 1% of nephrons, however, their growth progressively damages the surrounding tissue and impairs the surrounding nephrons to the point of complete loss of kidney function and eventual kidney failure (1). Disease progression is very variable, the reasons for which are unknown. In fact, individuals of the same family inheriting the same mutation may have very different rates of kidney degeneration (1).

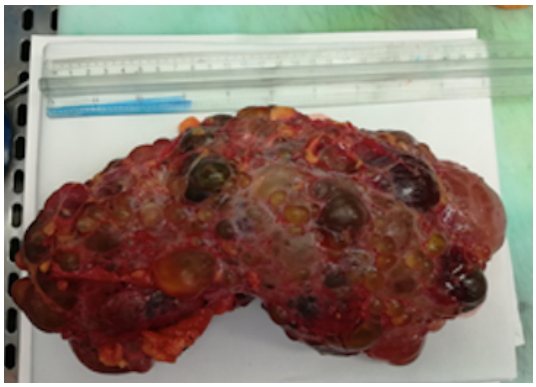

Figure 1.1 Kidney from a PKD patient. PKD causes multiple renal cysts and severe kidney enlargement. The picture was provided by our collaborator Dr. Albino Eccher, Department of Diagnostics and Public Health, University and Hospital Trust of Verona, Italy.

1.1.1. Genetics and pathways of PKD. The autosomal dominant form of PKD (ADPKD) is caused primarily by mutations in the *PKD1* (~80%) or *PKD2* (~15%) genes, while the recessive form (ARPKD) is caused by mutations in the *polycystic kidney and hepatic disease 1* (*PKHD1*) gene (1). *PKD1* encodes polycystin 1 (PC1), a large integral membrane protein and G-protein coupled receptor that is involved in ion transport, calcium (Ca^{2+}) signaling, and mechanistic target of rapamycin (mTOR, also called mammalian TOR) regulation (1-3). *PKD2* encodes polycystin 2 (PC2), a nonselective Ca^{2+} channel part of the transient receptor potential family of ion channels (1,3). PC1 and PC2 are distributed throughout the cell and a subset of the cellular pool is found in a PC1-PC2 complex. Such interaction is thought to play a role in primary cilia (1), and intracellular Ca^{2+} regulation (3). Several other genes have been associated with the onset of renal cysts. In ADPKD, mutations in other genes account for about 5% of the cases. Directly relevant for the research presented in this thesis, one gene implicated in PKD pathogenesis is *Bicaudal C* (called *BICC1* in humans, *Bicc1* in mice, and *BicC Drosophila*). BicC is an evolutionarily conserved RNA binding protein first discovered *in Drosophila* as a negative regulator of mRNA translation during oogenesis and early embryogenesis (4,5) which will be described in Section 1.2.1.

Several cellular defects are associated with PKD, such as changes in apical-basal and planar cell polarity, fluid transport, and, focus of this thesis, proliferation (1,6). Cystic cell growth and proliferation have been associated with the simultaneous disruption of several cellular pathways. Reduced intracellular Ca^{2+} signaling, increased cyclic adenosine monophosphate (cAMP) levels leading to abnormal activation of the RAS-RAF-ERK (respectively Rat sarcoma, rapidly accelerated fibrosarcoma, and extracellular signal-regulated kinase) pathway, as well as higher levels of epidermal growth factor receptor (EGFR) signaling are all thought to contribute to cystic growth and proliferation (1). Conversely, increasing Ca^{2+} concentrations raised Akt activity and blocked cAMP-dependent cystic cell proliferation (7). Additional pathways involved in PKD cystogenesis include the mTOR, Janus-family tyrosine kinase-signal transducer and activator of transcription (JAK-STAT), and Protein Kinase A pathways (1). Higher-than-normal levels of the c-Myc protein, encoded by the *c-myc* protooncogene often upregulated in cancer, have been found in both ARPKD and ADPKD (8-10). Compared to normal wild-type, ARPKD mice exhibited a two- to six-fold and 25- to 30-fold increase in *c-myc* mRNA levels at two and three weeks of age, respectively (8). In a previous

study, it was shown that *c-myc* overexpression (through a SV40 enhancer, β-globin promoter, and *c-myc* gene construct) could induce abnormal proliferation of renal epithelial cells and PKD in transgenic mice (9). *c-myc* overexpression reproduced two ADPKD features in apparent contrast with one another, the simultaneous increase of cell proliferation and apoptosis, that has been proposed to fuel cyst growth and tissue remodeling respectively (10). Moreover, it has been suggested that the local mechanical stress imposed by enlarging cysts may induce apoptosis of neighbouring renal epithelial cells (11). Ciliary dysfunction of renal epithelial cells was also thought to be important in the cystic process because the polycystin proteins PC1 and PC2 are in part co-localized to the primary cilium and primary cilia are functionally linked to several pathways implicated in PKD progression such as intracellular Ca^{2+} and cAMP signaling, growth factor regulation, and mTOR (12-15). Thus, PKD has historically been classified as a ciliopathy (16). Notably, PC1 and PC2 localize to numerous cellular locales besides the cilium (1), which implies complex functionality. While PC1 and PC2 functions are poorly understood, it has been proposed that in normal healthy kidneys they may inhibit cystogenesis through their ciliary function. However, surprising new evidence has shown that the absence of cilia in *Pkd1* mice slowed disease progression (1,17), instead of accelerating it as it was expected from the "ciliopathy" model (16). Thus, our understanding of the relationship between cilia and PKD is evolving.

1.1.2. PKD therapy. Although there is no cure for PKD, multiple strategies to modify the affected pathways have been attempted. The accidental discovery that targeting the mTOR pathway may have therapeutic potential occurred because of a peculiar type of kidney transplantation surgery. In this type of surgery, the affected kidneys are left in place and the (third) transplanted kidney is added. When rapamycin was used as an immunosuppressant for ADPKD patients who received such a kidney transplant (18), the post-operatory check-ups revealed that the affected kidneys had considerably improved, shrinking their overall and cystic size (2). Rapamycin displays antiproliferative properties and was found to greatly reduce PKD progression by slowing tubular epithelial cell proliferation. However, these effects were temporary (2,19-22). Rapamycin inhibits mTOR (23). Thus, several mTOR inhibitors were tested as potential PKD therapeutics in various animal models (2,21,24-26). While mTOR inhibitors appeared promising in PKD animal models, they did not display therapeutic potential

in the clinic, where they only partially slowed kidney growth in ADPKD patients, yet the progression of renal function degeneration remained unaltered (24,25). As well, several adverse effects were found in patients taking rapamycin or derivatives, including anemia, leukopenia, stomatitis, and diarrhea (24,25). Because cystic growth in PKD can be considered a neoplasia (27,28), several antineoplastics originally developed as anti-cancer drugs have been tested as PKD therapeutics. However, most are proving to be of limited applicability in PKD because of long-term toxicity.

A treatment showing promise in a PKD mouse model is the use of glucose analogs to reduce renal cysts (29). It was found that *Pkd1*$^{-/-}$ mice and microarrays from ADPKD patients both exhibit enhanced glycolysis compared to normal controls (29). Reminiscent of cancer cells (30), *Pkd1*$^{-/-}$ cells seemed to depend on aerobic glycolysis for their energy needs to fuel cellular growth and proliferation (29). Supporting this model, when glucose levels were depleted, cystic cells resumed to wild-type-level proliferation (29). Strongly suggesting that glucose deprivation reduces cystic cell proliferation while preserving wild-type cells, cystic cells displayed higher apoptotic rates in *Pkd1*$^{-/-}$ mice, whereas *Pkd1*$^{+/+}$ cells activated cell autophagy to survive (29). Treatment with 2-deoxyglucose, a non-metabolizable glucose analog, led to a reduced cyst number (called cystic index) without affecting other organs or the overall body weight. Two-deoxyglucose is being used in combination therapy to treat osteosarcomas and lung cancers in phase 2 clinical trials (31). With such encouraging preliminary results, 2-deoxyglucose is one candidate combination drug in PKD therapeutics (29).

As mentioned in Section 1.1.1, EGFR signaling is upregulated in PKD. Src is an important mediator of EGFR activation (32). Consistently, Src overexpression correlated with enlarged cystic kidneys from murine models of ARPKD (32). Therefore, one group sought to target this pathway by using Src inhibitor, SKI-606 (32). SKI606 administration to BPK mice (ARPKD model) significantly reduced both kidney size and renal cysts (32). Moreover, no renal toxicity was observed after 20 days of treatment and a dose of 30 mg/kg/day. Surprisingly, Src inhibition did not lower intracellular cAMP, which is normally elevated together with EGFR (32). This indicated that the observed kidney improvements were notably independent of cAMP (32), further highlighting how complex EGFR *in vivo* signaling and PKD pathophysiology are. Contingent on the pending results of long-term toxicity studies, the observed drug tolerability

and promising cyst reduction in murine models (32) suggest that Src inhibitors may offer potential for PKD therapeutics.

Currently, the only approved drug for PKD management is tolvaptan, a vasopressin V2 receptor antagonist already approved for heart disease treatment. Cystic fluid in the kidney is thought to arise in part from elevated cAMP concentrations (33). Tolvaptan is believed to inhibit V2R, which subsequently reduces cAMP levels in the kidney, thereby reducing cystic fluid accumulation and renal epithelial cell growth (33). Tolvaptan was found to be appropriate for only a subset of patients who were between the ages of 18 and 50, had fast disease progression, and low water and/or high salt intake (34). Tolvaptan reduced the increase in total kidney volume and slowed the deterioration of kidney function (35). However, its efficacy appeared to decrease during the three years tested and, troublingly, markers of liver toxicity increased (35,36). Unlike other treatment options mentioned above, tolvaptan appears to principally target the compensatory physiological mechanisms dependent on vasopressin signaling and may affect the core PKD cellular pathways indirectly. Thus, safe and effective PKD therapeutics suitable for a wider spectrum of patients are needed.

An additional class of compounds directly relevant for this thesis is being examined to reduce cellular proliferation in PKD. Such compounds are mimics of a cellular regulator called second mitochondria-derived activator of caspases (Smac) described below.

1.1.3. Smac-dependent regulation. Smac or DIABLO (direct inhibitor of apoptosis-binding protein with low pI) is a protein that activates a signaling cascade initiated by the targeting and ubiquitin-dependent degradation of inhibitors of apoptosis proteins (IAPs). Such cascade culminates with pro-apoptotic caspase activation. IAP antagonists were characterized in *Drosophila,* leading to the identification of the Reaper, Head involution defective (Hid) and Grim proteins containing an *N*-terminal 'RHG' motif (named after their initials). Despite the lack of mammalian orthologs, Reaper, Hid and Grim could induce cell death when expressed in mammalian cultured cells, which eventually led to the identification of the mammalian Smac/DIABLO protein the first of a few proteins that similarly function through an RHG motif (37,38). IAP proteins are found associated to the cytoplasmic side of several receptors. Here, we will examine the case of the TNF-α receptor, which is relevant to this thesis. In the presence of both TNF-α and a pro-apoptotic signal, Smac/DIABLO is released from the mitochondria

(Figure 1.2). Smac then binds IAPs on the cytoplasmic side of the TNF-α receptor complex, which leads to their ubiquitination and degradation (39-41). This in turn leads to TNF-α-mediated activation of caspases and apoptosis (41). Depending on the cellular context and the nature of the pro-apoptotic stimulus, the specific cell death pathway may differ. Smac mimicry leverages on this regulation by introducing just the RHG domain, *e.g.* as a peptide, to trigger the cascade in the presence of the TNF-α–TNFR interaction. This strategy has been used to induce apoptosis preferentially in TNF-α dependent cancer cells and some Smac mimics are currently in phase 2 clinical trials (42,43). TNF-α signaling can also give a pro-survival signal to cells (44), an opposing signal from apoptosis seen in cancer and cystic cells.

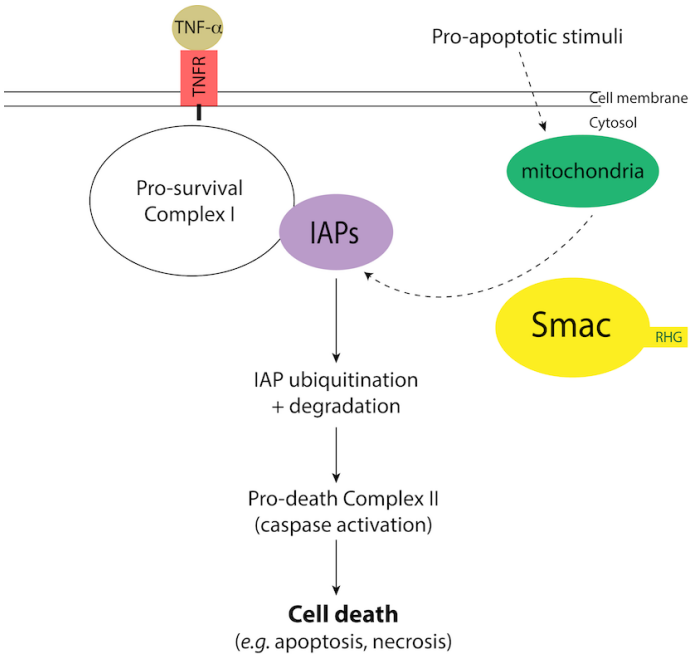

Figure 1.2 Essential Smac-dependent regulation pathway. Example of TNF-α-dependent Smac mechanism is shown. Only the main events and factors are shown. See text for details.

1.1.3.1. Smac mimicry in PKD. In both ADPKD patients and a *Pkd1*$^{-/-}$ mouse model, cystic fluid was found to contain high amounts of TNF-α (45,46). Cystic cells (but not the surrounding non-cystic tubular cells) also overexpress the TNF-α receptor 1 (TNFR1) (46). This creates a positive reinforcement of the TNF-α-dependent pro-survival signal between the cystic cells and the bathing cystic fluid, which is supposed to promote cyst growth (46). Potential contributions of the less studied TNF receptor TNFR2 are unknown. Similar to cancer, Smac mimicry can potentially be used to interfere with cystic cell proliferation. Based on these

considerations, the Smac-mimetic GT13072 was used to interfere with such cyst survival signal and induce cystic cell death in a TNF-α-dependent manner (46). This strategy aims to specifically target cystic cells (bathed in TNF-α-containing cystic fluid), while sparing the adjacent tubular cells in non-cystic regions (that do not accumulate TNF-α-containing fluid). Experiments on a murine PKD model suggest that when a Smac mimic is present, the TNF-α "pro-survival complex I" is disrupted and a "pro-death complex II" is, instead, formed as follows (Figure 1.3). Briefly, the Smac mimic targets cIAPs for ubiquitination and degradation, which leads to the dissociation of the pro-survival complex I (composed of TRADD, RIPK1, TRAF2, cIAP1 and cIAP2); then RIPK1, FADD and caspase-8 form the pro-death complex II (Figure 1.3). The latter subsequently activates downstream effector caspase-3 and apoptosis is initiated.

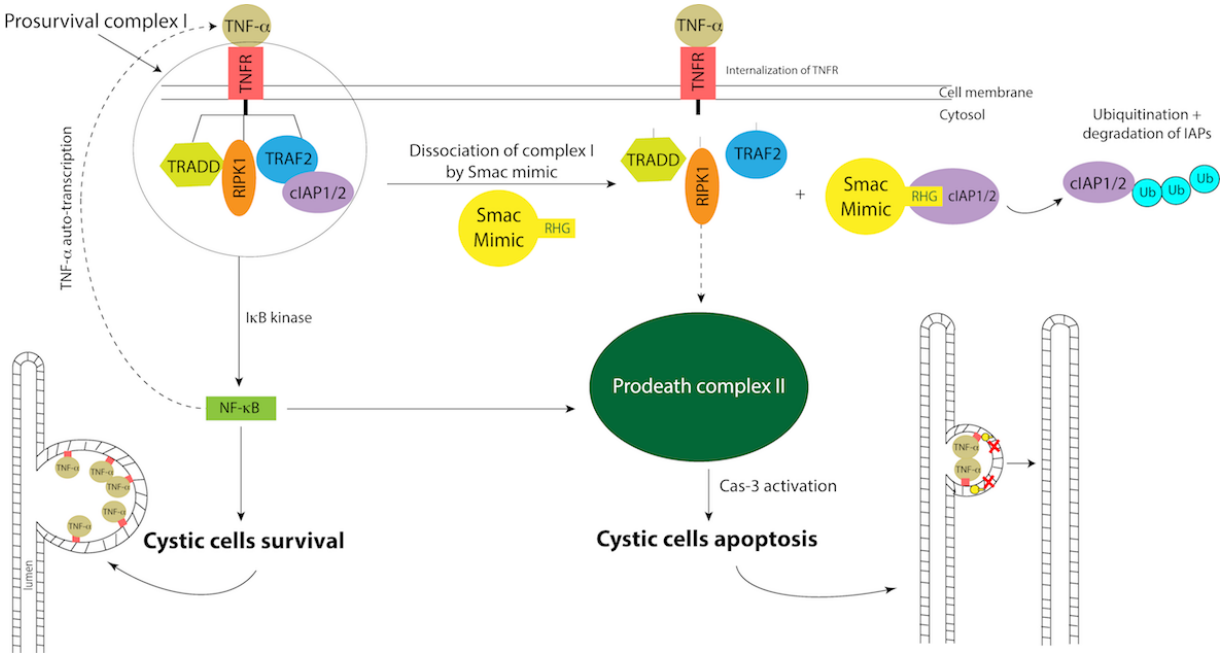

Figure 1.3 TNF-α dependent regulation in PKD and Smac mimicry. In ADPKD, cystic cells display upregulated TNF-α and TNFR. High TNF-α-TNFR signaling confers pro-survival signals through complex I (left). Introducing Smac mimics is thought to target cIAP and disassemble complex I, which causes the formation of pro-death complex II, and induce apoptosis (right). See text for more detail.

1.1.4. Conservation of the TNF pathway in Drosophila. The *Drosophila* genome contains two TNF orthologs, called *Eiger* and *Darth* (47-50) and two TNFR orthologs, called *Wengen* and

Grindenwald (48,50-52). Eiger and Wengen are thought to function together, similar to the mechanism of action of mammalian TNF-α and its receptors. Much less in known about the functions of the Darth and Grindelwald proteins. As well, how TNF and TNF signaling may contribute to the function of the Malpighian tubule is unknown. *Drosophila* orthologs of *FADD*, *TRAF* and *IAP* also exists and have been in part characterized in other epithelia (48). Because components of the TNF signaling appeared to be conserved in *Drosophila*, and the RHG-containing Reaper Hid and Grim can function in mammalian cells (53), we tested if Smac mimicry could also reduce cysts in the *Drosophila* PKD model.

1.2 **Modeling PKD in *Drosophila***

The anatomical complexity of the human and vertebrate kidney makes it difficult to study and probe it genetically (54). Genetic tractability refers to organisms and systems amenable to genetic manipulation. Therefore, the vertebrate kidney has been defined "relatively genetically intractable" (55), which complicates the study of the genetic underpinning of several pathologies. *Drosophila melanogaster* is useful to model vertebrate development and the molecular/cellular mechanisms of fundamental biological disease processes due to a 75% conservation of human disease pathways (56). Its genetic tractability enables studies of disease mechanisms. Moreover, *Drosophila* is inexpensive to culture in the laboratory and yields large populations for robust statistical analyses. Its short lifespan facilitates monitoring of the temporal progression of normal and diseased phenotypes. The large genetic toolkit for *Drosophila* research enables multiple rounds of experiments needed to refine mechanistic models. Specific to the renal system, *Drosophila* possesses two pairs of Malpighian tubules freely floating in the abdomen, that are analogous to the tubular part of the human nephron, as well as nephrocyte clusters separately located in the body cavity that are analogous to human renal podocytes in the glomerulus (57). Unlike vertebrate nephrons, *Drosophila* Malpighian (renal) tubules can be effectively micro-dissected enabling precise analyses. Important for the research presented here, a conserved feature of the Malpighian tubules is that distinct regions along the tubules carry out different functions, similar to the human nephron. Because the Malpighian tubules are anatomically separated, rather than embedded in an organ, they do not rely on salt gradients for urine concentration. The *Drosophila* small body size, short tubules and high transport rates all

contribute to proper urine concentration (detailed in Appendix II). *Drosophila melanogaster* has been successfully used to model human renal function (57).

Our laboratory has developed the first *Drosophila* PKD model. Similar to PKD, the cystic *Drosophila* exhibit renal cysts all along their Malpighian tubules, have impaired renal function, and display *myc* over-expression and mTOR activation (58). The cystic *Drosophila* model also displayed conserved pharmacological response to rapamycin (58). The cystic *D. melanogaster* used here carry mutations in the *BicC* gene, which encodes a conserved RNA-binding protein, described in Section 1.2.1. Notably, mutations in *BicC* orthologs in vertebrates, including humans, cause renal cysts (5,59,60).

1.2.1. BicC genetics. *BicC* was discovered in a genetic screen for maternal regulators of embryonic polarity (4,5). Oocytes from heterozygote *BicC* females were found to have disrupted anterior-posterior axis determination and yield embryos displaying various degrees of loss-of-segments phenotypes, including so-called "bicaudal" embryos consisting of two posterior ends juxtaposed in a mirror-image fashion (4,5). Homozygote *BicC* females, instead, exhibit oogenesis arrest at stage 10 (61). In the ovary, the BicC protein functions as a translational repressor for several mRNAs, including its own (5,62,63). On the other hand, BicC is ubiquitously expressed and it is unknown how it functions in somatic tissues (5). We have shown for the first time that *BicC* homozygote *Drosophila* develop cysts in the Malpighian tubules and display crucial PKD features (58). BicC is relevant for PKD, because we have found that *BicC* is genetically downstream of *PKD1* (58). In fact, the human *BICC1* mRNA was significantly downregulated in microarrays from cysts of *PKD1*-type ADPKD patients (58). Moreover, in the kidneys of *Pkd1*$^{-/-}$ mice the Bicc1 protein was significantly reduced (58). These results, combined with the fact that mutations of the *BicC* orthologs in several vertebrates (mice, *Xenopus*, zebrafish, humans) cause renal cysts, strongly suggest that BicC may be a key regulator of renal homeostasis and its mutation eventually results into cyst formation. Thus, the *BicC mutant Drosophila* can be used to model the aspects of PKD phenotypes due to *BicC* loss-of-function (58). Because of the BicC ovarian function, *BicC homozygote Drosophila* are sterile; thus, *BicC* mutants must be obtained by crossing heterozygotes for *BicC* alleles *in trans* to the CyO balancer.

1.3 Thesis Overview

My thesis consists of a published article reporting on the *in vivo* anti-cystic effects of four novel small molecule Smac mimics (64). The Smac mimics used here displayed proliferation-modulating properties in cancer cells (65) and were synthesized by our collaborators Dr. Ramesh Chingle and Dr. William D. Lubell from the Chemistry Department at the Université de Montreal. The Smac mimics were chosen in part as proof-of-principle for feasibility of drug discovery and development in *Drosophila* because of the precedent mentioned in Section 1.1.3.1, in which the Smac mimic and birinapant analog GT13072 could reduce cysts in a murine PKD model (46). The four Smac mimics (also called analogs) included the natural four-amino acids found at the *N*-terminal of the Smac protein, the sequence Alanine-Valine-Proline-Isoleucine (AVPI). Three analogs were azapeptides, in which nitrogen replaced the α-carbon of one or more of the amino acid residues with consequences on the peptide conformation, activity and pharmacokinetic properties (66). Structure-activity relationship revealed differential cyst-reducing activity of the of the four Smac mimics. Intriguingly, the different regions of the Malpighian tubules responded differentially to Smac mimicry, which was never observed in vertebrates, likely due to the kidney anatomical complexity. Such differential response has potential relevance in functional studies of Malpighian tubule function in *Drosophila*. If conserved to humans, a differential pharmacological response of the renal tubule may eventually be leveraged to develop optimized PKD therapeutics.

Chapter 2: Cyst reduction in a Polycystic Kidney Disease *Drosophila* Model Using Smac Mimics

Introduction to Chapter 2: The following research article reports the anti-cystic effects of Smac mimicry using our first-in-kind *Drosophila* model of PKD and novel Smac mimics synthesized from collaborating Lubell laboratory. This undertaking was a proof-of-principle investigation to validate drug-screening protocols in adult *Drosophila* using peptide and peptide analogs. Considering that TNF pathway components and the activity of RHG-domain containing proteins appear conserved from humans to *Drosophila*, these tests also served to probe if the cystic *BicC* mutants responded to Smac mimicry, similar to the PKD murine model.

Article summary and importance.

To test anti-cystic activity of the Smac mimics, populations of sibling *BicC* mutant *Drosophila* were probed in parallel by administering orally either Smac mimics or the solvent in which compounds were dissolved (vehicle) and in otherwise identical setups. Initial time course was performed to identify effective time of administration. Similarly, a dose-response was performed to identify effective compound concentration. To determine if the Smac mimics influenced cyst development, I established an assay based on the cystic index used in PKD research where cysts were scored based on the size of tubule dilation (*e.g.*, (29), also see section 1.1.2). The *Drosophila* Malpighian tubules can be examined in their entirety both overall and regionally. Therefore, cysts were recorded from 50 individuals per condition after 20 days of either Smac or vehicle treatment, assigned to the Malpighian tubule regions and analyzed statistically. Two allelic combinations for *BicC*, $BicC^{\Delta/YC33}$ (yielding milder cystic defects) and $BicC^{\Delta/IIF34}$ (yielding stronger cystic defects) were used. These two combinations were used as a mini allelic series to test the differential activities of the compounds in the mild and more severe *BicC* mutant phenotypes, similar to our previous research (58). The Smac mimics used were: peptide **1**, the natural Smac *N*-terminal four-residue sequence AVPI and three derived azapeptide mimics where the α-carbon(s) of one or more amino acids were replaced by nitrogen featured constrained structures. These were named mimic **2**-**4** (64). Peptide **1**, mimics **2** and **3** displayed

anti-cancer activity in breast cancer cells (66). Mimic **4** was a new molecule with modifications expected to improve its stability *in vivo*.

This research is important because it validated usefulness of the *Drosophila BicC* PKD model for drug discovery, it indicated activity of four Smac mimics that have never been used in PKD therapy, which extends and further confirms prior work from Fan and colleagues in the mouse (46) and further corroborated therapeutic potential for Smac mimicry in PKD.

Note: This article was published as "Millet-Boureima C., Chingle R., Lubell W.D., and Gamberi C. 2019. *Biomedicines, vol. 7(4),* 82." and the entirety of its content is being presented in this thesis. To fulfill the request of the committee members, the following edits to the published text were made in this thesis: Malpighian tubules are mentioned *in extenso*; "fly" and "flies" are replaced with "*Drosophila"* or "individuals", or deleted depending on context; one sentence in Section 2.3.2 that recalls a concept detailed in the Experimental Section, has been deleted; a few word changes that improve readability, yet do not change the meaning, have also been introduced. The published PDF version complete with supplementary files (that were excluded from the main body of this thesis) is available in Appendix I and online. DOI.

Abstract: Autosomal dominant polycystic kidney disease (ADPKD) is an inherited malady affecting 12.5 million people worldwide. Therapeutic options to treat PKD are limited, due in part to lack of precise knowledge of underlying pathological mechanisms. Mimics of the second mitochondria-derived activator of caspases (Smac) have exhibited activity as antineoplastic agents and reported recently to ameliorate cysts in a murine ADPKD model, possibly by differentially targeting cystic cells and sparing the surrounding tissue. A first-in-kind *Drosophila* PKD model has now been employed to probe further the activity of novel Smac mimics. Substantial reduction of cystic defects was observed in the Malpighian (renal) tubules of treated *Drosophila*, underscoring mechanistic conservation of the cystic pathways and potential for efficient testing of drug prototypes in this PKD model. Moreover, the observed differential rescue of the anterior and posterior tubules overall, and within their physiologically diverse intermediate and terminal regions implied a nuanced response in distinct tubular regions contingent upon the structure of the Smac mimic. Knowledge gained from studying Smac mimics reveals the capacity for the *Drosophila* model to precisely probe PKD pharmacology highlighting the value for such critical evaluation of factors implicated in renal

function and pathology.

2.1 Introduction

Autosomal dominant polycystic kidney disease (ADPKD) induces the formation of cysts along the entire renal tubule, predominantly at the terminal region and the collector tubule, as well as extra-renal manifestations (1). Inherited through a monogenic pattern with the most frequent mutations affecting *PKD1* or *PKD2*, ADPKD displays high heterogeneity in both phenotype and speed of progression (1). Abnormal proliferation of the epithelial tubular cells during development gives rise to cysts prenatally. Cysts become more numerous with age, gradually enlarging and filling with fluid (1). Animal models of PKD have been invaluable for defining disease progression and identifying key molecular alterations; however, the precise mechanisms underlying disease pathology remain to be elucidated at the molecular level (67). The most recent addition to the arsenal of PKD animal models has been the fruit fly, *Drosophila melanogaster*. Mutants for the *Bicaudal C* (*BicC*) gene (hereby *BicC Drosophila*) were found to recapitulate key molecular features of PKD, including *myc* over-expression and mechanistic target of rapamycin (mTOR) pathway activation (58). Consistent with ADPKD, the *BicC Drosophila* formed cysts along the entire length of the tubule, with higher frequency at the intermediate, terminal and collector tubule regions (58). Moreover, analogous to vertebrate PKD (2,19,21,68,69), pharmacological treatment of *BicC Drosophila* with rapamycin transiently reduced cysts (58). Consistent with the relevance of the *BicC* phenotype in PKD, *BICC1* mRNA and Bicc1 protein orthologues were respectively found to decrease in kidneys from *PKD1* patients and *Pkd1*$^{-/-}$ mice (58). Thus, *PKD1* dysfunction is associated with decreased *BicC* function.

An excellent model of human renal function, *Drosophila* has high genetic conservation and a streamlined anatomy (reviewed in (57)). In contrast to the human kidney, which contains one million tubular filtering units called nephrons, *Drosophila* harbors two pairs of Malpighian tubules, which are functionally equivalent to the tubular portion of the nephron. Suitable to the open circulatory system of *Drosophila*, the renal system does not have glomeruli and possesses nephrocytes, which exhibit re-adsorptive function analogous to the human glomerular podocytes (57). Originating from the interface between the mid- and hind-gut, the Malpighian tubules are asymmetrical with longer tubules anteriorly and shorter ones posteriorly. Reminiscent of the

different nephron types in the human kidney, the anterior and posterior Malpighian tubules have distinct transcriptomes (70). Like the human renal tubules, Malpighian tubules can be divided into distinct regions, which in *Drosophila* are called proximal, intermediate, and terminal. The proximal region excretes fluid into the tubules, the intermediate region secretes potassium chloride and water, and the terminal region is responsible for sodium and, possibly, water reabsorption (57). One key advantage of *the Drosophila* renal system is that the Malpighian tubules are anatomically distinct, float freely in the body cavity, and can be cleanly micro-dissected and examined in their entirety.

Antineoplastic mimics of the second mitochondria-derived activator of caspases (Smac, also called the direct inhibitor of apoptosis-binding protein with low pI, DIABLO) have been used to sensitize cancer cells to apoptosis by targeting inhibitors of apoptosis proteins (IAPs, (71,72)). Highly conserved, IAP proteins play a key role in balancing cell survival and cell death through multiple intersecting cellular pathways. Implicated in innate immunity (73,74), IAPs are often upregulated in cancer (75). First discovered in insect baculovirus as inhibitors of cellular apoptosis which enable viral replication, IAPs were found in both vertebrates and invertebrates ((76), reviewed in (71)). The best-known mammalian IAPs are X-linked IAP (XIAP), cellular IAP1 (cIAP1) and cIAP2 (71). The *Drosophila* genome encodes four IAPs, Diap1, Diap2, dBruce and Deterin (77-79). Multiple proteins have been shown to antagonize IAPs. First discovered in *Drosophila*, three proteins, Reaper (80), Hid, (81) and Grim (82), can induce apoptosis when transfected into mammalian cells, which demonstrated functional conservation of the apoptotic cellular machinery (53). Additional *Drosophila* IAP antagonists are Jafrac (83), Sickle (84-86) and HtrA2 (87-89). The search for the mammalian IAP antagonists yielded Smac/DIABLO (40,90), Omi/HtrA2 (91), apoptosis-related protein in the TGFβ signaling pathway (ARTS, (92)) and XIAP-associated factor 1 (XAF1, (93)). IAP antagonists function through an RHG motif, named after the prototypical Reaper, Hid and Grim *Drosophila* proteins. In the case of the well-studied human Smac/DIABLO and *Drosophila* Hid IAP antagonists, pro-apoptotic stimuli induce proteolytic cleavage exposing the RHG motif at the *N*-terminus enabling interaction with IAP proteins (94,95) and triggering their ubiquitination and degradation. In the appropriate cellular context, IAP degradation can eventually lead to cell death either by way of caspase activation or via tumor necrosis factor (TNF) signaling (71,96,97). The discovery that the Smac/DIABLO *N*-terminal peptide H-Ala-Val-Pro-Ile-NH_2 can recapitulate the pro-apoptotic

function of the entire protein has inspired the development of various Smac mimics, which enable sensitization of neoplastic cells to apoptosis (72).

Based on the premise that ADPKD is considered in part a neoplastic condition (27,28), and that various TNF complex components were upregulated in *Pkd1*$^{-/-}$ mouse embryonic kidney (MEK) cells, the Smac mimic and birinapant analog GT13072 was used to induce TNF-α-dependent cell death in both cultured cells and a rat model of PKD (46). The pro-apoptotic properties of GT13072 were specific for the TNF-positive renal epithelial cystic cells and spared surrounding non-cystic cells, offering therapeutic potential to ablate renal cystic cells to delay cystogenesis (46). The TNF pathway is highly conserved *in Drosophila* (47,48,51,52,98,99). The capacity for Smac mimics to reduce Malpighian tubule cystogenesis has now been tested in the *BicC* cystic *Drosophila*. The prototypical H-Ala-Val-Pro-Ile-NH_2 (peptide **1**, Figure 2.1) and three Smac mimics **2**–**4** were administered to the *BicC* cystic mutants to test their effect on cyst reduction.

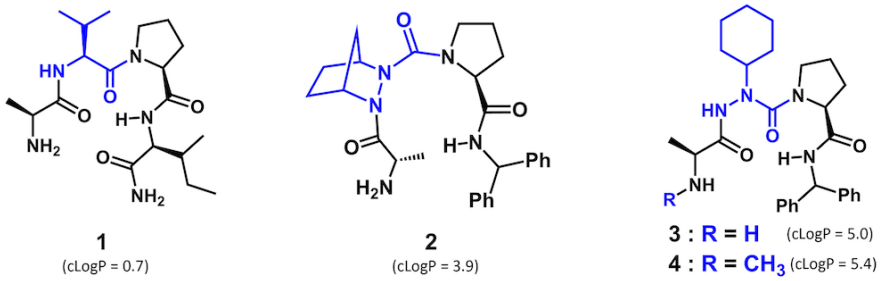

Figure 2.1 Second mitochondria-derived activator of caspases (Smac) analogs: peptide **1** and mimics **2**-**4** (Val, aza-residue and modifiend *N*-terminal in blue). Logarithm of the partition coefficient (clogP) values were calculated as described below.

2.2 Experimental Section

2.2.1. Drosophila Lines and Genetics. *Drosophila* care was previously described in detail (58). In brief, *Drosophila* were grown on cornmeal agar (Jazzmix, Fisher Scientific Canada, Ottawa, ON) at 25 °C and aged as indicated. *Oregon*^{R} (*Ore*^{R}) wild-types were maintained as in (58). *BicC* mutants were generated by crossing *Df(2L)RA5*/*CyO* (*BicC*-encompassing deletion obtained

from Bloomington *Drosophila* Stock Center) virgin females with one of the two hypomorphic *BicC* mutations, $BicC^{YC33}/CyO$ and $BicC^{IIF34}/CyO$ and selecting straight-winged progeny (*Df(2L)RA5*/$BicC^{YC33}$, $BicC^{\Delta/YC33}$ and *Df(2L)RA5*/$BicC^{IIF34}$, $BicC^{\Delta/IIF34}$). The two *BicC* allelic combinations produced truncated proteins and sterile *BicC* mutants (58). Eclosed adults were collected every two days to yield 0–2-day old populations and aged as described.

2.2.2. In Vivo and Ex Vivo Assays

2.2.2.1. Cystic Index. For the cyst analysis, 0–2-days *old Drosophila* were aged seven days (*i.e*., 7–9 days old) and were fed every three days with 2 mL of cornmeal food and equal volumes (50 µL) of either vehicle (water) or an aqueous solution containing peptide **1** or Smac mimic **2**–**4**. Each compound was used at 20 µM and was administered for 20 days (*i.e.,* until 27–29 days old). Malpighian tubules were micro-dissected from 25–50 females in phosphate buffered saline (PBS) and the number of cysts was scored separately in anterior and posterior tubules and assigned to each tubular region (*i.e*., proximal, intermediate and terminal (57,58)), as follows. At one extremity, the proximal region consists of about 15% of the tubule length, tends to have an opaque whitish content (posterior tubule), is thinner than adjacent regions (especially in the anterior tubule) and often exhibits a slight constriction terminally. The neighboring intermediate region has darker contents and consists of about 55% of the tubule length. The terminal region is often translucent, directly connected to the collecting tubule, and consists of the remaining 30% of the tubule length. Cysts were considered tubular deformations creating uni- or bi-laterally protuberant pouches. Extra-branches (as in (58)) were counted as cysts. Values were plotted using the Prism 8.0 software (Graphpad Software, San Diego, CA, USA) as nested distributions. Statistical analyses were performed as unpaired t tests with Welch's correction (the populations may not have equal standard deviations). The raw data counts are listed in supplementary Table S1.

2.2.2.2. Microscopy. Malpighian tubules from appropriately aged and treated *Drosophila* were micro-dissected in 1× PBS, equilibrated into a 3:1 1× PBS:glycerol solution and photographed on a Leica MZ FLIII Fluorescence Stereomicroscope with Leica MZ series 10×/21B Widefield adjustable eyepieces equipped with a Canon DS126201 EOS 5D MARK II camera, using visible light. Canon raw files (CR2) were converted into TIF format using the Adobe Lightroom 3.2 software (Adobe Systems, San Jose, CA, USA).

2.2.3. General Synthetic Methods. Chemicals were used as received from commercial sources without further purification unless stated otherwise. All glassware was stored in the oven or flame-dried and let cool under an inert atmosphere prior to use. Anhydrous solvents (DCM, and DMF) were obtained by passage through solvent filtration systems (Glass-Contour, Irvine, CA, USA). Silica gel chromatography was performed using 230–400 mesh silica gel (Silicycle), and TLC was on glass-backed silica plates visualizing the developed chromatogram by UV absorbance or staining with ceric ammonium molybdate or potassium permanganate solutions. Nuclear magnetic resonance spectra (^{1}H and ^{13}C) were recorded on a Bruker AV 500 spectrometer and referenced to residual solvent in CD_3OD (3.31 ppm, 49.0 ppm). Coupling constant *J* values and chemical shifts were measured in Hertz (Hz) and parts per million (ppm). Infrared spectra were recorded in the neat on a Perkin Elmer Spectrum One FTIR instrument and are reported in reciprocal centimeter (cm^{-1}). Liquid chromatography−mass spectrometry (LC−MS) was performed on an Agilent Technologies 1200 series instrument in positive electrospray ionization (ESI)-time-of-flight (TOF) mode at the Université de Montréal Mass Spectrometry Facility. Sodium and proton adducts ($[M + Na]^+$ and $[M + H]^+$) were used for empirical formula confirmation. The peptide H-Ala-Val-Pro-Ile-NH_2 (**1**), Smac mimics **2** and **3**, and aza-cyclohexylglycinyl-L-proline benzhydrylamide (**8**), all were synthesized according to published methods (65). *N*-Boc-*N*-Methyl-L-alanine and diisopropyl ethyl amine (DIEA) were purchased from Aldrich or Alfa Aesar and used without further purification. Benzotriazol-1-yl-oxytripyrrolidino-phosphoniumhexafluoro-phosphate (PyBop) was purchased from GL Biochem™, recrystallized prior to use from dry CH_2Cl_2/Et_2O (melting point, 156 °C), and stored in the dark.

N-Methyl alaninyl-aza-cyclohexylglycinyl-L-proline benzhydrylamide (**4**). A solution of aza-cyclohexylglycinyl-L-proline benzhydrylamide (**8**, 1 eq., 65 mg, 0.155 mmol, prepared according to (65)) and DIEA (2 eq., 40 mg, 53 µL, 0.309 mmol) was added to a solution of *N*-(*tert*-butoxycarbonyl)-*N*-methyl-L-alanine (1.2 eq., 38 mg, 0.186 mmol) and PyBOP (1.5 eq., 121 mg, 0.233 mmol) in DMF (3 mL), and the mixture was stirred overnight. The volatiles were removed under vacuum. The residue was dissolved in EtOAc (10 mL), washed with 5 mL of saturated aqueous $NaHCO_3$ and brine (10 mL), dried over Na_2SO_4, filtered, and evaporated. Without further purification, the residue was dissolved in a 25% solution of trifluoroacetic acid

in dichloromethane (2 mL) and stirred for 2 h. The volatiles were removed under vacuum. The residue was dissolved in CH_2Cl_2 and the solution was evaporated. The residue was suspended in 2 mL of 1N HCl, stirred for 30 min, and freeze-dried to give the hydrochloride salt as off white solid, which was purified by RP-HPLC on a reverse-phase Gemini® C18 column (Phenomenex® Inc., pore size: 110 Å, particle size: 5 μm, 250 x 21.2 mm) using a binary solvent system consisting of a gradient of 5–60% MeOH [0.1% formic acid (FA)] in water (0.1% FA) with a flow rate of 10.0 mL/min and UV detection at 214 nm. The desired fractions were combined and freeze-dried to white fluffy powder: azapeptide **4** (5.2 mg, 0.01 mmol, 7%): mp 93–94 °C; ^{1}H NMR (500 MHz, CD_3OD) δ 8.40 (s, 1H), 7.45–7.20 (m, 10H), 6.24 (s, 1H), 4.56–4.42 (m, 1H), 4.05–3.88 (m, 1H), 3.69–3.42 (m, 2H), 2.59–2.43 (m, 3H), 2.43–2.31 (m, 1H), 2.26–2.14 (m, 1H), 2.14–2.00 (m, 1H), 2.00–1.91 (m, 1H), 1.91–1.62 (m, 6H), 1.53–1.36 (m, 5H), 1.35–1.03 (m, 5H); ^{13}C NMR (125 MHz, MeOD) δ 174.1, 171.2, 161.4, 143.2, 139.1, 129.5 (2C), 129.4 (2C), 129.3 (2C), 128.8 (2C), 128.4, 128.2, 63.6, 57.9, 57.4, 49.6, 31.5, 31.3, 30.8, 26.9, 26.72 (2C), 26.69 (2C), 26.5, 17.5; IR (neat) vmax/cm^{-1} 2929, 1638, 1532, 1495, 1449, 1406, 1344, 1323, 1095; HRMS m/z calculated for $C_{29}H_{40}N_5O_3$ $[M+H]^+$ 506.3126; found 506.3139. (Supplementary File S1). The logarithm of the partition coefficient (clogP) values were calculated using Chemdraw 17.0 (Perkin Elmer, 2017, Waltham, MA, USA).

2.3 Results

2.3.1. Chemistry. Smac activity has been correlated to binding to IAP proteins and mimicked by its *N*-terminal four-residue amide sequence (H-Ala-Val-Pro-Ile-NH_2, **1**, Figure 2.3) (100-102). The purported turn conformation adopted about the central Val-Pro dipeptide in this sequence has led to the synthesis of various constrained analogs, exhibiting enhanced potency (72,103). Noting the similar conformational preferences of indolizidinone amino acid and aza-amino acyl proline turn mimics (104-107), and the relative ease of synthesis of the latter, a series of aza-analogs were synthesized and certain were shown to induce cell death by a caspase-9 mediated apoptotic pathway in cancer cell cultures (65,106). Notably, aza-methanopipecolate and aza-cyclohexylglycine analogs **2** and **3** were synthesized using pericyclic chemistry on the diazo dicarbonyl moiety of an azopeptide to examine the conformation of the Val residue in **1** (65,108,109). Specifically, the Alder-ene reaction of cyclohexadiene and the Diels-Alder reaction

of cyclopentadiene on N-(Cbz)azoglycinyl-proline benzhydrylamide **5** gave the unsaturated azapeptides **6** and **7**, which were hydrogenated with concomitant removal of the benzyloxycarbonyl group, coupled to N-protected alanine, and deprotected (Scheme 2.1, (65)). Considering the tolerance of N-methyl-alanine for alanine in the terminal position (110), a similar approach was used to prepare N-methyl analog **4** by hydrogenation of azapeptide **7**, coupling of the resulting aza-cyclohexylglycinyl-L-proline benzhydrylamide (**8**) to N-(Boc)-N-methylalanine using PyBop and cleavage of the Boc group with TFA in DCM. In cultured MCF7 breast cancer cells, aza-cyclohexylglycine analog **3** induced up to 60% cell death relative to vehicle (65).

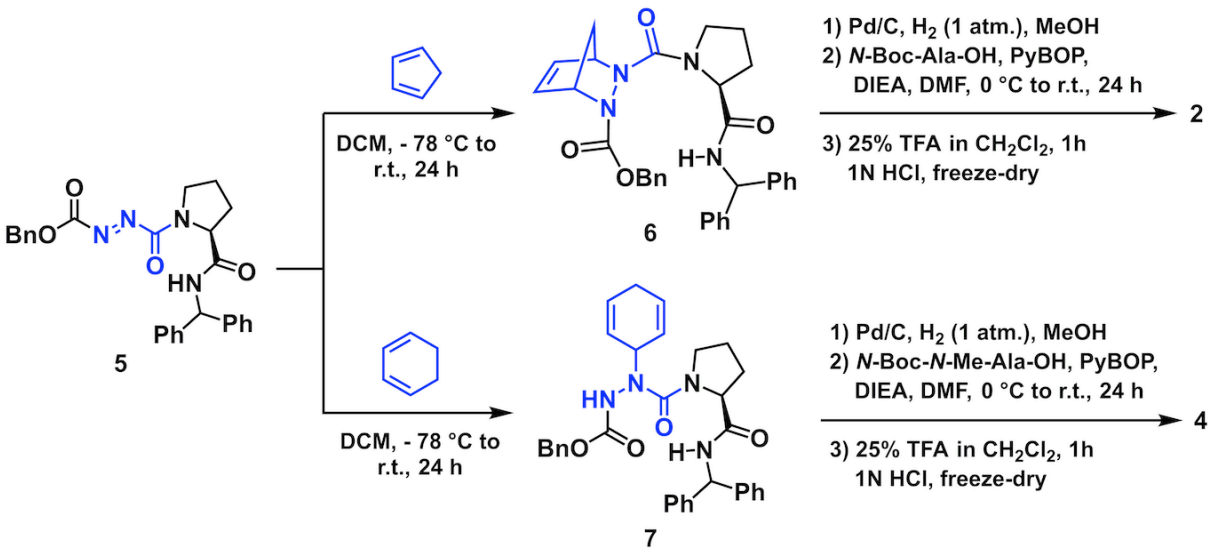

Scheme 2.1 Synthesis of Smac mimics **2** and **4** (dienes, azo- and aza-residues in blue).

2.3.2. Effect of Smac Mimic Administration in vivo. We have previously reported that *Drosophila* mutants in the *BicC* gene recapitulate key features of PKD (58). Considering that Smac mimics showed efficacy at reducing cysts in a rat PKD model (46), the results of Smac mimic administration were tested in the *BicC* cystic *Drosophila* using two different allelic combinations. The $BicC^{\Delta/YC33}$ combination induces milder cystic defects than the $BicC^{\Delta/IIF34}$ one (58). Straight-winged mutants ($BicC^{\Delta/YC33}$, $BicC^{\Delta/IIF34}$) from crosses were selected within two days of eclosion to yield pools of 0–2 days old *Drosophila* and aged for seven days (7–9 days old), during which time they were kept well-fed by transferring to fresh vials twice (Figure 2.2). Aged siblings were divided into fresh vials containing food spiked with either vehicle (water, 50 µL) or one of the Smac analogs **1**–**4** at 20 µM (50 µL). *Drosophila* were transferred into identical

fresh vials every three days. After 20 days of treatment, the Malpighian tubules were micro-dissected from 27–29 day old mutants and analyzed *ex vivo*.

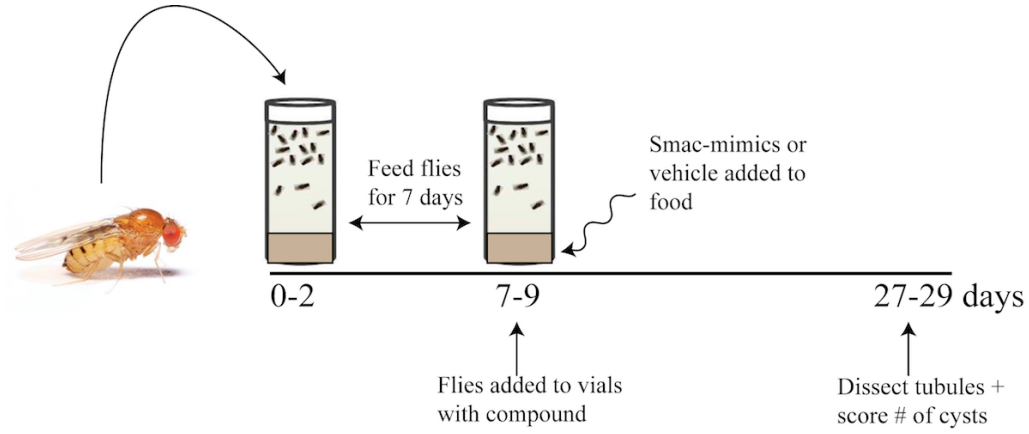

Figure 2.2 Testing protocol for Smac-mimic efficacy in cyst reduction. *Ore*^{R} wild-type, *BicC*$^{\Delta/YC33}$, and *BicC*$^{\Delta/IIF34}$ *Drosophila* (0-2 days old) were placed in food-containing vials at age 0-2 days and transferred into fresh vials every three days. Once the age of 7-9 days was reached, *Drosophila* were placed in vials containing one of each of the Smac mimics or vehicle control, respectively. Cysts were scored on the micro-dissected Malpighian tubules after 20 days, when animals reached age 27-29 days.

Per each condition, cystic deformities were scored using 25–50 female *BicC*$^{\Delta/IIF34}$ and *BicC*$^{\Delta/YC33}$ *Drosophila* (*i.e.*, 50–100 anterior and 50–100 posterior tubules). For each individual, cysts which were found in the two anterior and two posterior tubules were scored and charted as nested plots using the Prism 8.0 (Graphpad) software (Figures 2.3-2.6). Vehicle-treated *Drosophila* presented several cysts in both the anterior and posterior Malpighian tubules, especially in the terminal and intermediate regions, and fewer cysts in the proximal region, as reported previously (58). Similar to PKD patients (1), a variable number of cysts was found in different individuals (58). In general, Smac-mimics appeared to reduce tubular cysts in both *BicC* allelic combinations (Tables 2.1 and 2.2).

Effects of Smac mimic administration were recorded as overall cyst reduction (Tables 2.1 and 2.2). Nested plots were used to represent individual variability in cyst number in the analyzed populations. Administration of peptide **1** to *BicC*$^{\Delta/YC33}$ *Drosophila* (n = 50) reduced cystic deformities respectively by 44% and 20% (228 vs. 127 cysts and 276 vs. 220 cysts, p =

0.0005 and 0.0457) in the anterior and posterior tubules, respectively (Table 2.1, Figure 2.3A,B). Administration of mimic **2** to *BicC*$^{\Delta/YC33}$ mutants (n = 50) reduced tubular cysts by 24% and 34% (216 vs. 165 cysts, p = 0.0324 and 244 vs. 162 cysts, p = 0.0017) in the anterior and posterior tubules, respectively (Table 2.1, Figure 2.3A,B). Administration of mimic **3** to *BicC*$^{\Delta/YC33}$ *Drosophila* (n = 50) reduced cysts in the anterior and posterior tubules respectively by 21% and 34% (195 vs. 153 cysts, p = 0.1028 and 238 vs. 156 cysts, p = 0.0014, Table 2.1, Figure 2.3A,B). Finally, administration of mimic **4** to *BicC*$^{\Delta/YC33}$ mutants (n = 50) reduced cysts in the anterior and posterior tubules respectively by 31% and 18% (134 vs. 93 cysts, p = 0.0553 and 152 vs. 124 cysts, p = 0.1877, Table 2.1, Figure 2.3A,B).

Table 2.1 Overall cyst reduction upon Smac-mimic treatment of *BicC*$^{\Delta/YC33}$ *Drosophila*.

	Anterior Tubule				Posterior Tubule			
Mimic	**Cyst # Vehicle**	**Cyst # Treated**	**% Reduction**	***p* value**	**Cyst # Vehicle**	**Cyst # Treated**	**% Reduction**	***p* value**
1	228	127	44%	0.0005	276	220	20%	0.0457
2	216	165	24%	0.0324	244	162	34%	0.0017
3	195	153	*21%*	*0.1028*	238	156	34%	0.0014
4	134	93	*31%*	*0.0553*	152	124	*18%*	*0.1877*

P values > 0.05 and corresponding percentages are italicized.

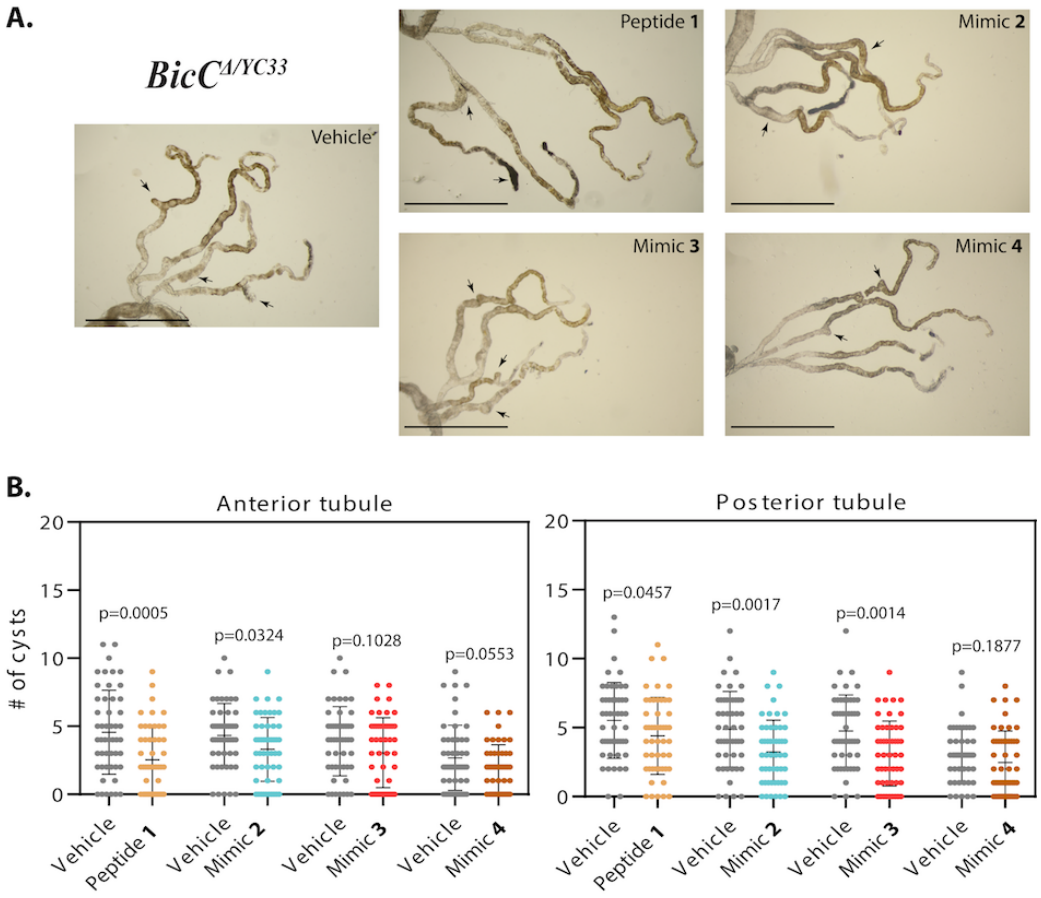

Figure 2.3 Smac mimics reduced cysts in *BicC*$^{\Delta/YC33}$ *Drosophila*. (**A**). Representative Malpighian tubules micro-dissected from *BicC*$^{\Delta/YC33}$ *Drosophila* treated with either vehicle or analogs **1**, **2**, **3**, and **4** (indicated) were photographed *ex vivo*. Arrows indicate cysts. In each image, anterior pairs are at the top, posterior pairs at the bottom. Scale bar: 1 mm. (**B**). Nested plots depicting number of cysts found in the anterior and posterior tubule pairs of vehicle- and Smac mimic-treated cystic *Drosophila* (indicated), with mean and standard deviation. *P* values (with Welch's correction) are indicated. Treatments are indicated with color: vehicle, grey; mimic **1**, sepia; **2**, blue; **3**, dark pink; **4**, brown.

The analogs were next administered to the *BicC*$^{\Delta/IIF34}$ *Drosophila* carrying the allelic combination which produced a more severe phenotype. Treatment with peptide **1** decreased cystic deformations respectively by 44% and 37% (total 357 vs. 199 cysts and 433 vs. 272 cysts, $p < 0.0001$ and 0.0002, respectively) in the anterior and posterior tubules of the micro-dissected *BicC*$^{\Delta/IIF34}$ mutants ($n = 50$, Table 2.2, Figure 2.4A,B). Administration of mimic **2** to *BicC*$^{\Delta/IIF34}$

Drosophila (n = 50) reduced cystic deformations by 39% in the anterior (233 vs. 142 cysts, p = 0.0011) and by 33% in the posterior (302 vs. 202 cysts, p = 0.0020) tubules (Table 2.2, Figure 2.4A,B). Administration of mimic **3** to $BicC^{\Delta/IIF34}$ mutants (n = 25) had a milder and highly variable effect on the renal tubules and reduced cystic deformities by 11% (114 vs. 102 cysts, p = 0.6317) and 21% (155 vs. 122 cysts, p = 0.2285) in the anterior and posterior tubules respectively (Table 2.2, Figure 2.4A,B), below statistical relevance thresholds. Finally, administration of mimic **4** to $BicC^{\Delta/IIF34}$ *Drosophila* (n = 50) reduced cysts in the anterior and posterior tubules by 40% (199 vs. 119 cysts, p = 0.0005) and 38% (243 vs. 151 cysts, p = 0.0002) respectively (Table 2.2, Figure 2.4A,B). Parallel respective administration of analogs **1**–**4** to control, non-cystic Ore^{R} wild type individuals did not change Malpighian tubule morphology.

Table 2.2 Overall cyst reduction upon Smac-mimic treatment of $BicC^{\Delta/IIF34}$ *Drosophila*

	Anterior Tubule				Posterior Tubule			
Mimic	**Cyst # Vehicle**	**Cyst # Treated**	**% Reduction**	***p* value**	**Cyst # Vehicle**	**Cyst # Treated**	**% Reduction**	***p* value**
1	357	199	44%	< 0.0001	433	272	37%	0.0002
2	233	142	39%	0.0011	302	202	33%	0.0020
3	114	102	*11%*	*0.6317*	155	122	*21%*	*0.2285*
4	199	119	40%	0.0005	243	151	38%	0.0002

P values > 0.05 and corresponding percentages are italicized.

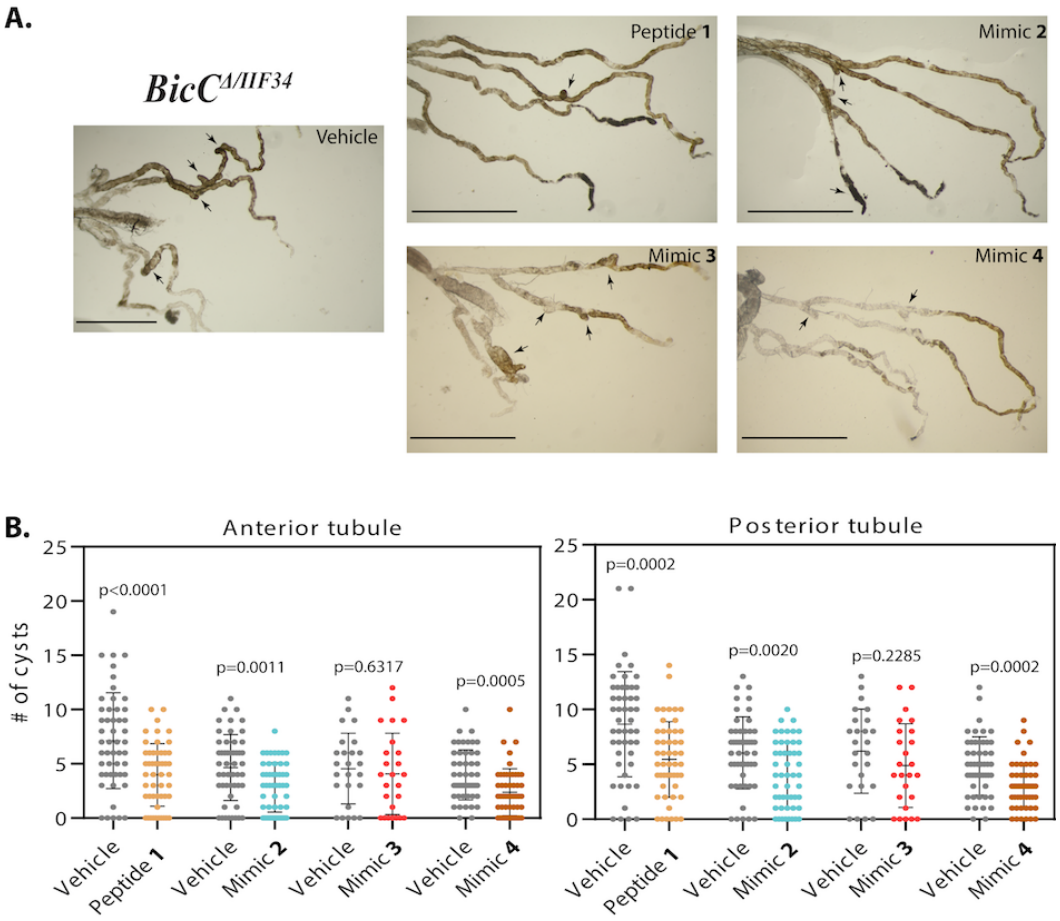

Figure 2.4 Smac mimics reduced cysts in *BicC*$^{\Delta/IIF34}$ *Drosophila*. (**A**). Representative Malpighian tubules micro-dissected from *BicC*$^{\Delta/IIF34}$ *Drosophila* treated with either vehicle or analogs **1**, **2**, **3**, and **4** (indicated) were photographed *ex vivo*. Arrows indicate cysts. In each image, anterior pairs are at the top, posterior pairs at the bottom. Scale bar: 1 mm. (**B**). Nested plots depicting number of cysts found in the anterior and posterior tubule pairs of vehicle- and Smac mimic-treated cystic *Drosophila* (indicated), with mean and standard deviation. *P* values (with Welch's correction) are indicated. Treatments are indicated with color: vehicle, grey; mimic **1**, sepia; **2**, blue; **3**, dark pink; **4**, brown.

Distinct Malpighian tubule regions in both the anterior and posterior tubules appeared to respond differentially to the Smac mimics. The cyst location was thus specifically mapped in the proximal, intermediate and terminal regions of the anterior and posterior tubules respectively (Tables 2.3 and 2.4), and individual variable cyst numbers similarly plotted (Figures 2.5 and 2.6). Absolute numbers for the cysts in each region described below are listed in Table S2.

2.3.2.1. Smac Mimics Differentially Affect Distinct Regions of the Malpighian Tubules. Administration of peptide **1** to the milder allelic combination $BicC^{\Delta/YC33}$ (n = 50) reduced cysts in the terminal and intermediate regions of the anterior tubules respectively by 53% and 34% (total 122 vs. 57, 104 vs. 69 cysts, $p < 0.0001$ and $p = 0.0381$, Table 2.3, Figure 2.5A). In the proximal region of the anterior tubules, two cysts were found in the control versus one cyst in the treated samples, precluding statistical analyses. In the posterior tubules, administration of peptide **1** diminished cysts in the intermediate region by 26% (total 109 vs. 80 cysts, $p = 0.0449$). In the terminal and proximal regions, a trend toward decreased cysts was observed, albeit without reaching a statistical threshold for significance (respectively 108 vs. 84 cysts, 22% reduction, $p = 0.1405$, and 59 vs. 56 cysts, 5% reduction, $p = 0.7531$, Table 2.3, Figure 2.5A).

Table 2.3 Percentage of cyst reduction upon treatment of $BicC^{\Delta/YC33}$ *Drosophila*.

Smac-mimic	Anterior tubule			Posterior tubule		
	Prox.	**Int.**	**Term.**	**Prox.**	**Int.**	**Term.**
1 (n = 50)	n/s	34% $p = 0.0381$	53% $p < 0.0001$	*5%* *$p = 0.7531$*	26% $p = 0.0449$	*22%* *$p = 0.1405$*
2 (n = 50)	n/s	*5%* *$p = 0.7599$*	41% $p = 0.0006$	47% $p = 0.0057$	29% $p = 0.0389$	32% $p = 0.0125$
3 (n = 50)	n/a	*2%* *$p = 0.9072$*	40% $p = 0.0041$	*21%* *$p = 0.2431$*	30% $p = 0.0465$	45% $p = 0.0007$
4 (n = 50)	n/a	36% $p = 0.0461$	*20%* *$p = 0.3377$*	n/s *$p = 0.4769$*	33% $p = 0.0130$	n/s *$p = 0.9245$*

P values > 0.05 and corresponding percentages are italicized; n/s = not significant; n/a = no cysts.

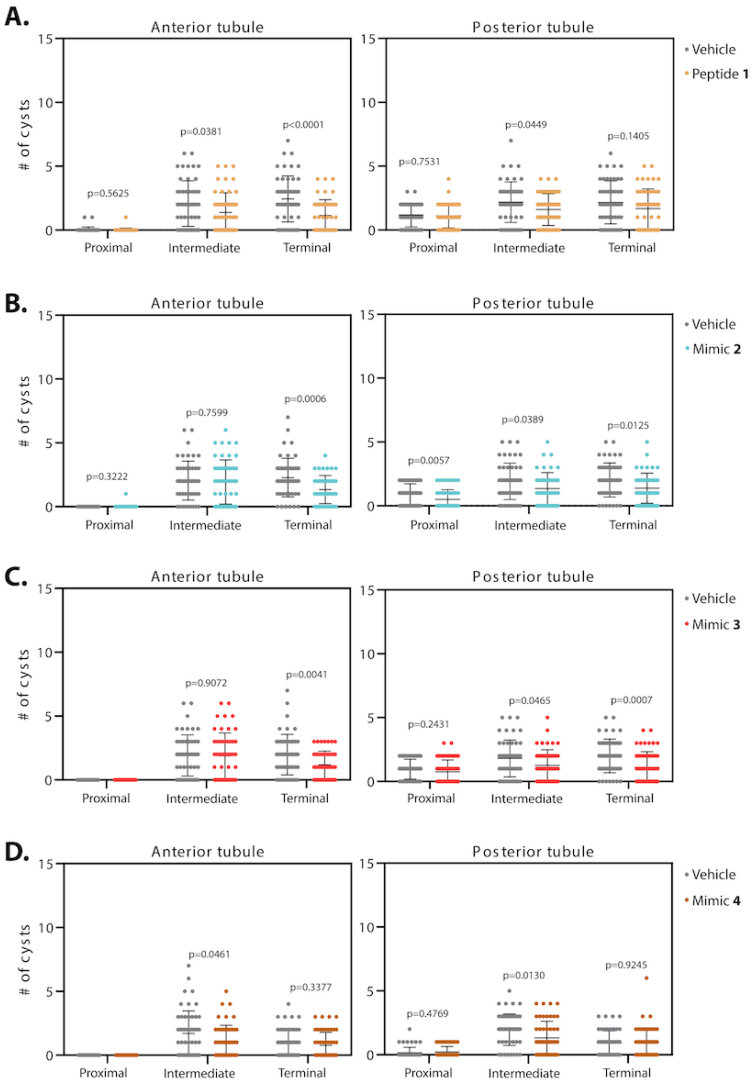

Figure 2.5 Smac mimics reduce cysts in *BicC*$^{\Delta/YC33}$ *Drosophila* with varying regional specificity. Malpighian tubules from 50 *BicC*$^{\Delta/YC33}$ *Drosophila* were micro-dissected after 20 days of treatment (age 27-29 days). Cysts were scored *ex vivo*. For each individual, cysts numbers were recorded for the terminal, intermediate and proximal region of the Malpighian tubules, independently for the anterior (left) and posterior (right) tubules. *Drosophila* were administered either vehicle (water, grey) or Smac mimics **1** (**A**, sepia), **2** (**B**, blue), **3** (**C**, dark pink), and **4** (**D**, brown). Mean and standard deviation are indicated. Analogs **1** and **2** best reduced tubular cysts, mimic **3** was effective at reducing cysts in the terminal region of the anterior tubules and mimic **4** had a mild effect in the intermediate region of both tubule pairs. *P* values (with Welch's correction) are indicated. *BicC*$^{\Delta/YC33}$ *Drosophila* exhibit the milder cystic defects.

Administration of peptide **1** to *BicC*$^{\Delta/IIF34}$ *Drosophila* reduced cysts in the anterior tubules by 40% and 48% (total 156 vs. 94 and 193 *vs* 100 cysts, $p = 0.0038$ and $p < 0.0001$) in the terminal and intermediate regions, respectively (Table 2.4, Figure 2.6A). In the proximal region of the anterior tubules, a trend of cyst reduction was observed, albeit fewer cysts (eight and five in vehicle- and peptide **1**-treated tubules) and high individual variability precluded a margin of confidence. In the posterior tubules, administration of peptide **1** reduced cysts in the terminal, intermediate and proximal regions by 32%, 41% and 39% (total 180 vs. 122, 167 vs. 98, 86 vs. 52 cysts, $p = 0.0022$, 0.0008 and 0.0150), respectively (Table 2.4, Figure 2.6A).

Table 2.4 Percentage of cyst reduction upon treatment of *BicC*$^{\Delta/IIF34}$ *Drosophila*.

Smac-mimic	Anterior tubule			Posterior tubule		
	Prox.	**Int.**	**Term.**	**Prox.**	**Int.**	**Term.**
1 ($n = 50$)	n/s	48% $p < 0.0001$	40% $p = 0.0038$	39% $p = 0.0150$	41% $p = 0.0008$	32% $p = 0.0022$
2 ($n = 50$)	n/a	41% $p = 0.0045$	37% $p = 0.0161$	43% $p = 0.0080$	*27%* *$p = 0.0703$*	32% $p = 0.0086$
3 ($n = 25$)	n/a	*9%* *$p = 0.7140$*	*11%* *$p = 0.6746$*	*40%* *$p = 0.1325$*	*10%* *$p = 0.7038$*	*21%* *$p = 0.2429$*
4 (n = 50)	n/s	42% $p = 0.0014$	38% $p = 0.0195$	*35%* *$p = 0.1069$*	*22%* *$p = 0.1231$*	51% $p < 0.0001$

P values > 0.05 and corresponding percentages are italicized; n/s = not significant; n/a = no cysts.

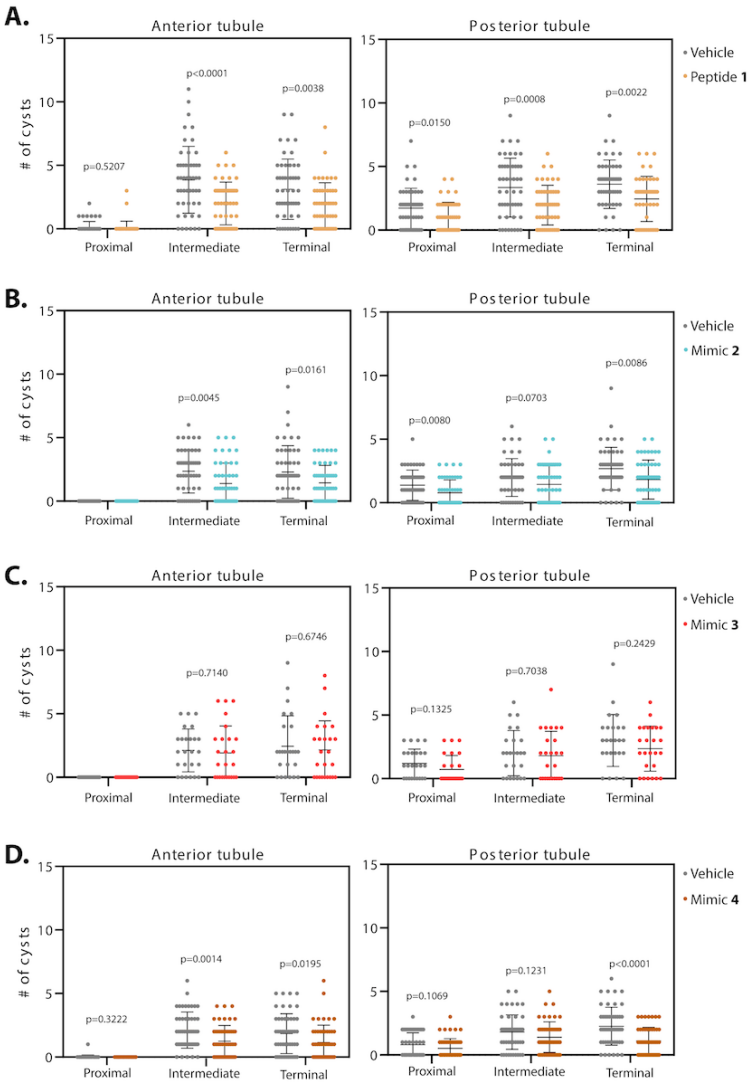

Figure 2.6 Smac mimics reduce cysts in *BicC*$^{\Delta/IIF34}$ *Drosophila* with varying regional specificity. Malpighian tubules from 50 *BicC*$^{\Delta/IIF34}$ *Drosophila* were micro-dissected after 20 days of treatment (age 27-29 days). Cysts were scored *ex vivo*. For each individual, cysts numbers were recorded for the terminal, intermediate and proximal region of the Malpighian tubules, independently for the anterior (left) and posterior (right) tubules. *Drosophila* were administered either vehicle (water, grey) or Smac mimics **1** (**A**, sepia), **2** (**B**, blue), **3** (**C**, dark pink), and **4** (**D**, brown). Mean and standard deviation are indicated. Peptide **1** was the most effective at reducing cysts in the treated tubules. Mimics **2** and 4 showed great improvements in all regions except for the intermediate region of the posterior tubules and mimic **3** showed a very mild to no effect in cyst reduction. *P* values (with Welch's correction) are indicated. *BicC*$^{\Delta/IIF34}$ *Drosophila* exhibit the more severe cystic defects.

Treatment with mimic **2** diminished cysts in the terminal region of the anterior tubules of *BicC*$^{\Delta/YC33}$ *Drosophila* (n = 50) by 41% (114 vs. 67 cysts, p = 0.0006). In the intermediate region, a mild 5% reduction was observed that did not approach a statistical significance threshold (102 vs. 97 cysts, p = 0.7599, Table 2.3, Figure 2.5B). Precluding statistical analyses, no (control) and one cyst (mimic **2**-treated) were detected in the proximal region of the anterior tubules. In contrast, in the posterior tubule, administration of mimic **2** reduced cysts in the terminal, intermediate and proximal regions by 32%, 29% and 47% (101 vs. 69 cysts, p = 0.0125, 96 vs. 68 cysts, p = 0.0389 and 47 vs. 25 cysts, p = 0.0057), respectively (Table 2.3, Figure 2.5B).

Administration of mimic **2** to the more severely cystic *BicC*$^{\Delta/IIF34}$ mutants (n = 50) reduced cysts in the terminal and intermediate regions of the anterior tubules by 37% and 41% (average 115 vs. 72 cysts, p = 0.0161, 118 vs. 70 cysts, p = 0.0045), respectively. No cysts were found in the proximal regions of control and treated tubules (Table 2.4, Figure 2.6B). Administration of mimic **2** reduced cysts in the terminal and proximal regions of the posterior tubules by 32% and 43% (134 vs. 91 cysts, p = 0.0086 and 69 vs. 39 cysts, p = 0.0080), respectively. The intermediate region displayed a 27% reduction that approached statistical significance threshold (99 vs. 72 cysts, p = 0.0703, Table 2.4, Figure 2.6B).

After treatment with mimic **3**, the *BicC*$^{\Delta/YC33}$ *Drosophila* (n = 50) harbored 40% fewer cysts in the terminal region of the anterior tubules (99 vs. 59 cysts, p = 0.0041). In the intermediate region, the effect was negligible (2% reduction, 96 vs. 94 cysts, p = 0.9072). No cysts were detected in the proximal region of both control and treated tubules (Table 2.3, Figure 2.5C). On the contrary, administration of mimic **3** reduced strongly cysts in the terminal and intermediate regions of the posterior tubules by 45% and 30% (100 vs. 55 cysts, p = 0.0007 and 90 vs. 63 cysts, p = 0.0465), respectively. The proximal region displayed a trend towards cyst reduction with high individual variability (21% reduction, 48 vs. 38 cysts, p = 0.2431, Table 2.3, Figure 2.5C).

Mimic **3** did not ameliorate the more severely cystic *BicC*$^{\Delta/IIF34}$ mutants (n = 25). After treatment with mimic **3**, the *BicC*$^{\Delta/IIF34}$ mutants displayed respectively 11% and 9% (61 vs. 54 cysts, p = 0.6746 and 53 vs. 48 cysts, p = 0.7140) fewer cysts in the terminal and intermediate regions of the anterior tubules; no cysts were observed in the proximal region of both control and treated tubules (Table 2.4, Figure 2.6C). Similarly, mimic **3** caused respectively 21%, 10% and 40% (75 vs. 59 cysts, p = 0.2429, 50 vs. 45 cysts, p = 0.7038 and 30 vs. 18 cysts, p = 0.1325)

reductions in cysts in the terminal, intermediate and proximal regions of the posterior tubules (Table 2.4, Figure 2.6C).

Mimic **4** reduced cysts in the intermediate region of the anterior tubules of $BicC^{\Delta/YC33}$ *Drosophila* (n = 50) by 36% (85 vs. 55 cysts, p = 0.0461). In the terminal region, a 20% decrease was observed, that did not reach a threshold of statistical significance (49 vs. 39 cysts, p = 0.3377). No cysts were detected in the proximal region of both control and treated tubules (Table 2.3, Figure 2.5D). Treatment with mimic **4** reduced cysts in the intermediate region of the posterior tubules by 33% (98 vs. 66 cysts, p = 0.0130), but did not reduce cysts in the terminal and proximal regions (Table 2.3, Figure 2.5D).

Upon treatment with mimic **4**, cysts were lessened in the terminal and intermediate regions of the anterior tubules of $BicC^{\Delta/IIF34}$ *Drosophila* (n = 50) by 38% and 42% (92 vs. 57 cysts, p = 0.0195 and 106 vs. 62 cysts, p = 0.0014), respectively (Table 2.4, Figure 2.6D). Precluding statistical analysis, only one cyst was detected in the proximal region of control tubules and no cysts in the treated tubules. Administration of mimic **4** reduced cysts in the terminal region of the posterior tubules by 51% (113 vs. 55 cysts, $p < 0.0001$). Less cysts were also scored in the intermediate and proximal regions, although values did not reach the significance threshold (respectively 22% reduction, 90 vs. 70 cysts, p = 0.1231, and 35% reduction, 40 vs. 26 cysts, p = 0.1069, Table 2.4, Figure 2.6D).

Ineffective cyst reduction could be partly due to *Drosophila* refusing to ingest the Smac mimics. To assess their ingestion, the analogs were mixed with food and dye, and fed to mutants for four days. The green dye could be seen through the semi-transparent abdominal cuticle for all mimics, confirming analog ingestion (Figure S2.1). As a measure of hydrophilicity, the clogP values were calculated for the different Smac mimics (Figure 2.1) and found to be sufficiently low to be consistent with absorption: **1** (0.7), **2** (3.9), **3** (5.0), **4** (5.4). Together these results support the conclusion that the Smac analogs may have differential activities and/or processing.

2.4 Discussion

A systematic analysis of the influences of the Smac mimic H-Ala-Val-Pro-Ile-NH_2 (**1**) and constrained analogs **2**–**4** on renal cystogenesis has been performed using the novel *BicC Drosophila* model to recapitulate features of PKD (58). Two allelic combinations for *BicC* were used that yield cystic phenotypes of different severity, namely $BicC^{\Delta/YC33}$ and $BicC^{\Delta/IIF34}$.

Previously, the Smac mimic GT13072 reduced cystogenesis in a rat ADPKD model (46). In the *BicC Drosophila*, Smac mimics **1**–**4** ameliorated similarly the cystic condition with the strongest effects displayed in the more severely affected $BicC^{\Delta/IIF34}$ genotype. Peptide **1** exhibited the highest overall efficacy reducing cyst occurrence by 20–44% across genotypes at the anterior and posterior tubules. Moreover, aza-methanopipecolate **2** caused a 24–39% reduction of cysts. Aza-cyclohexylglycine **3** displayed least efficacy, but still improved significantly the posterior tubules of the $BicC^{\Delta/YC33}$ mutants. The related *N*-methyl-alaninyl-aza-cyclohexylglycine analog **4** exhibited differential activity in the two *BicC* mutants, reducing cysts by ~40% in both tubules of the $BicC^{\Delta/IIF34}$ mutants. In contrast, analog **4** only showed a trend towards reducing cysts in the anterior tubule of the $BicC^{\Delta/YC33}$ *Drosophila* close to the significance threshold ($p = 0.0553$). The Smac mimics tested appeared to differentially affect the anterior and posterior tubule pairs overall, consistent with the report of the latter having distinct transcriptomes (70) and thus different physiological specialization. Mimics **1, 2** and **3** were found to induce death of 20% (**1**, **2**) and 60% (**3**) of cultured MCF7 adenocarcinoma cells (65). Their efficacy in other PKD models and patients is unknown. Smac mimics function in context-dependent ways, likely through different IAPs to affect apoptosis via several mechanisms (72). Due to its methyl group, *N*-methyl-alaninyl-aza-cyclohexylglycine analog **4** was expected to be more stable than aza-cyclohexylglycine **3** *in vivo* (111-113), which was consistent with the observed higher cyst-reducing activity.

The tubular sections responded differentially to treatment with the Smac mimics. The terminal region consistently exhibited greater improvement, especially in the weaker $BicC^{\Delta/YC33}$ allelic combination. *Drosophila* were shown to ingest the Smac mimics. The clogP values of mimics **1**–**4** were also within the range consistent with effective absorption. The distinct pharmacological responses observed at different regions of the Malpighian tubules may be related to variability in absorption, metabolism and response to Smac mimics within cystic cells in such regions. Regional specialization of Malpighian tubules has been observed despite the tubular epithelium being composed by only two major cell types (reviewed in (57), (114)). Cystogenesis may perturb cells and reduce the threshold for initiating cell death pathways either through caspase-dependent apoptosis or the TNF signaling pathway. The contribution of apoptosis to the early phases of ADPKD is a matter of debate (115); however, the TNF pathway has been implicated in ADPKD-type renal cystogenesis and suggested to be the primary target of

Smac mimics in a rat model of *Pkd1*-dependent ADPKD (46). The results presented here predict that the *BicC* mutation may feature dysregulated TNF signaling in the epithelial cells of the Malpighian tubules, as observed in ADPKD-type cystogenesis. The expression of TNF (Eiger) and TNF pathway components in the Malpighian tubules and their respective contributions to tubular function are however unknown. The human *BicC* orthologue *BICC1* has been found to be genetically downstream of the main *PKD1* gene (58). The pharmacological response to Smac mimics was herein demonstrated to be conserved in *Drosophila* illustrating further the phenotypic and molecular similarities between *PKD1*-induced and *BicC*-induced renal cystogenesis.

Notably, pharmacological binding sites have been found to be conserved in *Drosophila* (116). Chemical probing in *Drosophila in vivo* may thus rapidly pinpoint the involvement of specific pathways with complementarity to genetic analyses, indicate conserved biological activity of drug-prototypes, and provide a rapid read-out for effectiveness of pharmacological modulation of specific pathways involved in cystic pathogenesis. The Smac mimics affected different tubular regions differentially. Considering that such specificity may be conserved to humans, the development of personalized pharmacological treatments for cystic renal diseases such as PKD will benefit from precise knowledge of the cyst-ameliorating potential of different Smac mimics.

2.5 Supplementary Materials to Chapter 2

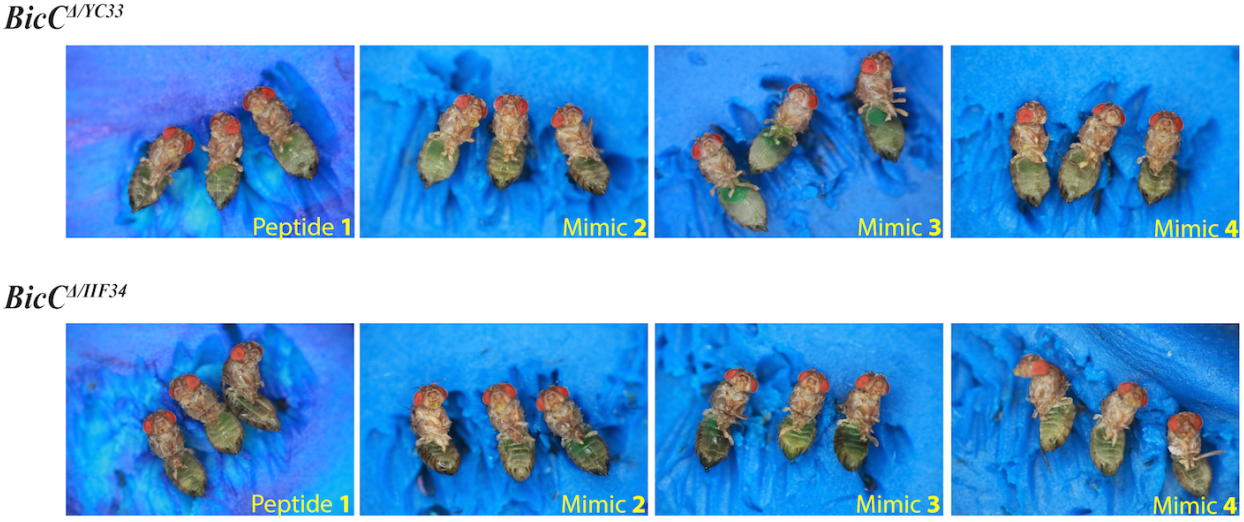

Figure S2.1 Analog feeding control. *BicC* mutants fed Smac mimics mixed with green dye for four days, displayed ingested food contents visible through their semi-transparent abdominal cuticle. Legs were clipped for better visualization.

Chapter 3: General conclusions and future directions

My thesis consists of a primary research article published in 2019 and also a review published in 2018, which is included in Appendix II. I have discussed how *Drosophila* can be valuable to model human renal cystic diseases due to remarkable conservation of genes, pathways and morphological features. Of specific advantage to the study of diseases causing the formation of cysts of the renal tubule such as PKD, anatomically separated Malpighian tubules enable detailed phenotypic analyses such as the ones shown in this thesis. Particularly suitable to drug discovery, the small size of *Drosophila* also facilitates drug-screening *in vivo* using analytical amounts of compounds. Mutations in the human *BICC1*, murine *Bicc1* and other *BicC* vertebrate orthologs all cause the formation of renal cysts. We have shown that in PKD mutation of the human *PKD1* and murine *Pkd1* genes cause reduced function respectively of the *BICC1* and *Bicc1* orthologs (58). Together with the observation that *BicC* loss of function is sufficient to induce renal cysts, this suggests that BicC is a contributor to renal cystic pathogenesis in human *PKD1* and murine *Pkd1* mutants. Thus, characterization of the effects of *BicC* loss of function may help unravel the complex events of renal cyst formation.

BicC mutation in *Drosophila* produces a phenotype reminiscent of PKD, characterized by a degenerative trajectory. In *Drosophila BicC* mutants, cysts form along all regions of the Malpighian tubules, with highest frequency in the terminal and intermediate regions. The *BicC Drosophila* model also displays several molecular markers of PKD, including Myc and mTOR up-regulation (58). Therefore, the *BicC Drosophila* model can be leveraged to study conserved aspects of the complex processes of renal cysts. This thesis shows a first proof-of-principle application of such model for drug discovery.

Because multiple pathways promoting cell proliferation are dysregulated in PKD, including c-Myc and mTOR, several anti-cancer drugs have been and are being tested to reduce cysts in PKD. Among these, Smac mimetics neutralize IAPs leading to activation of caspases and apoptosis (75). In ADPKD, TNF-α accumulates in the cystic fluid, which offers opportunity to target preferentially cystic cells and not neighbouring renal epithelial cells (46). The role of TNF signaling in Malpighian tubules is unknown, however, TNF, its receptor and downstream factors are conserved in *Drosophila,* although their functions need to be explored. Additionally, Reaper, Hid and Grim proteins (which are all *Drosophila* IAP antagonists similar to Smac) could

induce apoptosis when transfected in mammalian cells (53). Such extensive conservation suggested that Smac mimicry may function in the cystic *Drosophila* model, should TNF be dys-regulated in the *BicC* mutant, similar to PKD.

Overall, Smac mimics **1**-**4** all reduced cystogenesis of the $BicC^{\Delta/YC33}$ and $BicC^{\Delta/IIF34}$ *Drosophila*. Smac mimic **1** was the most efficient reducing cysts overall by 44% for both allelic combinations, followed by mimic **2** (34 and 39%, respectively), and **4** (31 and 40%, respectively). As well, distinct regions of the Malpighian tubules showed differential improvements to Smac mimic treatment, highlighting functional differences along the tubule that will be further characterized in future. The cystic index scored here is qualitative, because it exclusively tallied cysts and did not include other parameters that may be consequential, such as cyst size and morphology. How these may influence the cysts and the cystic portions of the epithelium (compared to the non-cystic surroundings) is unknown in both PKD and in the recently-established *Drosophila* PKD model. Cyst size, especially in the context of the vertebrate kidney where nephrons are embedded in parenchymal tissue, is expected to impact both mechanical deformation and, likely, the induction of stress-induced apoptosis of the surrounding tissues (11). In fact, in PKD only 1% of the nephrons are cystic, yet the kidneys are eventually damaged completely and irreparably (*e.g.*, see Figure 1.1). Therefore, slowing cyst enlargement is also expected to delay kidney damage and prolong the time before dialysis and transplant are needed. The way I counted cysts may be considered particularly stringent because of the lack of accounting of cystic size. However, cyst size and morphology are largely uncharacterized, and their appropriate quantification is a matter of debate in the field of PKD studies. Because of the likely relevance of these parameters and the accessibility of the *Drosophila* Malpighian tubules facilitating direct examination, our laboratory is developing tools to measure such parameters as we tease apart the underlying biology of renal cyst formation using the streamlined *Drosophila* model. In future studies, these tools, together with increased knowledge of how Smac mimicry affects the complex mechanisms of cyst formation, may reveal that the numerical cyst reduction observed from Smac mimic treatment may indeed be accompanied by a higher overall rescue of the cystic phenotype.

The observation that Smac mimics could reduce cysts in the *Drosophila* PKD model without the addition of exogenous TNF, also suggests that TNF and its receptor may be up-regulated in the *BicC Drosophila* Malpighian tubules, a possibility consistent with preliminary

data from our ongoing research. If confirmed, this finding would further extend the similarities between human PKD and the cystic *Drosophila* model and add a novel aspect to the complex *BicC* mutant phenotype. In perspective, using this model appears a valid first step to characterize the conserved molecular pathways involved in renal cystic growth, including cell proliferation, apoptosis, cell-cell contacts and the associated molecular markers, including proliferation factors, cell junction proteins, signal transduction and TNF pathway components. The *BicC Drosophila* model will likely help to elucidate the functions of the TNF pathway in *Drosophila* Malpighian tubules and decipher the mechanism of action for Smac mimics in *Drosophila.* Albeit cyst reduction in vertebrates is expected to retard loss of kidney function, it is unclear if Smac mimics can also rescue polarization of the tubular epithelium and the filtration function of the renal tubules. These fundamental aspects can be efficiently studied in isolated *Drosophila* Malpighian tubules in which epithelial and other cell markers can be monitored by immunoblots and immunostaining. Moreover, individual tubule filtration indicative of physiological function, can be measured by *Drosophila* Ramsay assays (117) and can be used to compare fluid secretion from Malpighian tubules of vehicle and Smac-mimic-treated *Drosophila*.

To fully confirm efficacy and drug potential for Smac mimicry in PKD, these studies will have to be extended to vertebrate models and, eventually, clinical trials. Because of the influence of cellular context on TNF upregulation levels and signaling, Smac mimic response in patients may ultimately vary depending on factors such as the individual *PKD1* mutations and the random variable of which tubular region(s) may have developed most cysts. Optimal administration to effectively reach and improve the cystic tubules embedded in the (vertebrate) kidney, long-term efficacy and safety will also have to be determined.

One interesting observation is that in both the murine and *Drosophila* cystic models, Smac mimics appeared to reduce, yet not completely eliminate cysts (46,64). Smac mimics are considered combination drugs in oncology(43) and may similarly be more effective when used jointly to other compounds in PKD. However, lacking a cure for renal cystic diseases such as PKD, a safe way of inducing cyst reduction is considered a milestone because it would delay the need for costly procedures such as dialysis and transplant and lead to a better quality of life for the patients, as kidney enlargement cause severe abdominal pain from compression and painful events of cyst rupture that may lead to secondary infections.

While the biological underpinning of renal cyst formation is complex and there is a lot more to investigate about its molecular pathways, our research begins to offer some clues as to the conserved molecular players in the cystic process. One of such players with implications on our understanding of PKD pathology appears to be *BicC*. My research presented here, demonstrated feasibility of discovering drug candidates displaying cyst-reducing activity *in vivo* using the *BicC Drosophila* model of PKD. Further drug development potential will be evaluated for such identified molecules. The drug-testing protocols presented here can be scaled up for increased throughput and testing other compounds and libraries that can be combined with the genetic approaches well established in *Drosophila*. Intriguingly, this research has also provided clues to novel BicC functions in the Malpighian tubule as a potential TNF modulator, either direct or indirect. Thus, chemical testing in *Drosophila* may also benefit efforts to tease apart the conserved, fundamental molecular underpinning of *BicC* mutation-dependent renal cyst formation and ultimately contribute to expanding our understanding of PKD pathology.

References

(1) Bergmann C, Guay-Woodford LM, Harris PC, Horie S, Peters DJ, Torres VE. Polycystic kidney disease. Nat Rev Dis Primers 2018;4(1):1-24.

(2) Shillingford JM, Murcia NS, Larson CH, Low SH, Hedgepeth R, Brown N, et al. The mTOR pathway is regulated by polycystin-1, and its inhibition reverses renal cystogenesis in polycystic kidney disease. Proc Natl Acad Sci U S A 2006;103(14):5466-5471.

(3) Harris PC, Torres VE. Polycystic kidney disease. Annu Rev Med 2009;60:321-337.

(4) Mohler J, Wieschaus EF. Dominant maternal-effect mutations of *Drosophila melanogaster* causing the production of double-abdomen embryos. Genetics 1986;112(4):803-822.

(5) Gamberi C, Lasko P. The Bic-C family of developmental translational regulators. Comp Funct Genomics 2012;2012.

(6) Fischer E, Legue E, Doyen A, Nato F, Nicolas J, Torres V, et al. Defective planar cell polarity in polycystic kidney disease. Nat Genet 2006;38(1):21.

(7) Yamaguchi T, Hempson SJ, Reif GA, Hedge AM, Wallace DP. Calcium restores a normal proliferation phenotype in human polycystic kidney disease epithelial cells. J Am Soc Nephrol 2006;17(1):178-187.

(8) Cowley BD,Jr, Smardo FL,Jr, Grantham JJ, Calvet JP. Elevated c-myc protooncogene expression in autosomal recessive polycystic kidney disease. Proc Natl Acad Sci U S A 1987;84(23):8394-8398.

(9) Trudel M, D'Agati V, Costantini F. C-myc as an inducer of polycystic kidney disease in transgenic mice. Kidney Int 1991;39(4):665-671.

(10) Lanoix J, D'Agati V, Szabolcs M, Trudel M. Dysregulation of cellular proliferation and apoptosis mediates human autosomal dominant polycystic kidney disease (ADPKD). Oncogene 1996;13(6):1153-1160.

(11) Leonhard WN, Zandbergen M, Veraar K, van den Berg S, van der Weerd L, Breuning M, et al. Scattered deletion of PKD1 in kidneys causes a cystic snowball effect and recapitulates polycystic kidney disease. J Am Soc Nephrol 2015;26(6):1322-1333.

(12) Nauli SM, Alenghat FJ, Luo Y, Williams E, Vassilev P, Li X, et al. Polycystins 1 and 2 mediate mechanosensation in the primary cilium of kidney cells. Nat Genet 2003;33(2):129.

(13) Christensen ST, Pedersen SF, Satir P, Veland IR, Schneider L. The primary cilium coordinates signaling pathways in cell cycle control and migration during development and tissue repair. Curr Top Dev Biol 2008;85:261-301.

(14) Masyuk AI, Gradilone SA, Banales JM, Huang BQ, Masyuk TV, Lee S, et al. Cholangiocyte primary cilia are chemosensory organelles that detect biliary nucleotides via P2Y12 purinergic receptors. Am J Physiol Gastrointest Liver Physiol 2008;295(4):G725-G734.

(15) Ibraghimov-Beskrovnaya O, Natoli TA. mTOR signaling in polycystic kidney disease. Trends Mol Med 2011;17(11):625-633.

(16) Hildebrandt F, Benzing T, Katsanis N. Ciliopathies. New Engl J Med 2011;364(16):1533-1543.

(17) Ma M, Tian X, Igarashi P, Pazour GJ, Somlo S. Loss of cilia suppresses cyst growth in genetic models of autosomal dominant polycystic kidney disease. Nat Genet 2013;45(9):1004.

(18) Flechner SM, Goldfarb D, Modlin C, Feng J, Krishnamurthi V, Mastroianni B, et al. Kidney transplantation without calcineurin inhibitor drugs: a prospective, randomized trial of sirolimus versus cyclosporine1. Transplantation 2002;74(8):1070-1076.

(19) Tao Y, Kim J, Schrier RW, Edelstein CL. Rapamycin markedly slows disease progression in a rat model of polycystic kidney disease. J Am Soc Nephrol 2005;16(1):46-51.

(20) Gattone II VH, Sinders RM, Hornberger TA, Robling AG. Late progression of renal pathology and cyst enlargement is reduced by rapamycin in a mouse model of nephronophthisis. Kidney Int 2009;76(2):178-182.

(21) Shillingford JM, Piontek KB, Germino GG, Weimbs T. Rapamycin ameliorates PKD resulting from conditional inactivation of Pkd1. J Am Soc Nephrol 2010;21(3):489-497.

(22) Novalic Z, Van Der Wal AM, Leonhard WN, Koehl G, Breuning MH, Geissler EK, et al. Dose-dependent effects of sirolimus on mTOR signaling and polycystic kidney disease. J Am Soc Nephrol 2012;23(5):842-853.

(23) Raught B, Gingras AC, Sonenberg N. The target of rapamycin (TOR) proteins. Proc Natl Acad Sci U S A 2001;98(13):7037-7044.

(24) Serra AL, Poster D, Kistler AD, Krauer F, Raina S, Young J, et al. Sirolimus and kidney growth in autosomal dominant polycystic kidney disease. N Engl J Med 2010;363(9):820-829.

(25) Walz G, Budde K, Mannaa M, Nürnberger J, Wanner C, Sommerer C, et al. Everolimus in patients with autosomal dominant polycystic kidney disease. N Engl J Med 2010;363(9):830-840.

(26) Renken C, Fischer D-, Kundt G, Gretz N, Haffner D. Inhibition of mTOR with sirolimus does not attenuate progression of liver and kidney disease in PCK rats. Nephrol Dial Transplant 2011;26(1):92-100.

(27) Harris PC, Watson ML. Autosomal dominant polycystic kidney disease: neoplasia in disguise? Nephrol Dial Transplant 1997;12(6):1089-1090.

(28) Grantham JJ. Polycystic kidney disease: neoplasia in disguise. Am J Kidney Dis 1990;15(2):110-116.

(29) Rowe I, Chiaravalli M, Mannella V, Ulisse V, Quilici G, Pema M, et al. Defective glucose metabolism in polycystic kidney disease identifies a new therapeutic strategy. Nat Med 2013;19(4):488-493.

(30) Vander Heiden MG, Cantley LC, Thompson CB. Understanding the Warburg effect: the metabolic requirements of cell proliferation. Science 2009;324(5930):1029-1033.

(31) Csibi A, Blenis J. Appetite for destruction: the inhibition of glycolysis as a therapy for tuberous sclerosis complex-related tumors. BMC Biol 2011;9(1):69.

(32) Sweeney WE,Jr, von Vigier RO, Frost P, Avner ED. Src inhibition ameliorates polycystic kidney disease. J Am Soc Nephrol 2008;19(7):1331-1341.

(33) Irazabal MV, Torres VE, Hogan MC, Glockner J, King BF, Ofstie TG, et al. Short-term effects of tolvaptan on renal function and volume in patients with autosomal dominant polycystic kidney disease. Kidney Int 2011;80(3):295-301.

(34) Sans-Atxer L, Joly D. Tolvaptan in the treatment of autosomal dominant polycystic kidney disease: patient selection and special considerations. Int J Nephrol Renovasc Dis 2018;11:41-51.

(35) Torres VE, Chapman AB, Devuyst O, Gansevoort RT, Grantham JJ, Higashihara E, et al. Tolvaptan in patients with autosomal dominant polycystic kidney disease. N Engl J Med 2012;367(25):2407-2418.

(36) Torres VE, Chapman AB, Devuyst O, Gansevoort RT, Perrone RD, Koch G, et al. Tolvaptan in later-stage autosomal dominant polycystic kidney disease. N Engl J Med 2017;377(20):1930-1942.

(37) Clavería C, Albar JP, Serrano A, Buesa JM, Barbero JL, Martínez-A C, et al. *Drosophila* Grim induces apoptosis in mammalian cells. EMBO J 1998;17(24):7199-7208.

(38) McCarthy JV, Dixit VM. Apoptosis induced by *Drosophila* Reaper and Grim in a human system. Attenuation by inhibitor of apoptosis proteins (cIAPs). J Biol Chem 1998;273(37):24009-24015.

(39) Wang CY, Mayo MW, Korneluk RG, Goeddel DV, Baldwin AS,Jr. NF-kappa antiapoptosis: induction of TRAF1 and TRAF2 and c-IAP1 and c-IAP2 to suppress caspase-8 activation. Science 1998;281(5383):1680-1683.

(40) Verhagen AM, Ekert PG, Pakusch M, Silke J, Connolly LM, Reid GE, et al. Identification of DIABLO, a mammalian protein that promotes apoptosis by binding to and antagonizing IAP proteins. Cell 2000;102(1):43-53.

(41) Deng Y, Ren X, Yang L, Lin Y, Wu X. A JNK-dependent pathway is required for TNFα-induced apoptosis. Cell 2003;115(1):61-70.

(42) Runckel K, Barth MJ, Mavis C, Gu JJ, Hernandez-Ilizaliturri FJ. The SMAC mimetic LCL-161 displays antitumor activity in preclinical models of rituximab-resistant □-cell lymphoma. Blood Adv 2018;2(23):3516-3525.

(43) Pemmaraju N, Carter BZ, Kantarjian HM, Cortes JE, Bose P, Kadia TM, et al. Final results of phase 2 clinical trial of LCL161, a novel oral SMAC mimetic/IAP antagonist, for patients with intermediate to high risk myelofibrosis 2019. ASH Annual Meeting.

(44) O'Donnell MA, Legarda-Addison D, Skountzos P, Yeh WC, Ting AT. Ubiquitination of RIP1 regulates an NF-κ□-independent cell-death switch in TNF signaling. Curr Biol 2007;17(5):418-424.

(45) Li X, Magenheimer BS, Xia S, Johnson T, Wallace DP, Calvet JP, et al. A tumor necrosis factor-α–mediated pathway promoting autosomal dominant polycystic kidney disease. Nat Med 2008;14(8):863.

(46) Fan LX, Zhou X, Sweeney WE,Jr, Wallace DP, Avner ED, Grantham JJ, et al. Smac-mimetic-induced epithelial cell death reduces the growth of renal cysts. J Am Soc Nephrol 2013;24(12):2010-2022.

(47) Igaki T, Kanda H, Yamamoto-Goto Y, Kanuka H, Kuranaga E, Aigaki T, et al. Eiger, a TNF superfamily ligand that triggers the *Drosophila* JNK pathway. EMBO J 2002;21(12):3009-3018.

(48) Igaki T, Miura M. The *Drosophila* TNF ortholog Eiger: emerging physiological roles and evolution of the TNF system. Semin Immunol: Elsevier; 2014.

(49) Li M, Sun S, Priest J, Bi X, Fan Y. Characterization of TNF-induced cell death in *Drosophila* reveals caspase-and JNK-dependent necrosis and its role in tumor suppression. Cell Death & Disease 2019;10(8):1-14.

(50) Igaki T, Kanda H, Okano H, Xu T, Miura M. Eiger and Wengen: the *Drosophila* orthologs of TNF/TNFR. Advances in TNF Family Research: Springer; 2011. 45-50.

(51) Kanda H, Igaki T, Kanuka H, Yagi T, Miura M. Wengen, a member of the *Drosophila* tumor necrosis factor receptor superfamily, is required for Eiger signaling. J Biol Chem 2002;277(32):28372-28375.

(52) Kauppila S, Maaty WS, Chen P, Tomar RS, Eby MT, Chapo J, et al. Eiger and its receptor, Wengen, comprise a TNF-like system in *Drosophila*. Oncogene 2003;22(31):4860.

(53) Verhagen A, Vaux D. Cell death regulation by the mammalian IAP antagonist Diablo/Smac. Apoptosis 2002;7(2):163-166.

(54) Costantini F, Kopan R. Patterning a complex organ: branching morphogenesis and nephron segmentation in kidney development. Dev Cell 2010;18(5):698-712.

(55) Hildebrandt F. Genetic kidney diseases. The Lancet 2010;375(9722):1287-1295.

(56) Chien S, Reiter LT, Bier E, Gribskov M. Homophila: human disease gene cognates in Drosophila. Nucleic Acids Res 2002;30(1):149-151.

(57) Millet-Boureima C, Porras Marroquin J, Gamberi C. Modeling Renal Disease "On the Fly". BioMed Res Int 2018;2018.

(58) Gamberi C, Hipfner DR, Trudel M, Lubell WD. Bicaudal C mutation causes myc and TOR pathway up-regulation and polycystic kidney disease-like phenotypes in *Drosophila*. PLoS Genet 2017;13(4).

(59) Tran U, Pickney LM, Özpolat BD, Wessely O. Xenopus Bicaudal-C is required for the differentiation of the amphibian pronephros. Dev Biol 2007;307(1):152-164.

(60) Bouvrette DJ, Sittaramane V, Heidel JR, Chandrasekhar A, Bryda EC. Knockdown of bicaudal C in zebrafish (*Danio rerio*) causes cystic kidneys: A nonmammalian model of polycystic kidney disease. Comp Med 2010;60(2):96-106.

(61) Mahone M, Saffman EE, Lasko PF. Localized Bicaudal-C RNA encodes a protein containing a KH domain, the RNA binding motif of FMR1. EMBO J 1995;14(9):2043-2055.

(62) Saffman EE, Styhler S, Rother K, Li W, Richard S, Lasko P. Premature translation of oskar in oocytes lacking the RNA-binding protein Bicaudal-C. Mol Cell Biol 1998;18(8):4855-4862.

(63) Chicoine J, Benoit P, Gamberi C, Paliouras M, Simonelig M, Lasko P. Bicaudal-C recruits CCR4-NOT deadenylase to target mRNAs and regulates oogenesis, cytoskeletal organization, and its own expression. Dev Cell 2007;13(5):691-704.

(64) Millet-Boureima C, Chingle R, Lubell WD, Gamberi C. Cyst reduction in a polycystic kidney disease *Drosophila* model using Smac mimics. Biomedicines 2019;7(4):82.

(65) Chingle R, Ratni S, Claing A, Lubell WD. Application of constrained aza-valine analogs for Smac mimicry. Peptide Science 2016;106(3):235-244.

(66) Chingle R, Proulx C, Lubell WD. Azapeptide synthesis methods for expanding side-chain diversity for biomedical applications. Acc Chem Res 2017;50(7):1541-1556.

(67) Happé H, Peters DJM. Translational research in ADPKD: Lessons from animal models. Nat Rev Nephrol 2014;10(10):587-601.

(68) Wahl PR, Serra AL, Le Hir M, Molle KD, Hall MN, Wüthrich RP. Inhibition of mTOR with sirolimus slows disease progression in Han:SPRD rats with autosomal dominant polycystic kidney disease (ADPKD). Nephrol Dial Transplant 2006;21(3):598-604.

(69) Wu M, Wahl PR, Le Hir M, Wackerle-Men Y, Wuthrich RP, Serra AL. Everolimus retards cyst growth and preserves kidney function in a rodent model for polycystic kidney disease. Kidney Blood Press Res 2007;30(4):253-259.

(70) Wang J, Kean L, Yang J, Allan AK, Davies SA, Herzyk P, et al. Function-informed transcriptome analysis of *Drosophila* renal tubule. Genome Biol 2004;5(9).

(71) Lalaoui N, Vaux DL. Recent advances in understanding inhibitor of apoptosis proteins. F1000Research 2018;7.

(72) Cong H, Xu L, Wu Y, Qu Z, Bian T, Zhang W, et al. Inhibitor of apoptosis protein (IAP) antagonists in anticancer agent discovery: Current status and perspectives. J Med Chem 2019;62(12):5750-5772.

(73) Damgaard RB, Nachbur U, Yabal M, Wong WW, Fiil BK, Kastirr M, et al. The ubiquitin ligase XIAP recruits LUBAC for NOD2 signaling in inflammation and innate immunity. Mol Cell 2012;46(6):746-758.

(74) Damgaard RB, Fiil BK, Speckmann C, Yabal M, Zur Stadt U, Bekker-Jensen S, et al. Disease-causing mutations in the XIAP BIR2 domain impair NOD2-dependent immune signalling. EMBO Mol Med 2013;5(8):1278-1295.

(75) Fulda S, Vucic D. Targeting IAP proteins for therapeutic intervention in cancer. Nat Rev Drug Discov 2012;11(2):109.

(76) Duckett C, Nava VE, Gedrich RW, Clem RJ, Van Dongen JL, Gilfillan MC, et al. A conserved family of cellular genes related to the baculovirus iap gene and encoding apoptosis inhibitors. EMBO J 1996;15(11):2685-2694.

(77) Hay BA, Wassarman DA, Rubin GM. *Drosophila* homologs of baculovirus inhibitor of apoptosis proteins function to block cell death. Cell 1995;83(7):1253-1262.

(78) Jones G, Jones D, Zhou L, Steller H, Chu Y. Deterin, a new inhibitor of apoptosis from *Drosophila melanogaster*. J Biol Chem 2000;275(29):22157-22165.

(79) Vernooy SY, Chow V, Su J, Verbrugghe K, Yang J, Cole S, et al. *Drosophila* Bruce can potently suppress Rpr-and Grim-dependent but not Hid-dependent cell death. Curr Biol 2002;12(13):1164-1168.

(80) White K, Grether ME, Abrams JM, Young L, Farrell K, Steller H. Genetic control of programmed cell death in *Drosophila*. Science 1994;264(5159):677-683.

(81) Grether ME, Abrams JM, Agapite J, White K, Steller H. The head involution defective gene of *Drosophila melanogaster* functions in programmed cell death. Genes Dev 1995;9(14):1694-1708.

(82) Chen P, Nordstrom W, Gish B, Abrams JM. grim, a novel cell death gene in *Drosophila*. Genes Dev 1996;10(14):1773-1782.

(83) Tenev T, Zachariou A, Wilson R, Paul A, Meier P. Jafrac2 is an IAP antagonist that promotes cell death by liberating Dronc from DIAP1. EMBO J 2002;21(19):5118-5129.

(84) Christich A, Kauppila S, Chen P, Sogame N, Ho S, Abrams JM. The damage-responsive *Drosophila* gene sickle encodes a novel IAP binding protein similar to but distinct from reaper, grim, and hid. Curr Biol 2002;12(2):137-140.

(85) Srinivasula SM, Datta P, Kobayashi M, Wu J, Fujioka M, Hegde R, et al. sickle, a novel *Drosophila* death gene in the reaper/hid/grim region, encodes an IAP-inhibitory protein. Curr Biol 2002;12(2):125-130.

(86) Wing JP, Karres JS, Ogdahl JL, Zhou L, Schwartz LM, Nambu JR. *Drosophila* sickle is a novel grim-reaper cell death activator. Curr Biol 2002;12(2):131-135.

(87) Challa M, Malladi S, Pellock BJ, Dresnek D, Varadarajan S, Yin YW, et al. *Drosophila* Omi, a mitochondrial-localized IAP antagonist and proapoptotic serine protease. EMBO J 2007;26(13):3144-3156.

(88) Igaki T, Suzuki Y, Tokushige N, Aonuma H, Takahashi R, Miura M. Evolution of mitochondrial cell death pathway: proapoptotic role of HtrA2/Omi in *Drosophila*. Biochem Biophys Res Commun 2007;356(4):993-997.

(89) Khan F, Fujioka M, Datta P, Fernandes-Alnemri T, Jaynes J, Alnemri E. The interaction of DIAP1 with dOmi/HtrA2 regulates cell death in *Drosophila*. Cell Death Differ 2008;15(6):1073.

(90) Du C, Fang M, Li Y, Li L, Wang X. Smac, a mitochondrial protein that promotes cytochrome c–dependent caspase activation by eliminating IAP inhibition. Cell 2000;102(1):33-42.

(91) van Loo G, Van Gurp M, Depuydt B, Srinivasula S, Rodriguez I, Alnemri E, et al. The serine protease Omi/HtrA2 is released from mitochondria during apoptosis. Omi interacts with caspase-inhibitor XIAP and induces enhanced caspase activity. Cell Death Differ 2002;9(1):20.

(92) Gottfried Y, Rotem A, Lotan R, Steller H, Larisch S. The mitochondrial ARTS protein promotes apoptosis through targeting XIAP. EMBO J 2004;23(7):1627-1635.

(93) Liston P, Fong WG, Kelly NL, Toji S, Miyazaki T, Conte D, et al. Identification of XAF1 as an antagonist of XIAP anti-Caspase activity. Nat Cell Biol 2001;3(2):128.

(94) Wing JP, Schwartz LM, Nambu JR. The RHG motifs of Drosophila Reaper and Grim are important for their distinct cell death-inducing abilities. Mech Dev 2001;102(1-2):193-203.

(95) Saita S, Nolte H, Fiedler KU, Kashkar H, Venne AS, Zahedi RP, et al. PARL mediates Smac proteolytic maturation in mitochondria to promote apoptosis. Nat Cell Biol 2017;19(4):318.

(96) Xu D, Woodfield SE, Lee TV, Fan Y, Antonio C, Bergmann A. Genetic control of programmed cell death (apoptosis) in *Drosophila*. Fly 2009;3(1):78-90.

(97) Brenner D, Blaser H, Mak TW. Regulation of tumour necrosis factor signalling: live or let die. Nat Rev Immunol 2015;15(6):362-374.

(98) Moreno E, Yan M, Basler K. Evolution of TNF signaling mechanisms: JNK-dependent apoptosis triggered by Eiger, the *Drosophila* homolog of the TNF superfamily. Curr Biol 2002;12(14):1263-1268.

(99) Andersen DS, Colombani J, Palmerini V, Chakrabandhu K, Boone E, Röthlisberger M, et al. The *Drosophila* TNF receptor Grindelwald couples loss of cell polarity and neoplastic growth. Nature 2015;522(7557):482.

(100) Liu Z, Sun C, Olejniczak ET, Meadows RP, Betz SF, Oost T, et al. Structural basis for binding of Smac/DIABLO to the XIAP BIR3 domain. Nature 2000;408(6815):1004.

(101) Wu G, Chai J, Suber TL, Wu J, Du C, Wang X, et al. Structural basis of IAP recognition by Smac/DIABLO. Nature 2000;408(6815):1008.

(102) Fadeel B, Orrenius S. Apoptosis: a basic biological phenomenon with wide-ranging implications in human disease. J Intern Med 2005;258(6):479-517.

(103) Sun H, Nikolovska-Coleska Z, Yang C, Qian D, Lu J, Qiu S, et al. Design of small-molecule peptidic and nonpeptidic Smac mimetics. Acc Chem Res 2008;41(10):1264-1277.

(104) Boeglin D, Hamdan FF, Melendez RE, Cluzeau J, Laperriere A, Héroux M, et al. Calcitonin gene-related peptide analogues with aza and indolizidinone amino acid residues reveal conformational requirements for antagonist activity at the human calcitonin gene-related peptide 1 receptor. J Med Chem 2007;50(6):1401-1408.

(105) Bourguet CB, Goupil E, Tassy D, Hou X, Thouin E, Polyak F, et al. Targeting the prostaglandin F2α receptor for preventing preterm labor with azapeptide tocolytics. J Med Chem 2011;54(17):6085-6097.

(106) Bourguet CB, Boulay P, Claing A, Lubell WD. Design and synthesis of novel azapeptide activators of apoptosis mediated by caspase-9 in cancer cells. Bioorg Med Chem Lett 2014;24(15):3361-3365.

(107) Mir FM, Atmuri NP, Bourguet CB, Fores JR, Hou X, Chemtob S, et al. Paired utility of aza-amino acyl proline and indolizidinone amino acid residues for peptide mimicry: conception of prostaglandin F2α receptor allosteric modulators that delay preterm birth. J Med Chem 2019;62(9):4500-4525.

(108) Chingle R, Mulumba M, Chung NN, Nguyen TM, Ong H, Ballet S, et al. Solid-phase azopeptide Diels–Alder chemistry for aza-pipecolyl residue synthesis to study peptide conformation. J Org Chem 2019;84(10):6006-6016.

(109) Chingle R, Lubell WD. Azopeptides: Synthesis and pericyclic chemistry. Org Lett 2015;17(21):5400-5403.

(110) Oost TK, Sun C, Armstrong RC, Al-Assaad A, Betz SF, Deckwerth TL, et al. Discovery of potent antagonists of the antiapoptotic protein XIAP for the treatment of cancer. J Med Chem 2004;47(18):4417-4426.

(111) Chatterjee J, Gilon C, Hoffman A, Kessler H. N-methylation of peptides: a new perspective in medicinal chemistry. Acc Chem Res 2008;41(10):1331-1342.

(112) Chatterjee J, Rechenmacher F, Kessler H. N-methylation of peptides and proteins: an important element for modulating biological functions. Angewandte Chemie International Edition 2013;52(1):254-269.

(113) Merlino F, Billard É, Yousif AM, Di Maro S, Brancaccio D, Abate L, et al. Functional selectivity revealed by N-methylation scanning of human urotensin II and related peptides. J Med Chem 2019;62(3):1455-1467.

(114) Sözen MA, Armstrong JD, Yang M, Kaiser K, Dow JAT. Functional domains are specified to single-cell resolution in a *Drosophila* epithelium. Proc Natl Acad Sci U S A 1997;94(10):5207-5212.

(115) Goilav B. Apoptosis in polycystic kidney disease. Biochimica et Biophysica Acta (BBA)-Molecular Basis of Disease 2011;1812(10):1272-1280.

(116) Ziehm M, Kaur S, Ivanov DK, Ballester PJ, Marcus D, Partridge L, et al. Drug repurposing for aging research using model organisms. Aging Cell 2017;16(5):1006-1015.

(117) O'Donnell MJ, Maddrell SH. Fluid reabsorption and ion transport by the lower Malpighian tubules of adult female *Drosophila*. J Exp Biol 1995;198(8):1647-1653.

Appendix I

biomedicines

MDPI

Article

Cyst Reduction in a Polycystic Kidney Disease *Drosophila* Model Using Smac Mimics

Cassandra Millet-Boureima [1], Ramesh Chingle [2], William D. Lubell [2] and Chiara Gamberi [1,*]

[1] Biology Department, Concordia University, Montreal, QC H4B 1R6, Canada; cassandra.millet@mail.concordia.ca
[2] Département de Chimie, Université de Montréal, Montreal, QC H3T 1J4, Canada; ramesh.chingle@nih.gov (R.C.); lubell@chimie.umontreal.ca (W.D.L.)
* Correspondence: chiara.gamberi@concordia.ca; Tel.: +1-524-848-2424 (ext. 3395)

Received: 21 September 2019; Accepted: 15 October 2019; Published: 18 October 2019

Abstract: Autosomal dominant polycystic kidney disease (ADPKD) is an inherited malady affecting 12.5 million people worldwide. Therapeutic options to treat PKD are limited, due in part to lack of precise knowledge of underlying pathological mechanisms. Mimics of the second mitochondria-derived activator of caspases (Smac) have exhibited activity as antineoplastic agents and reported recently to ameliorate cysts in a murine ADPKD model, possibly by differentially targeting cystic cells and sparing the surrounding tissue. A first-in-kind *Drosophila* PKD model has now been employed to probe further the activity of novel Smac mimics. Substantial reduction of cystic defects was observed in the Malpighian (renal) tubules of treated flies, underscoring mechanistic conservation of the cystic pathways and potential for efficient testing of drug prototypes in this PKD model. Moreover, the observed differential rescue of the anterior and posterior tubules overall, and within their physiologically diverse intermediate and terminal regions implied a nuanced response in distinct tubular regions contingent upon the structure of the Smac mimic. Knowledge gained from studying Smac mimics reveals the capacity for the *Drosophila* model to precisely probe PKD pharmacology highlighting the value for such critical evaluation of factors implicated in renal function and pathology.

Keywords: renal cystogenesis; *Drosophila*; disease models; Smac mimicry; polycystic kidney disease; azapeptide

1. Introduction

Autosomal dominant polycystic kidney disease (ADPKD) induces the formation of cysts along the entire renal tubule, predominantly at the terminal region and the collector tubule, as well as extra-renal manifestations [1]. Inherited through a monogenic pattern with the most frequent mutations affecting the *PKD1* or *PKD2* gene, ADPKD displays high heterogeneity in both phenotype and speed of progression [1]. Abnormal proliferation of the epithelial tubular cells during development gives rise to cysts prenatally. Cysts become more numerous with age, gradually enlarging and filling with fluid [1]. Animal models of PKD have been invaluable for defining disease progression and identifying key molecular alterations; however, the precise mechanisms underlying disease pathology remain to be elucidated at the molecular level [2]. The most recent addition to the arsenal of PKD animal models has been the fruit fly, *Drosophila melanogaster*. Mutants for the *Bicaudal C* (*BicC*) gene (hereby *BicC* flies) were found to recapitulate key molecular features of PKD, including *myc* over-expression and mechanistic target of rapamycin (mTOR) pathway activation [3]. Consistent with ADPKD, the *BicC* flies formed cysts along the entire length of the tubule, with higher frequency at the intermediate, terminal and

collector tubule regions [3]. Moreover, analogous to vertebrate PKD [4–8], pharmacological treatment of *BicC* flies with rapamycin transiently reduced cysts [3]. Consistent with the relevance of the *BicC* phenotype in PKD, *BICC1* mRNA and Bicc1 protein orthologues were respectively found to decrease in kidneys from *PKD1* patients and *Pkd1*$^{-/-}$ mice [3]. Thus, *PKD1* dysfunction is associated with decreased *BicC* function.

An excellent model of human renal function, the fly has high genetic conservation and a streamlined anatomy (reviewed in [9]). In contrast to the human kidney, which contains one million tubular filtering units called nephrons, *Drosophila* harbors two pairs of Malpighian tubules (MTs), which are functionally equivalent to the tubular portion of the nephron. Suitable to the open circulatory system of the fly, the renal system does not have glomeruli and possesses nephrocytes, which exhibit re-adsorptive function analogous to the human glomerular podocytes [9]. Originating from the interface between the mid- and hind-gut, the MTs are asymmetrical with longer tubules anteriorly and shorter ones posteriorly. Reminiscent of the different nephron types in the human kidney, the anterior and posterior MTs have distinct transcriptomes [10]. Like the human renal tubules, MTs can be divided into distinct regions, which in the fly are called proximal, intermediate, and terminal. The proximal region excretes fluid into the tubules, the intermediate region secretes potassium chloride and water, and the terminal region is responsible for sodium and, possibly, water reabsorption [9]. One key advantage of the fly renal system is that the MTs are anatomically distinct, float freely in the fly body cavity, and can be cleanly micro-dissected and examined in their entirety.

Antineoplastic mimics of the second mitochondria-derived activator of caspases (Smac, also called the direct inhibitor of apoptosis-binding protein with low pI, DIABLO) have been used to sensitize cancer cells to apoptosis by targeting inhibitors of apoptosis proteins (IAPs, [11,12]). Highly conserved, IAP proteins play a key role in balancing cell survival and cell death through multiple intersecting cellular pathways. Implicated in innate immunity [13,14], IAPs are often upregulated in cancer [15]. First discovered in insect baculovirus as inhibitors of cellular apoptosis which enable viral replication, IAPs were found in both vertebrates and invertebrates [16] (reviewed in [11]). The best-known mammalian IAPs are X-linked IAP (XIAP), cellular IAP1 (cIAP1) and cIAP2 [11]. The *Drosophila* genome encodes four IAPs, Diap1, Diap2, dBruce and Deterin [17–19]. Multiple proteins have been shown to antagonize IAPs. First discovered in *Drosophila*, three proteins, Reaper [20], Head involution defective (Hid, [21]) and Grim [22], can induce apoptosis when transfected into mammalian cells, which demonstrated functional conservation of the apoptotic cellular machinery [23]. Additional fly IAP antagonists are Jafrac [24], Sickle [25–27] and HtrA2 [28–30]. The search for the mammalian IAP antagonists yielded Smac/DIABLO [31,32], Omi/HtrA2 [33], apoptosis-related protein in the TGFβ signaling pathway (ARTS, [34]) and XIAP-associated factor 1 (XAF1, [35]). IAP antagonists function through an RHG motif, named after the prototypical Reaper, Hid and Grim fly proteins. In the case of the well-studied human Smac/DIABLO and fly Hid IAP antagonists, pro-apoptotic stimuli induce proteolytic cleavage exposing the RHG motif at the *N*-terminus enabling interaction with IAP proteins [36,37] and triggering their ubiquitination and degradation. In the appropriate cellular context, IAP degradation can eventually lead to cell death either by way of caspase activation or via tumor necrosis factor (TNF) signaling [11,38,39]. The discovery that the Smac/DIABLO *N*-terminal peptide H-Ala-Val-Pro-Ile-NH_2 can recapitulate the pro-apoptotic function of the entire protein has inspired the development of various Smac mimics, which enable sensitization of neoplastic cells to apoptosis [12].

Based on the premise that ADPKD is considered in part a neoplastic condition [40,41], and that various TNF complex components were upregulated in *Pkd1*$^{-/-}$ mouse embryonic kidney (MEK) cells, the Smac mimic and birinapant analog GT13072 was used to induce TNF-α-dependent cell death in both cultured cells and a rat model of PKD [42]. The pro-apoptotic properties of GT13072 were specific for the TNF-positive renal epithelial cystic cells and spared surrounding non-cystic cells, offering therapeutic potential to ablate renal cystic cells to delay cystogenesis [42].

The TNF pathway is highly conserved in the fly [43–48]. The capacity for Smac mimics to reduce MT cystogenesis has now been tested in the *BicC* cystic flies. The prototypical H-Ala-Val-Pro-Ile-NH_2

(peptide **1**, Figure 1) and three Smac mimics **2**–**4** were administered to the *BicC* cystic flies to reduce cyst formation.

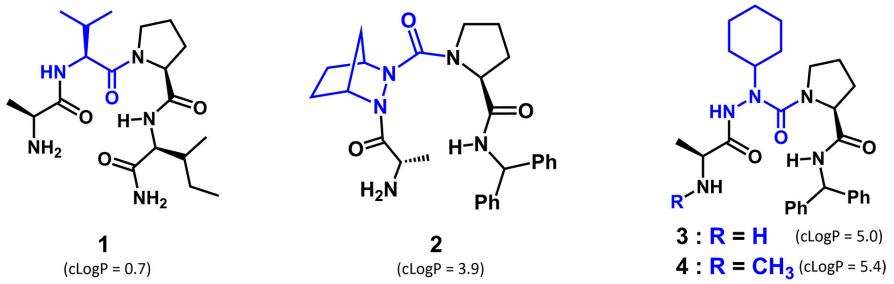

Figure 1. Second mitochondria-derived activator of caspases (Smac) analogs: peptide **1** and mimics **2**–**4** (Val, aza-residue and modified *N*-terminal in blue). Logarithm of the partition coefficient (clogP) values were calculated as described below.

2. Experimental Section

2.1. Fly Lines and Genetics

Fly breeding and care were previously described in detail [3]. In brief, flies were grown on cornmeal agar (Jazzmix, Fisher Scientific Canada, Ottawa, ON) at 25 °C and aged as indicated. *Oregon*^{R} (*Ore*^{R}) wild-type flies were maintained as in [3]. *BicC* mutants were generated by crossing *Df(2L)RA5/CyO* (*BicC*-encompassing deletion obtained from Bloomington *Drosophila* Stock Center) virgin females with one of the two hypomorphic *BicC* mutations, *BicC*^{YC33}*/CyO* and *BicC*^{IIF34}*/CyO* and selecting straight-winged progeny (*Df(2L)RA5/BicC*^{YC33}, *BicC*$^{\Delta/YC33}$ and *Df(2L)RA5/BicC*^{IIF34}, *BicC*$^{\Delta/IIF34}$). The two *BicC* allelic combinations produced truncated proteins and sterile *BicC* flies [3]. Eclosed adult flies were collected every two days to yield 0–2-day old populations and aged as described.

2.2. In Vivo and Ex Vivo Assays

2.2.1. Cystic Index

For the cyst analysis, 0–2-days old flies were aged seven days (i.e., 7–9 days old) and were fed every three days with 2 mL of cornmeal food and equal volumes (50 µL) of either vehicle (water) or an aqueous solution containing peptide **1** or Smac mimic **2**–**4**. Each compound was used at 20 µM and was administered for 20 days (i.e., until 27–29 days old). Malpighian tubules were micro-dissected from 25–50 female flies in phosphate buffered saline (PBS) and the number of cysts was scored separately in anterior and posterior tubules and assigned to each tubular region (i.e., proximal, intermediate and terminal [3,9]), as follows. At one extremity, the proximal region consists of about 15% of the tubule length, tends to have an opaque whitish content (posterior tubule), is thinner than adjacent regions (especially in the anterior tubule) and often exhibits a slight constriction terminally. The neighboring intermediate region has darker contents and consists of about 55% of the tubule length. The terminal region is often translucent, directly connected to the collecting tubule, and consists of the remaining 30% of the tubule length. Cysts were considered tubular deformations creating uni- or bi-laterally protuberant pouches. Extra-branches (as in [3]) were counted as cysts. Values were plotted using the Prism 8.0 software (Graphpad Software, San Diego, CA, USA) as nested distributions. Statistical analyses were performed as unpaired t tests with Welch's correction (the populations may not have equal standard deviations). The raw data counts are listed in Supplementary Table S1.

2.2.2. Microscopy

Malpighian tubules from appropriately aged and treated flies were micro-dissected in 1× PBS, equilibrated into a 3:1 1× PBS:glycerol solution and photographed on a Leica MZ FLIII Fluorescence

Stereomicroscope with Leica MZ series 10×/21B Widefield adjustable eyepieces equipped with a Canon DS126201 EOS 5D MARK II camera, using visible light. Canon raw files (CR2) were converted into TIF format using the Adobe Lightroom 3.2 software (Adobe Systems, San Jose, CA, USA).

2.3. General Synthetic Methods

Chemicals were used as received from commercial sources without further purification unless stated otherwise. All glassware was stored in the oven or flame-dried and let cool under an inert atmosphere prior to use. Anhydrous solvents (DCM, and DMF) were obtained by passage through solvent filtration systems (Glass-Contour, Irvine, CA, USA). Silica gel chromatography was performed using 230–400 mesh silica gel (Silicycle), and TLC was on glass-backed silica plates visualizing the developed chromatogram by UV absorbance or staining with ceric ammonium molybdate or potassium permanganate solutions. Nuclear magnetic resonance spectra (^{1}H and ^{13}C) were recorded on a Bruker AV 500 spectrometer and referenced to residual solvent in CD_3OD (3.31 ppm, 49.0 ppm). Coupling constant *J* values and chemical shifts were measured in Hertz (Hz) and parts per million (ppm). Infrared spectra were recorded in the neat on a Perkin Elmer Spectrum One FTIR instrument and are reported in reciprocal centimeter (cm^{-1}). Liquid chromatography−mass spectrometry (LC−MS) was performed on an Agilent Technologies 1200 series instrument in positive electrospray ionization (ESI)-time-of-flight (TOF) mode at the Université de Montréal Mass Spectrometry Facility. Sodium and proton adducts ($[M + Na]^+$ and $[M + H]^+$) were used for empirical formula confirmation. The peptide H-Ala-Val-Pro-Ile-NH_2 (**1**), Smac mimics **2** and **3**, and aza-cyclohexylglycinyl-L-proline benzhydrylamide (**8**), all were synthesized according to published methods [49]. *N*-Boc-*N*-Methyl-L-alanine and diisopropyl ethyl amine (DIEA) were purchased from Aldrich or Alfa Aesar and used without further purification. Benzotriazol-1-yl-oxytripyrrolidino-phosphoniumhexafluoro-phosphate (PyBop) was purchased from GL Biochem™, recrystallized prior to use from dry CH_2Cl_2/Et_2O (melting point, 156 °C), and stored in the dark.

N-Methyl alaninyl-aza-cyclohexylglycinyl-L-proline benzhydrylamide (**4**). A solution of aza-cyclohexylglycinyl-L-proline benzhydrylamide (**8**, 1 eq., 65 mg, 0.155 mmol, prepared according to [49]) and DIEA (2 eq., 40 mg, 53 µL, 0.309 mmol) was added to a solution of *N*-(*tert*-butoxycarbonyl)-*N*-methyl-L-alanine (1.2 eq., 38 mg, 0.186 mmol) and PyBOP (1.5 eq., 121 mg, 0.233 mmol) in DMF (3 mL), and the mixture was stirred overnight. The volatiles were removed under vacuum. The residue was dissolved in EtOAc (10 mL), washed with 5 mL of saturated aqueous $NaHCO_3$ and brine (10 mL), dried over Na_2SO_4, filtered, and evaporated. Without further purification, the residue was dissolved in a 25% solution of trifluoroacetic acid in dichloromethane (2 mL) and stirred for 2 h. The volatiles were removed under vacuum. The residue was dissolved in CH_2Cl_2 and the solution was evaporated. The residue was suspended in 2 mL of 1N HCl, stirred for 30 min, and freeze-dried to give the hydrochloride salt as off white solid, which was purified by RP-HPLC on a reverse-phase Gemini® C18 column (Phenomenex® Inc., pore size: 110 Å, particle size: 5 µm, 250 × 21.2 mm) using a binary solvent system consisting of a gradient of 5–60% MeOH [0.1% formic acid (FA)] in water (0.1% FA) with a flow rate of 10.0 mL/min and UV detection at 214 nm. The desired fractions were combined and freeze-dried to white fluffy powder: azapeptide **4** (5.2 mg, 0.01 mmol, 7%): mp 93–94 °C; ^{1}H NMR (500 MHz, CD_3OD) δ 8.40 (s, 1H), 7.45–7.20 (m, 10H), 6.24 (s, 1H), 4.56–4.42 (m, 1H), 4.05–3.88 (m, 1H), 3.69–3.42 (m, 2H), 2.59–2.43 (m, 3H), 2.43–2.31 (m, 1H), 2.26–2.14 (m, 1H), 2.14–2.00 (m, 1H), 2.00–1.91 (m, 1H), 1.91–1.62 (m, 6H), 1.53–1.36 (m, 5H), 1.35–1.03 (m, 5H); ^{13}C NMR (125 MHz, MeOD) δ 174.1, 171.2, 161.4, 143.2, 139.1, 129.5 (2C), 129.4 (2C), 129.3 (2C), 128.8 (2C), 128.4, 128.2, 63.6, 57.9, 57.4, 49.6, 31.5, 31.3, 30.8, 26.9, 26.72 (2C), 26.69 (2C), 26.5, 17.5; IR (neat) vmax/cm^{-1} 2929, 1638, 1532, 1495, 1449, 1406, 1344, 1323, 1095; HRMS m/z calculated for $C_{29}H_{40}N_5O_3$ $[M+H]^+$ 506.3126; found 506.3139. (Supplementary File S1). The logarithm of the partition coefficient (clogP) values were calculated using Chemdraw 17.0 (Perkin Elmer, 2017, Waltham, MA, USA).

3. Results

3.1. Chemistry

Smac activity has been correlated to binding to IAP proteins and mimicked by its *N*-terminal four residue amide sequence (H-Ala-Val-Pro-Ile-NH_2, **1**, Figure 1) [50–52]. The purported turn conformation adopted about the central Val-Pro dipeptide in this sequence has led to the synthesis of various constrained analogs, exhibiting enhanced potency [12,53]. Noting the similar conformational preferences of indolizidinone amino acid and aza-amino acyl proline turn mimics [54–57], and the relative ease of synthesis of the latter, a series of aza-analogs were synthesized and certain were shown to induce cell death by a caspase-9 mediated apoptotic pathway in cancer cell cultures [49,57]. Notably, aza-methanopipecolate and aza-cyclohexylglycine analogs **2** and **3** were synthesized using pericyclic chemistry on the diazo dicarbonyl moiety of an azopeptide to examine the conformation of the Val residue in **1** [49,58,59]. Specifically, the Alder-ene reaction of cyclohexadiene and the Diels-Alder reaction of cyclopentadiene on N-(Cbz)azoglycinyl-proline benzhydrylamide **5** gave the unsaturated azapeptides **6** and **7**, which were hydrogenated with concomitant removal of the benzyloxycarbonyl group, coupled to N-protected alanine, and deprotected (Scheme 1, [49]). Considering the tolerance of N-methyl-alanine for alanine in the terminal position [60], a similar approach was used to prepare N-methyl analog **4** by hydrogenation of azapeptide **7**, coupling of the resulting aza-cyclohexylglycinyl-L-proline benzhydrylamide (**8**) to N-(Boc)-N-methylalanine using PyBop and cleavage of the Boc group with TFA in DCM. In cultured MCF7 breast cancer cells, aza-cyclohexylglycine analog **3** induced up to 60% cell death relative to vehicle [49].

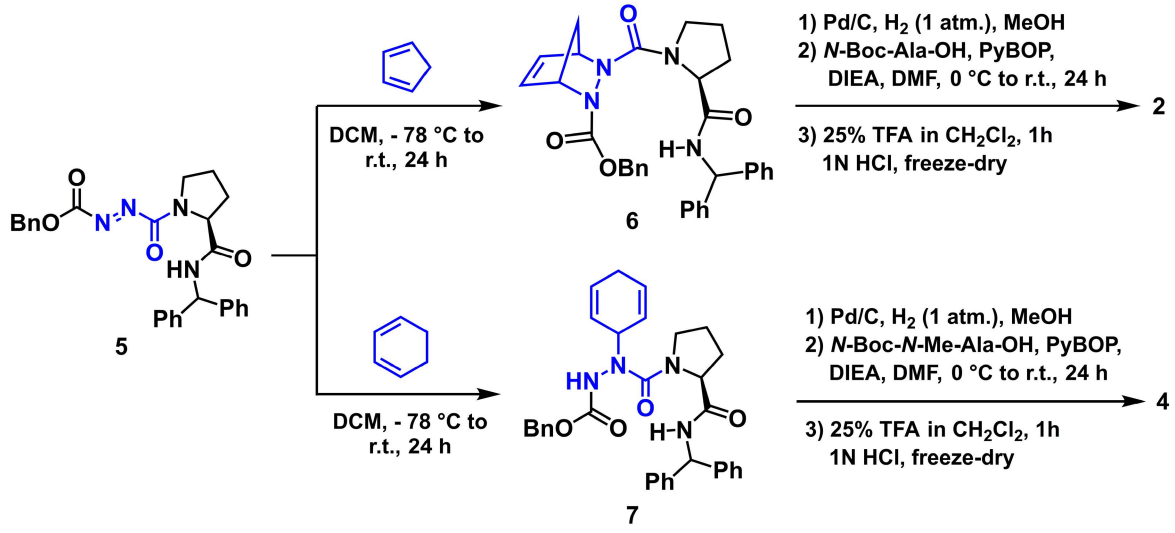

Scheme 1. Synthesis of Smac mimics **2** and **4** (dienes, azo- and aza-residues in blue).

3.1.1. Effect of Smac Mimic Administration In Vivo

We have previously reported that flies mutant in the *BicC* gene recapitulate key features of PKD [3]. Considering that Smac mimics showed efficacy at reducing cysts in a rat PKD model [42], the results of Smac mimic administration were tested in the *BicC* cystic flies using two different allelic combinations. *BicC* mutant flies were obtained from genetic crosses of heterozygote parents consisting of CyO-balanced flies containing *Df(2L)RA5* (Δ, a *BicC*-encompassing deletion), and either the $BicC^{YC33}$ or $BicC^{IIF34}$ alleles similarly balanced with CyO. The $BicC^{\Delta/YC33}$ fly exhibits milder cystic defects than the $BicC^{\Delta/IIF34}$ fly [3]. Straight-winged mutants ($BicC^{\Delta/YC33}$, $BicC^{\Delta/IIF34}$) from crosses were selected within two days of eclosion to yield pools of 0–2 days old flies and aged for seven days (7–9 days old), during which time the flies were kept well-fed by transferring to fresh vials twice (Figure 2). Aged sibling flies were divided into fresh vials containing food spiked with either vehicle (water, 50 µL)

or one of the Smac analogs **1**–**4** at 20 µM (50 µL). Flies were transferred into identical fresh vials every three days. After 20 days of treatment, the Malpighian tubules were micro-dissected from 27–29 day old flies and analyzed ex vivo. Per each condition, cystic deformities were scored using 25–50 female $BicC^{\Delta/IIF34}$ and $BicC^{\Delta/YC33}$ flies (i.e., 50–100 anterior and 50–100 posterior tubules). For each fly, cysts which were found in the two anterior and two posterior tubules were scored and charted as nested plots using the Prism 8.0 (Graphpad) software (Figures 3–6). Vehicle-treated flies presented several cysts in both the anterior and posterior MTs, especially in the terminal and intermediate regions, and fewer cysts in the proximal region, as reported previously [3]. Similar to PKD patients [1], a variable number of cysts was found in different individuals [3]. In general, Smac-mimics appeared to reduce tubular cysts in both *BicC* allelic combinations (Tables 1 and 2).

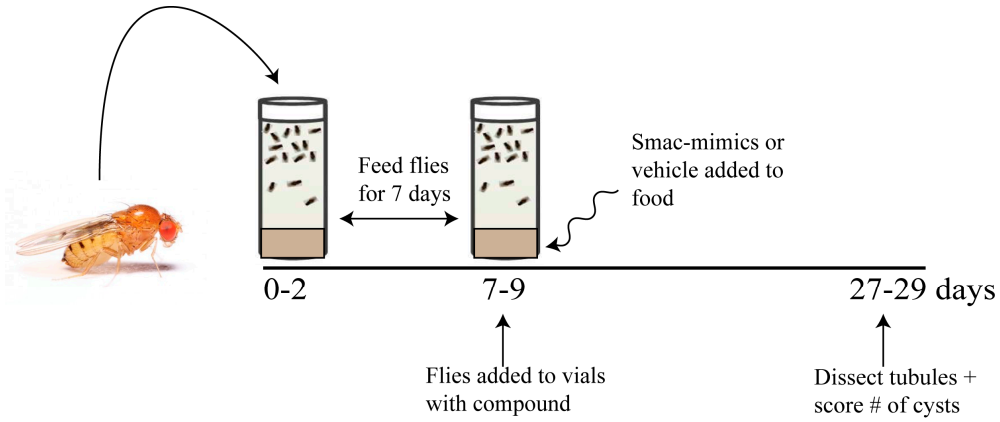

Figure 2. Testing protocol for Smac-mimic efficacy in cyst reduction. Ore^{R} wild-type, $BicC^{\Delta/YC33}$, and $BicC^{\Delta/IIF34}$ flies (0–2 days old) were placed in food-containing vials at age 0–2 days and transferred into fresh vials every three days. Once the age of 7–9 days was reached, flies were placed in vials containing one of each of the Smac-mimics or vehicle control, respectively. Cysts were scored on the micro-dissected MTs after 20 days, when flies reached age 27–29 days.

Table 1. Overall cyst reduction upon Smac-mimic treatment of $BicC^{\Delta/YC33}$ flies.

	Anterior Tubule				Posterior Tubule			
Mimic	**Cyst # Vehicle**	**Cyst # Treated**	**% Reduction**	***p* Value**	**Cyst # Vehicle**	**Cyst # Treated**	**% Reduction**	***p* Value**
1	228	127	44%	0.0005	276	220	20%	0.0457
2	216	165	24%	0.0324	244	162	34%	0.0017
3	195	153	*21%*	*0.1028*	238	156	34%	0.0014
4	134	93	*31%*	*0.0553*	152	124	*18%*	*0.1877*

P values > 0.05 and corresponding percentages are italicized.

Table 2. Overall cyst reduction upon Smac-mimic treatment of $BicC^{\Delta/IIF34}$ flies.

	Anterior Tubule				Posterior Tubule			
Mimic	**Cyst # Vehicle**	**Cyst # Treated**	**% Reduction**	***p* Value**	**Cyst # Vehicle**	**Cyst # Treated**	**% Reduction**	***p* Value**
1	357	199	44%	<0.0001	433	272	37%	0.0002
2	233	142	39%	0.0011	302	202	33%	0.0020
3	114	102	*11%*	*0.6317*	155	122	*21%*	*0.2285*
4	199	119	40%	0.0005	243	151	38%	0.0002

P values > 0.05 and corresponding percentages are italicized.

Effects of Smac mimic administration were recorded as overall cyst reduction (Table 1, Table 2). Nested plots were used to represent individual variability in cyst number in the analyzed fly populations. Administration of peptide **1** to $BicC^{\Delta/YC33}$ flies (n = 50) reduced cystic deformities respectively by 44% and 20% (228 vs. 127 cysts and 276 vs. 220 cysts, p = 0.0005 and 0.0457) in the anterior and posterior tubules, respectively (Table 1, Figure 3A,B). Administration of mimic **2** to $BicC^{\Delta/YC33}$ flies (n = 50) reduced tubular cysts by 24% and 34% (216 vs. 165 cysts, p = 0.0324 and 244 vs. 162 cysts, p = 0.0017) in the anterior and posterior tubules, respectively (Table 1, Figure 3A,B). Administration of mimic **3** to $BicC^{\Delta/YC33}$ flies (n = 50) reduced cysts in the anterior and posterior tubules respectively by 21% and 34% (195 vs. 153 cysts, p = 0.1028 and 238 vs. 156 cysts, p = 0.0014, Table 1, Figure 3A,B). Finally, administration of mimic **4** to $BicC^{\Delta/YC33}$ flies (n = 50) reduced cysts in the anterior and posterior tubules respectively by 31% and 18% (134 vs. 93 cysts, p = 0.0553 and 152 vs. 124 cysts, p = 0.1877, Table 1, Figure 3A,B).

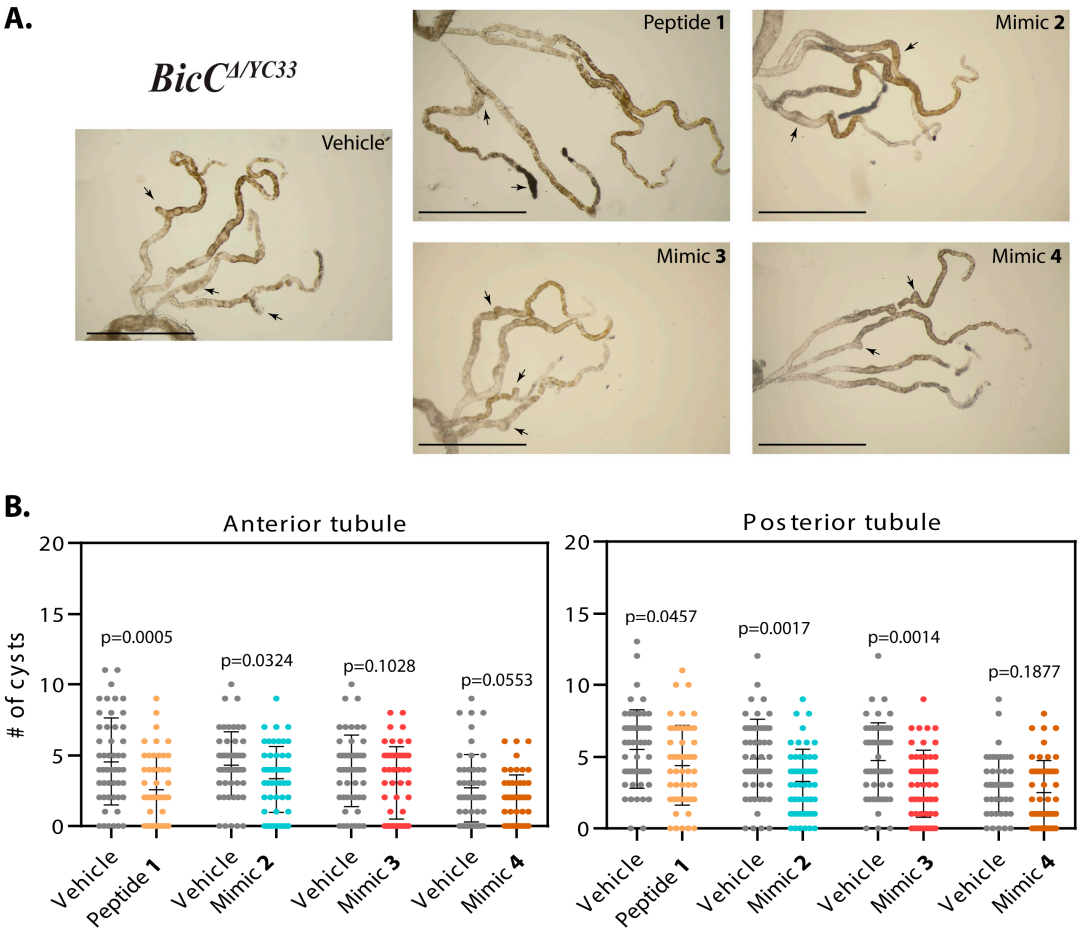

Figure 3. Smac-mimics reduced cysts in $BicC^{\Delta/YC33}$ flies. (**A**). Representative Malpighian tubules micro-dissected from $BicC^{\Delta/YC33}$ flies treated with either vehicle or analogs **1**, **2**, **3**, and **4** (indicated) were photographed *ex vivo*. Arrows indicate cysts. In each image, anterior pairs are at the top, posterior pairs at the bottom. Scale bar: 1 mm. (**B**). Nested plots depicting number of cysts found in the anterior and posterior tubule pairs of vehicle- and Smac mimic-treated cystic flies (indicated), with mean and standard deviation. *P* values (with Welch's correction) are indicated. Treatments are indicated with color: vehicle, grey; mimic **1**, sepia; **2**, blue; **3**, dark pink; **4**, brown.

The analogs were next administered to the $BicC^{\Delta/IIF34}$ flies carrying the allelic combination which produced a more severe phenotype. Treatment with peptide **1** decreased cystic deformations respectively by 44% and 37% (total 357 vs. 199 cysts and 433 vs. 272 cysts, $p < 0.0001$ and 0.0002, respectively) in the anterior and posterior tubules of the micro-dissected $BicC^{\Delta/IIF34}$ flies (n = 50, Table 2,

Figure 4A,B). Administration of mimic **2** to $BicC^{\Delta/IIF34}$ flies (n = 50) reduced cystic deformations by 39% in the anterior (233 vs. 142 cysts, p = 0.0011) and by 33% in the posterior (302 vs. 202 cysts, p = 0.0020) tubules (Table 2, Figure 4A,B). Administration of mimic **3** to $BicC^{\Delta/IIF34}$ flies (n = 25) had a milder and highly variable effect on the renal tubules and reduced cystic deformities by 11% (114 vs. 102 cysts, p = 0.6317) and 21% (155 vs. 122 cysts, p = 0.2285) in the anterior and posterior tubules respectively (Table 2, Figure 4A,B), below statistical relevance thresholds. Finally, administration of mimic **4** to $BicC^{\Delta/IIF34}$ flies (n = 50) reduced cysts in the anterior and posterior tubules by 40% (199 vs. 119 cysts, p = 0.0005) and 38% (243 vs. 151 cysts, p = 0.0002) respectively (Table 2, Figure 4A,B). Parallel respective administration of analogs **1**–**4** to control, non-cystic Ore^{R} wild type flies did not change MT morphology.

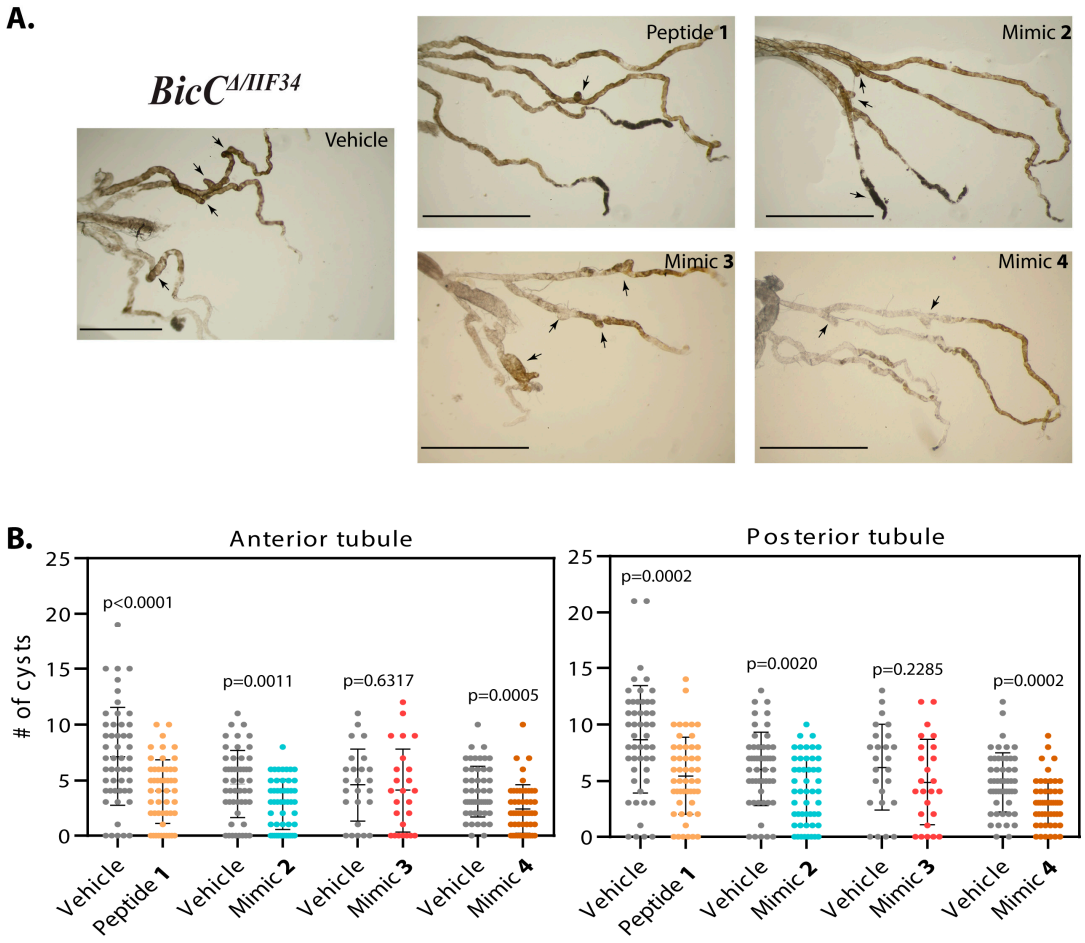

Figure 4. Smac-mimics reduced cysts in $BicC^{\Delta/IIF34}$ flies. (**A**). Representative Malpighian tubules micro-dissected from $BicC^{\Delta/IIF34}$ flies treated with either vehicle or analogs **1**, **2**, **3**, and **4** (indicated) were photographed *ex vivo*. Arrows indicate cysts. In each image, anterior pairs are at the top, posterior pairs at the bottom. Scale bar: 1 mm. (**B**). Nested plots depicting number of cysts found in the anterior and posterior tubule pairs of vehicle- and Smac mimic-treated cystic flies (indicated), with mean and standard deviation. *P* values (with Welch's correction) are indicated. Treatments are indicated with color: vehicle, grey; mimic **1**, sepia; **2**, blue; **3**, dark pink; **4**, brown.

Distinct MT regions in both the anterior and posterior tubules appeared to respond differentially to the Smac mimics. The cyst location was thus specifically mapped in the proximal, intermediate and terminal regions of the anterior and posterior tubules respectively (Tables 3 and 4), and individual variable cyst numbers similarly plotted (Figures 5 and 6). Absolute numbers for the cysts in each region described below are listed in Table S2.

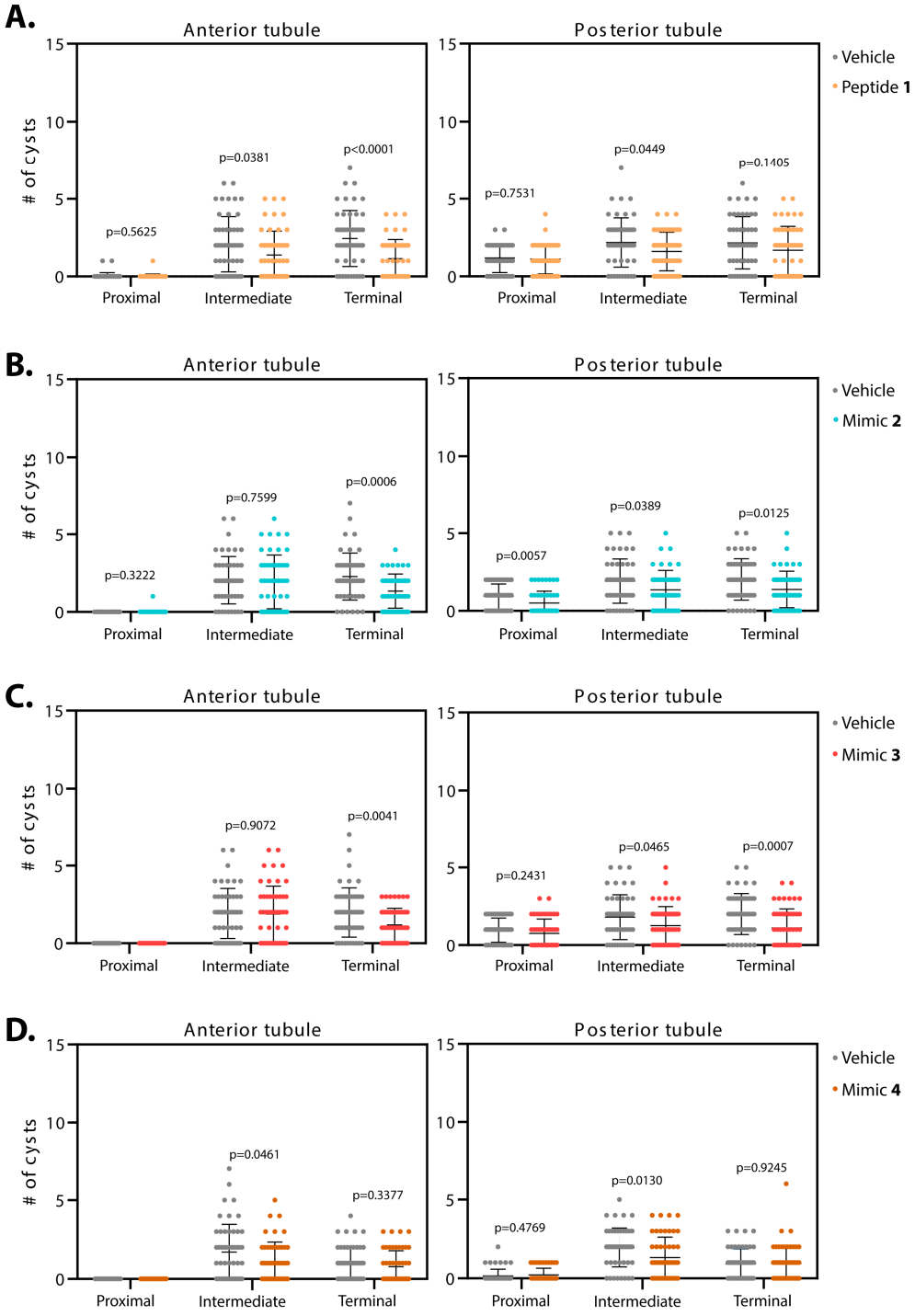

Figure 5. Smac-mimics reduce cysts in *BicC*$^{\Delta YC33}$ flies with varying regional specificity. Malpighian tubules from 50 *BicC*$^{\Delta YC33}$ flies were micro-dissected after 20 days of treatment (age 27–29 days). Cysts were scored *ex vivo*. For each fly, cysts numbers were recorded for the terminal, intermediate and proximal region of the Malpighian tubules, independently for the anterior (left) and posterior (right) tubules. Flies were administered either vehicle (water, grey) or Smac mimics **1** (**A**, sepia), **2** (**B**, blue), **3** (**C**, dark pink), and **4** (**D**, brown). Mean and standard deviation are indicated. Analogs **1** and **2** best reduced tubular cysts, mimic **3** was effective at reducing cysts in the terminal region of the anterior tubules and mimic **4** had a mild effect in the intermediate region of both tubule pairs. *P* values (with Welch's correction) are indicated. *BicC*$^{\Delta YC33}$ flies exhibit the milder cystic defects.

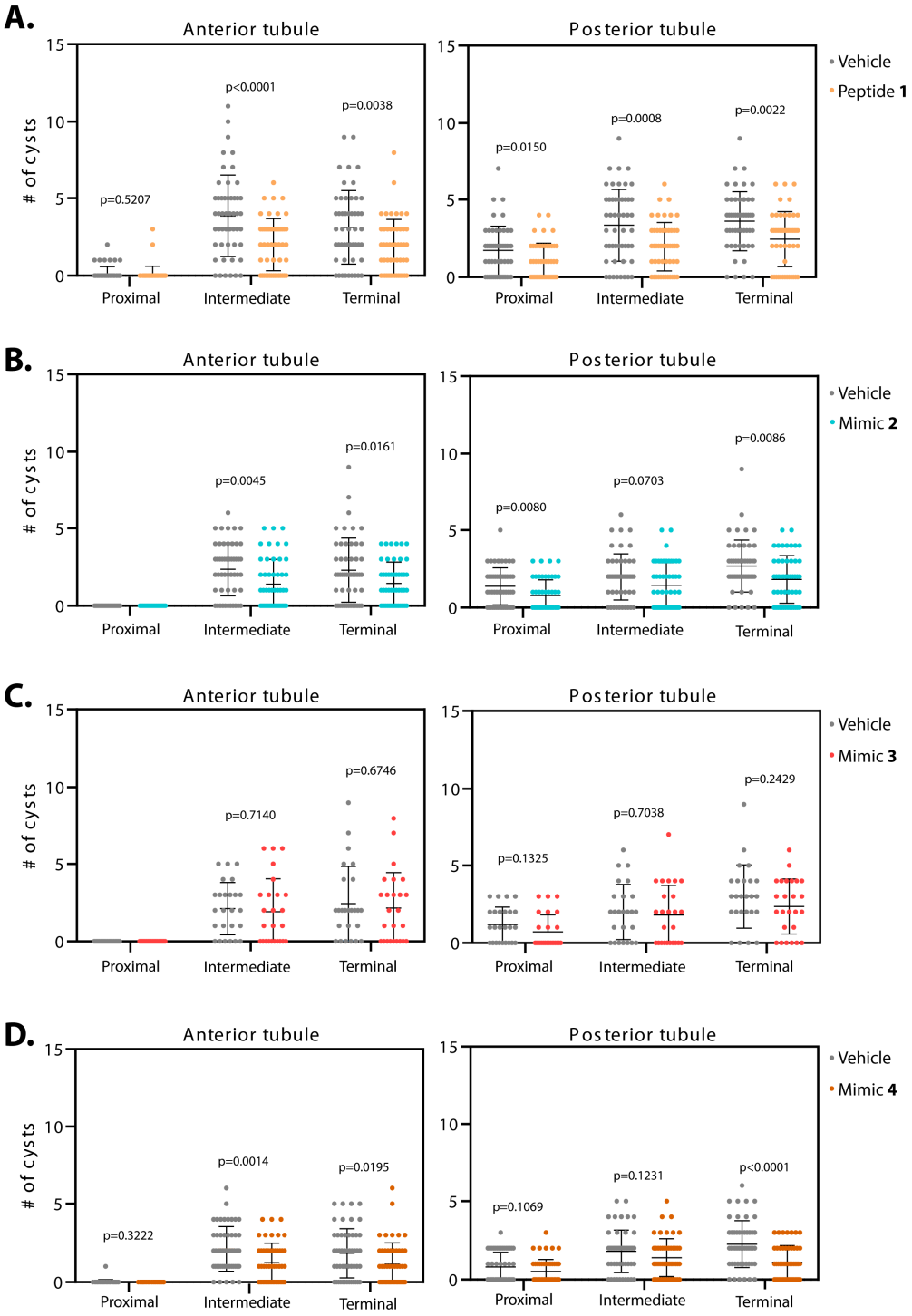

Figure 6. Smac-mimics reduce cysts in $BicC^{\Delta/IIF34}$ flies with varying regional specificity. Malpighian tubules from 25 to 50 $BicC^{\Delta/IIF34}$ flies were micro-dissected after 20 d of treatment (age 27–29 days). Cysts were scored *ex vivo*. For each fly, cysts numbers were recorded for the terminal, intermediate and proximal region of the Malpighian tubules, independently for the anterior (left) and posterior (right) tubules. Flies were administered either vehicle (water, grey) or Smac mimics **1** (**A**, sepia), **2** (**B**, blue), **3** (**C**, dark pink), and **4** (**D**, brown). Mean and standard deviation are indicated. Peptide 1 was the most effective at reducing cysts in the treated tubules. Mimics **2** and **4** showed great improvements in all regions except for the intermediate region of the posterior tubules and mimic **3** showed a very mild to no effect in cyst reduction. *P* values (with Welch's correction) are indicated. $BicC^{\Delta/IIF34}$ flies exhibit the more severe cystic defects.

Table 3. Percentage of cyst reduction upon treatment of *BicC*$^{\Delta/YC33}$ flies.

Smac-Mimic	Anterior Tubule			Posterior Tubule		
	Prox.	**Int.**	**Term.**	**Prox.**	**Int.**	**Term.**
1 (n = 50)	n/s	34% p = 0.0381	53% p < 0.0001	*5%* *p = 0.7531*	26% p = 0.0449	*22%* *p = 0.1405*
2 (n = 50)	n/s	*5%* *p = 0.7599*	41% p = 0.0006	47% p = 0.0057	29% p = 0.0389	32% p = 0.0125
3 (n = 50)	n/a	*2%* *p = 0.9072*	40% p = 0.0041	*21%* *p = 0.2431*	30% p = 0.0465	45% p = 0.0007
4 (n = 50)	n/a	36% p = 0.0461	*20%* *p = 0.3377*	n/s *p = 0.4769*	33% p = 0.0130	n/s *p = 0.9245*

P values > 0.05 and corresponding percentages are italicized; n/s = not significant; n/a = no cysts.

Table 4. Percentage of cyst reduction upon treatment of *BicC*$^{\Delta/IIF34}$ flies.

Smac-Mimic	Anterior Tubule			Posterior Tubule		
	Prox.	**Int.**	**Term.**	**Prox.**	**Int.**	**Term.**
1 (n = 50)	n/s	48% p < 0.0001	40% p = 0.0038	39% p = 0.0150	41% p = 0.0008	32% p = 0.0022
2 (n = 50)	n/a	41% p = 0.0045	37% p = 0.0161	43% p = 0.0080	*27%* *p = 0.0703*	32% p = 0.0086
3 (n = 25)	n/a	*9%* *p = 0.7140*	*11%* *p = 0.6746*	*40%* *p = 0.1325*	*10%* *p = 0.7038*	*21%* *p = 0.2429*
4 (n = 50)	n/s	42% p = 0.0014	38% p = 0.0195	*35%* *p = 0.1069*	*22%* *p = 0.1231*	51% p < 0.0001

P values > 0.05 and corresponding percentages are italicized; n/s = not significant; n/a = no cysts.

3.1.2. Smac Mimics Differentially Affect Distinct Regions of the MTs

Administration of peptide **1** to the milder allelic combination *BicC*$^{\Delta/YC33}$ (n = 50) reduced cysts in the terminal and intermediate regions of the anterior tubules respectively by 53% and 34% (total 122 vs. 57, 104 vs. 69 cysts, p < 0.0001 and p = 0.0381, Table 3, Figure 5A). In the proximal region of the anterior tubules, two cysts were found in the control versus one cyst in the treated samples, precluding statistical analyses. In the posterior tubules, administration of peptide **1** diminished cysts in the intermediate region by 26% (total 109 vs. 80 cysts, p = 0.0449). In the terminal and proximal regions, a trend toward decreased cysts was observed, albeit without reaching a statistical threshold for significance (respectively 108 vs. 84 cysts, 22% reduction, p = 0.1405, and 59 vs. 56 cysts, 5% reduction, p = 0.7531, Table 3, Figure 5A).

Administration of peptide **1** to *BicC*$^{\Delta/IIF34}$flies reduced cysts in the anterior tubules by 40% and 48% (total 156 vs. 94 and 193 vs. 100 cysts, p = 0.0038 and p < 0.0001) in the terminal and intermediate regions, respectively (Table 4, Figure 6A). In the proximal region of the anterior tubules, a trend of cyst reduction was observed, albeit fewer cysts (eight and five in vehicle- and peptide **1**-treated tubules) and high individual variability precluded a margin of confidence. In the posterior tubules, administration of peptide **1** reduced cysts in the terminal, intermediate and proximal regions by 32%, 41% and 39% (total 180 vs. 122, 167 vs. 98, 86 vs. 52 cysts, p = 0.0022, 0.0008 and 0.0150), respectively (Table 4, Figure 6A).

Treatment with mimic **2** diminished cysts in the terminal region of the anterior tubules of *BicC*$^{\Delta/YC33}$ flies (n = 50) by 41% (114 vs. 67 cysts, p = 0.0006). In the intermediate region, a mild 5% reduction was observed that did not approach a statistical significance threshold (102 vs. 97 cysts, p = 0.7599, Table 3, Figure 5B). Precluding statistical analyses, no (control) and one cyst (mimic **2**-treated) were detected in the proximal region of the anterior tubules. In contrast, in the posterior tubule, administration of mimic **2** reduced cysts in the terminal, intermediate and proximal regions by 32%, 29% and 47% (101 vs. 69 cysts, p = 0.0125, 96 vs. 68 cysts, p = 0.0389 and 47 vs. 25 cysts, p = 0.0057), respectively (Table 3, Figure 5B).

Administration of mimic **2** to the more severely cystic $BicC^{\Delta/IIF34}$ flies ($n = 50$) reduced cysts in the terminal and intermediate regions of the anterior tubules by 37% and 41% (average 115 vs. 72 cysts, $p = 0.0161$, 118 vs. 70 cysts, $p = 0.0045$), respectively. No cysts were found in the proximal regions of control and treated tubules (Table 4, Figure 6B). Administration of mimic **2** reduced cysts in the terminal and proximal regions of the posterior tubules by 32% and 43% (134 vs. 91 cysts, $p = 0.0086$ and 69 vs. 39 cysts, $p = 0.0080$), respectively. The intermediate region displayed a 27% reduction that approached statistical significance threshold (99 vs. 72 cysts, $p = 0.0703$, Table 4, Figure 6B).

After treatment with mimic **3**, the $BicC^{\Delta/YC33}$ flies ($n = 50$) harbored 40% fewer cysts in the terminal region of the anterior tubules (99 vs. 59 cysts, $p = 0.0041$). In the intermediate region, the effect was negligible (2% reduction, 96 vs. 94 cysts, $p = 0.9072$). No cysts were detected in the proximal region of both control and treated tubules (Table 3, Figure 5C). On the contrary, administration of mimic **3** reduced strongly cysts in the terminal and intermediate regions of the posterior tubules by 45% and 30% (100 vs. 55 cysts, $p = 0.0007$ and 90 vs. 63 cysts, $p = 0.0465$), respectively. The proximal region displayed a trend towards cyst reduction with high individual variability (21% reduction, 48 vs. 38 cysts, $p = 0.2431$, Table 3, Figure 5C).

Mimic **3** did not ameliorate the more severely cystic $BicC^{\Delta/IIF34}$ flies ($n = 25$). After treatment with mimic **3**, the $BicC^{\Delta/IIF34}$ flies displayed respectively 11% and 9% (61 vs. 54 cysts, $p = 0.6746$ and 53 vs. 48 cysts, $p = 0.7140$) fewer cysts in the terminal and intermediate regions of the anterior tubules; no cysts were observed in the proximal region of both control and treated tubules (Table 4, Figure 6C). Similarly, mimic **3** caused respectively 21%, 10% and 40% (75 vs. 59 cysts, $p = 0.2429$, 50 vs. 45 cysts, $p = 0.7038$ and 30 vs. 18 cysts, $p = 0.1325$) reductions in cysts in the terminal, intermediate and proximal regions of the posterior tubules (Table 4, Figure 6C).

Mimic **4** reduced cysts in the intermediate region of the anterior tubules of $BicC^{\Delta/YC33}$ flies ($n = 50$) by 36% (85 vs. 55 cysts, $p = 0.0461$). In the terminal region, a 20% decrease was observed, that did not reach a threshold of statistical significance (49 vs. 39 cysts, $p = 0.3377$). No cysts were detected in the proximal region of both control and treated tubules (Table 3, Figure 5D). Treatment with mimic **4** reduced cysts in the intermediate region of the posterior tubules by 33% (98 vs. 66 cysts, $p = 0.0130$), but did not reduce cysts in the terminal and proximal regions (Table 3, Figure 5D).

Upon treatment with mimic **4**, cysts were lessened in the terminal and intermediate regions of the anterior tubules of $BicC^{\Delta/IIF34}$ flies ($n = 50$) by 38% and 42% (92 vs. 57 cysts, $p = 0.0195$ and 106 vs. 62 cysts, $p = 0.0014$), respectively (Table 4, Figure 6D). Precluding statistical analysis, only one cyst was detected in the proximal region of control tubules and no cysts in the treated tubules. Administration of mimic **4** reduced cysts in the terminal region of the posterior tubules by 51% (113 vs. 55 cysts, $p < 0.0001$). Less cysts were also scored in the intermediate and proximal regions, although values did not reach the significance threshold (respectively 22% reduction, 90 vs. 70 cysts, $p = 0.1231$, and 35% reduction, 40 vs. 26 cysts, $p = 0.1069$, Table 4, Figure 6D).

Ineffective cyst reduction could be partly due to flies refusing to ingest the Smac mimics. To assess their ingestion, the analogs were mixed with food and dye, and fed to the flies for four days. The green dye could be seen through the semi-transparent abdominal cuticle of the *BicC* flies for all mimics, confirming analog ingestion (Figure S1). As a measure of hydrophilicity, the clogP values were calculated for the different Smac mimics (Figure 1) and found to be sufficiently low to be consistent with absorption: **1** (0.7), **2** (3.9), **3** (5.0), **4** (5.4). Together these results support the conclusion that the Smac analogs may have differential activities and/or processing.

4. Discussion

A systematic analysis of the influences of the Smac mimic H-Ala-Val-Pro-Ile-NH_2 (**1**) and constrained analogs **2**–**4** on renal cystogenesis has been performed using the novel *BicC* fly model to recapitulate features of PKD [3]. Two allelic combinations for *BicC* were used that yield cystic phenotypes of different severity, namely $BicC^{\Delta/YC33}$ and $BicC^{\Delta/IIF34}$. Previously, the Smac mimic GT13072 reduced cystogenesis in a rat ADPKD model [42]. In the *BicC* flies, Smac mimics **1**–**4** ameliorated similarly the

cystic condition with the strongest effects displayed in the more severely affected $BicC^{\Delta/IIF34}$ genotype. Peptide **1** exhibited the highest overall efficacy reducing cyst occurrence by 20–44% across genotypes at the anterior and posterior tubules. Moreover, aza-methanopipecolate **2** caused a 24–39% reduction of cysts. Aza-cyclohexylglycine **3** displayed least efficacy, but still improved significantly the posterior tubules of the $BicC^{\Delta/YC33}$ flies. The related *N*-methyl-alaninyl-aza-cyclohexylglycine analog **4** exhibited differential activity in the two *BicC* mutants, reducing cysts by ~40% in both tubules of the $BicC^{\Delta/IIF34}$ flies. In contrast, analog **4** only showed a trend towards reducing cysts in the anterior tubule of the $BicC^{\Delta/YC33}$ flies close to the significance threshold ($p = 0.0553$). The Smac mimics tested appeared to differentially affect the anterior and posterior tubule pairs overall, consistent with the report of the latter having distinct transcriptomes [10] and thus different physiological specialization. Mimics **1, 2** and **3** were found to induce death of 20% (**1**, **2**) and 60% (**3**) of cultured MCF7 adenocarcinoma cells [49]. Their efficacy in other PKD models and patients is unknown. Smac mimics function in context-dependent ways, likely through different IAPs to affect apoptosis via several mechanisms [12]. Due to its methyl group, *N*-methyl-alaninyl-aza-cyclohexylglycine analog **4** was expected to be more stable than aza-cyclohexylglycine **3** in vivo [61–63], which was consistent with the observed higher cyst-reducing activity.

The tubular sections responded differentially to treatment with the Smac mimics. The terminal region consistently exhibited better improvement, especially in the weaker $BicC^{\Delta/YC33}$ allelic combination. The flies were shown to ingest the Smac mimics. The clogP values of mimics **1–4** were also within the range consistent with effective absorption. The distinct pharmacological responses observed at different regions of the MTs may be related to variability in absorption, metabolism and response to Smac mimics within cystic cells in such regions. Regional specialization of fly MTs has been observed despite the tubular epithelium being composed by only two major cell types (reviewed in [9,64]). Cystogenesis may perturb cells and reduce the threshold for initiating cell death pathways either through caspase-dependent apoptosis or the TNF signaling pathway. The contribution of apoptosis to the early phases of ADPKD is a matter of debate [65]; however, the TNF pathway has been implicated in ADPKD-type renal cystogenesis and suggested to be the primary target of Smac mimics in a rat model of *Pkd1*-dependent ADPKD [42]. The results presented here predict that the *BicC* mutation may feature dysregulated TNF signaling in the epithelial cells of the MTs, as observed in ADPKD-type cystogenesis. The expression of TNF (Eiger) and TNF pathway components in the MT and their respective contributions to tubular function are however unknown. The human *BicC* orthologue *BICC1* has been found to be genetically downstream of the main *PKD1* gene [3]. The pharmacological response to Smac mimics was herein demonstrated to be conserved in the fly illustrating further the phenotypic and molecular similarities between *PKD1*-induced and *BicC*-induced renal cystogenesis.

Notably, pharmacological binding sites have been found to be conserved in *Drosophila* [66]. Chemical probing in the fly in vivo may thus rapidly pinpoint the involvement of specific pathways with complementarity to genetic analyses, indicate conserved biological activity of drug-prototypes, and provide a rapid read-out for effectiveness of pharmacological modulation of specific pathways involved in cystic pathogenesis. The Smac mimics affected different tubular regions differentially. Considering that such specificity may be conserved to humans, the development of personalized pharmacological treatments for cystic renal diseases such as PKD will benefit from precise knowledge of the cyst-ameliorating potential of different Smac mimics.

Supplementary Materials: The following are available online at http://www.mdpi.com/2227-9059/7/4/82/s1. Supplementary file S1: spectral and chromatographic characterization of mimic 4, Table S1: Cystic index analysis raw data, Table S2: Regional cystic index for BicC flies. Figure S1: Analog feeding control.

Author Contributions: Conceptualization, C.M.B., W.D.L., and C.G.; methodology, C.M.B., R.C., W.D.L. and C.G.; validation, C.M.B., R.C., W.D.L. and C.G.; formal analysis, C.M.B., R.C., W.D.L. and C.G.; investigation, C.M.B., and R.C.; resources, W.D.L and C.G.; data curation, C.M.B., R.C. and C.G.; writing—original draft preparation, C.M.B., W.D.L. and C.G.; writing—review and editing, C.M.B., R.C., W.D.L. and C.G.; visualization, C.M.B., R.C. and C.G.; supervision, W.D.L. and C.G.; project administration, W.D.L. and C.G.; funding acquisition, W.D.L. and C.G.

Funding: This research was funded by the Natural Sciences and Engineering Research Council of Canada (NSERC) Discovery Research Project #04079, the Fonds de recherche nature et technologie Quebec for the Centre in Green Chemistry and Catalysis (FRQNT-2020-RS4-265155-CCVC), the Université de Montréal to W.D.L., and a Concordia University CUPFA Professional Development Grant to C.G.

Acknowledgments: We wish to thank C. Charbonneau (Institute for Research in Immunology and Cancer, IRIC, Université de Montréal) and C. Law (Centre for Microscopy and Cellular Imaging, CMCI, Concordia University) for sharing their expertise in microscopy and analyses; J. Oliver, T.B.U. Le and S. He for help with fly work; J. Pelletier (Université de Montréal), M. Therrien (IRIC) and their groups, for welcoming hospitality and shared resources; The Bloomington *Drosophila* Stock Center for fly lines.

Conflicts of Interest: The authors declare no conflict of interest. The funders had no role in the design of the study; in the collection, analyses, or interpretation of data; in the writing of the manuscript, or in the decision to publish the results.

References

1. Bergmann, C.; Guay-Woodford, L.M.; Harris, P.C.; Horie, S.; Peters, D.J.M.; Torres, V.E. Polycystic kidney disease. *Nat. Rev. Dis. Primers.* **2018**, *80*. [CrossRef] [PubMed]
2. Happé, H.; Peters, J.D.M. Translational research in ADPKD: Lessons from animal models. *Nat. Rev. Neph.* **2014**, *10*, 587–601. [CrossRef] [PubMed]
3. Gamberi, C.; Hipfner, D.R.; Trudel, M.; Lubell, W.D. *Bicaudal C* mutation causes *myc* and TOR pathway up-regulation and polycystic kidney disease-like phenotypes in *Drosophila*. *PLoS Gen.* **2017**, *13*, e1006694. [CrossRef] [PubMed]
4. Tao, Y.; Kim, J.; Shrier, R.W.; Edelstein, C.L. Rapamycin markedly slows disease progression in a rat model of polycystic kidney disease. *J. Am. Soc. Nephrol.* **2005**, *16*, 46–51. [CrossRef]
5. Shillingford, J.M.; Murcia, N.S.; Larson, C.H.; Low, S.H.; Hedgepeth, R.; Brown, N.; Flask, C.A.; Novick, A.C.; Goldfarb, D.A.; Kramer-Zucker, A.; et al. The mTOR pathway is regulated by polycystin-1, and its inhibition reverses renal cystogenesis in polycystic kidney disease. *Proc. Natl. Acad. Sci. USA* **2006**, *103*, 5466–5471. [CrossRef]
6. Wahl, P.R.; Serra, A.L.; Le Hir, M.; Molle, K.D.; Hall, M.N.; Wuthrich, R.P. Inhibition of mTOR with sirolimus slows disease progression in Han:SPRD rats with autosomal dominant polycystic kidney disease (ADPKD). *Nephrol. Dial. Transplant* **2006**, *21*, 598–604. [CrossRef]
7. Wu, M.; Wahl, P.R.; Le Hir, M.; Wackerie-Men, Y.; Wuthrich, R.P. Everolimus retards cyst growth and preserves kidney function in a rodent model for polycystic kidney disease. *Kidney Blood Press. Res.* **2007**, *30*, 253–259. [CrossRef]
8. Shillingford, J.M.; Piontek, K.B.; Germino, G.G.; Weimbs, T. Rapamycin ameliorates PKD resulting from conditional inactivation of *Pkd1*. *J. Am. Soc. Nephrol.* **2010**, *21*, 489–497. [CrossRef]
9. Millet-Boureima, C.; Marroquin, J.P.; Gamberi, C. Modeling renal disease "on the fly". *Biomed. Res. Int.* **2018**, *2018*, 13. [CrossRef]
10. Wang, J.; Kean, L.; Yang, J.; Allan, A.K.; Davies, S.A.; Herzyk, P.; Dow, J.A.T. Function-informed transcriptome analysis of *Drosophila* renal tubule. *Genome Biology* **2004**, *5*, R69. [CrossRef]
11. Lalaoui, N.; Vaux, D.L. Recent advances in understanding inhibitor of apoptosis proteins. *F1000Res.* **2018**, *7*, 30631429. [CrossRef] [PubMed]
12. Cong, H.; Xu, L.; Wu, Y.; Qu, Z.; Bian, T.; Zhang, W.; Xing, C.; Zhuang, C. Inhibitor of apoptosis protein (IAP) antagonists in anticancer agent discovery: Current status and perspectives. *J. Med. Chem.* **2019**, *62*, 5750–5772. [CrossRef] [PubMed]
13. Damgaard, R.B.; Nachbur, U.; Yabal, M.; Wong, W.W.; Fiil, B.K.; Kastirr, M.; Rieser, E.; Rickard, J.A.; Bankovacki, A.; Peschel, C.; et al. The ubiquitin ligase XIAP recruits LUBAC for NOD2 signaling in inflammation and innate immunity. *Mol. Cell* **2012**, *46*, 746–758. [CrossRef] [PubMed]
14. Damgaard, R.B.; Fiil, B.K.; Speckmann, C.; Yabal, M.; zur Stadt, U.; Bekker-Jensen, S.; Jost, P.J.; Ehl, S.; Mailand, N.; Gyrd-Hansen, M. Disease-causing mutations in the XIAPBIR2 domain impair NOD2-dependent immune signalling. *EMBO Mol. Med.* **2013**, *5*, 1278–1295. [CrossRef]
15. Fulda, S.; Vucic, D. Targeting IAP proteins for therapeutic intervention in cancer. *Nat. Rev. Drg. Disc.* **2012**, *11*, 109–124. [CrossRef]

16. Duckett, C.S.; Nava, V.E.; Gedrich, R.W.; Clem, R.J.; Van Dongen, J.L.; Gilfillan, M.C.; Shiels, H.; Hardwick, J.; Thompson, C.B. A conserved family of cellular genes related to the baculovirus *iap* gene and encoding apoptosis inhibitors. *EMBO J.* **1996**, *15*, 2685–2694. [CrossRef]
17. Hay, B.A.; Wassarman, D.A.; Rubin, G.M. *Drosophila* homologs of baculovirus inhibitor of apoptosis proteins function to block cell death. *Cell* **1995**, *83*, 1253–1262. [CrossRef]
18. Jones, G.; Jones, D.; Zhou, L.; Steller, H.; Chu, Y. Deterin, a new inhibitor of apoptosis from *Drosophila melanogaster*. *J. Biol. Chem.* **2000**, *275*, 22157–22165. [CrossRef]
19. Vernooy, S.Y.; Chow, V.; Su, J.; Verbrugghe, K.; Yang, J.; Cole, S.; Olson, M.R.; Hay, B.A. *Drosophila* Bruce can potently suppress Rpr- and Grim-dependent but not Hid-dependent cell death. *Curr. Biol.* **2002**, *12*, 1164–1168. [CrossRef]
20. White, K.; Grether, M.E.; Abrams, J.M.; Young, L.; Farrell, K.; Steller, H. Genetic control of programmed cell death in *Drosophila*. *Science* **1994**, *264*, 677–683. [CrossRef]
21. Grether, M.E.; Abrams, J.M.; Agapite, J.; White, K.; Steller, H. The head involution defective gene of *Drosophila melanogaster* functions in programmed cell death. *Genes Dev.* **1995**, *9*, 1694–1708.
22. Chen, P.; Nordstrom, W.; Gish, B.; Abrams, J.M. grim, a novel cell death gene in *Drosophila*. *Genes Dev.* **1996**, *10*, 1773–1782.
23. Verhagen, A.M.; Vaux, D.L. Cell death regulation by the mammalian IAP antagonist Diablo/Smac. *Apoptosis* **2002**, *7*, 163–166. [CrossRef] [PubMed]
24. Tenev, T.; Zachariou, A.; Wilson, R.; Paul, A.; Meier, P. Jafrac2 is an IAP antagonist that promotes cell death by liberating Dronc from DIAP1. *EMBO J.* **2002**, *21*, 5118–5129. [CrossRef] [PubMed]
25. Christich, A.; Kauppila, S.; Chen, P.; Sogame, N.; Ho, S.; Abrams, J.M. The damage-responsive *Drosophila* gene *sickle* encodes a novel IAP binding protein similar to but distinct from *reaper*, *grim*, and *hid*. *Curr. Biol.* **2002**, *12*, 137–140. [CrossRef]
26. Srinivasula, S.M.; Datta, P.; Kobayashi, M.; Wu, J.; Fujioka, M.; Hegde, R.; Zhang, Z.; Mukattash, R.; Fernandes-Alnemri, T.; Shi, Y.; et al. *sickle*, a novel *Drosophila* death gene in the *reaper/hid/grim* region, encodes an IAP-inhibitory protein. *Curr. Biol.* **2002**, *12*, 125–130. [CrossRef]
27. Wing, J.P.; Karres, J.S.; Ogdahl, J.L.; Zhou, L.; Schwartz, L.M.; Nambu, J.R. *Drosophila sickle* is a novel *grim-reaper* cell death activator. *Curr. Biol.* **2002**, *12*, 131–135. [CrossRef]
28. Challa, M.; Malladi, S.; Pellock, B.J.; Dresnek, D.; Varadarajan, S.; Yin, Y.W.; White, K.; Bratton, S.B. *Drosophila* Omi, a mitonchondrial-localized IAP antagonist and proapoptotic serine protease. *EMBO J.* **2007**, *26*, 3144–3156. [CrossRef]
29. Igaki, T.; Suzuki, Y.; Tokushige, N.; Aonuma, H.; Takahashi, R.; Miura, M. Evolution of mitochondrial cell death pathway: Proapoptotic role of HtrA2/Omi in *Drosophila*. *Biochem. Biophys. Res. Commun.* **2007**, *356*, 993–997. [CrossRef]
30. Khan, F.S.; Fujioka, M.; Datta, P.; Fernandes-Alnemri, T.; Jaynes, J.B.; Alnemri, E.S. The interaction of DIAP1 with dOmi/HtrA2 regulates cell death in *Drosophila*. *Cell Death Diff.* **2008**, *15*, 1073–1083. [CrossRef]
31. Du, C.; Fang, M.; Li, Y.; Li, L.; Wang, X. Smac, a mitochondrial protein that promotes cytochrome c-dependent caspase activation by eliminating IAP inhibition. *Cell* **2000**, *102*, 33–42. [CrossRef]
32. Verhagen, A.M.; Ekert, P.G.; Pakusch, M.; Silke, J.; Connolly, L.M.; Reid, G.E.; Moritz, R.L.; Simpson, R.J.; Vaux, D.L. Identification of DIABLO, a mammalian protein that promotes apoptosis by binding to and antagonizing IAP proteins. *Cell* **2000**, *102*, 43–53. [CrossRef]
33. van Loo, G.; van Gurp, M.; Depuydt, B.; Srinivasula, S.M.; Rodriguez, I.; Alnemri, E.S.; Gevaert, K.; Vandekerckhove, J.; Declercq, W.; Vandenabeele, P. The serine protease Omi/HtrA2 is released from mitochondria during apoptosis. Omi interacts with caspase-inhibitor XIAP and induces enhanced caspase activity. *Cell Death Diff.* **2002**, *9*, 20–26. [CrossRef] [PubMed]
34. Gottfried, Y.; Rotem, A.; Lotan, R.; Steller, H.; Larisch, S. The mitochondrial ARTS protein promotes apoptosis through targeting XIAP. *EMBO J.* **2004**, *23*, 1627–1635. [CrossRef] [PubMed]
35. Liston, P.; Fong, W.G.; Kelly, N.L.; Toji, S.; Miyazaki, T.; Conte, D.; Tamai, K.; Craig, C.G.; McBurney, M.W.; Korneluk, R.G. Identification of XAF1 as an antagonist of XIAP anti-caspase activity. *Nat. Cell. Biol.* **2001**, *3*, 128–133. [CrossRef] [PubMed]
36. Wing, J.P.; Schwartz, L.M.; Nambu, J.R. The RHG motifs of *Drosophila* Reaper and Grim are important for their distinct cell death-inducing abilities. *Mechan. Dev.* **2001**, *102*, 193–203. [CrossRef]

37. Saita, S.; Nolte, H.; Fiedler, K.U.; Kashkar, H.; Venne, A.S.; Zahedi, R.P.; Kruger, M.; Langer, T. PARL mediates Smac proteolytic maturation in mitochondria to promote apoptosis. *Nat. Cell Biol.* **2017**, *19*, 318–328. [CrossRef]
38. Xu, D.; Woodfield, S.E.; Lee, T.V.; Fan, Y.; Antonio, C.; Bergmann, A. Genetic control of programmed cell death (apoptosis) in *Drosophila*. *Fly* **2009**, *3*, 78–90. [CrossRef]
39. Brenner, D.; Blaser, H.; Mak, T.W. Regulation of tumour necrosis factor signaling: Live or let die. *Nat. Rev. Immunol.* **2015**, *15*, 362–374. [CrossRef]
40. Harris, P.C.; Watson, M.L. Autosomal dominant polycystic kidney disease: Neoplasia in disguise? *Nephrol. Dial. Transplant* **1997**, *12*, 1089–1090. [CrossRef]
41. Grantham, J.J. Polycystic kidney disease: Neoplasia in disguise. *Am. J. Kidney Dis.* **1990**, *15*, 110–116. [CrossRef]
42. Fan, L.X.; Zhou, X.; Sweeney, W.E.; Wallace, D.P.; Avner, E.D.; Grantham, J.J.; Li, X. Smac-mimetic-induced epithelial cell death reduces the growth of renal cysts. *J. Am. Soc. Nephrol.* **2013**, *24*, 2010–2022. [CrossRef] [PubMed]
43. Igaki, T.; Kanda, H.; Yamamoto-Goto, Y.; Kanuka, H.; Kuranaga, E.; Aigaki, T.; Miura, M. Eiger, a TNF superfamily ligand that triggers the *Drosophila* JNK pathway. *EMBO J.* **2002**, *21*, 3009–3018. [CrossRef] [PubMed]
44. Kanda, H.; Igaki, T.; Kanuka, H.; Yagi, T.; Miura, M. Wengen, a member of the *Drosophila* Tumor Necrosis Factor receptor superfamily, is required for Eiger signaling. *J. Biol. Chem.* **2002**, *277*, 28372–28375. [CrossRef]
45. Moreno, E.; Yan, M.; Basler, K. Evolution of TNF signaling mechanisms: JNK-dependent apoptosis triggered by Eiger, the *Drosophila* homolog of the TNF superfamily. *Curr. Biol.* **2002**, *12*, 1263–1268. [CrossRef]
46. Kauppila, S.; Maaty, W.S.A.; Chen, P.; Tomar, R.S.; Eby, M.T.; Chapo, J.; Chew, S.; Rathore, N.; Zachariah, S.; Sinha, S.K.; et al. Eiger and its receptor, Wengen, comprise a TNF-like system in *Drosophila*. *Oncogene* **2003**, *22*, 4860–4867. [CrossRef]
47. Igaki, T.; Miura, M. The *Drosophila* TNF ortholog Eiger: Emerging physiological roles and evolution of the TNF system. *Semin. Immunol.* **2014**, *26*, 267–274. [CrossRef]
48. Andersen, D.S.; Colombani, J.; Palmerini, V.; Chakrabandhu, K.; Boone, E.; Rothlisberger, M.; Toggweiler, J.; Basler, K.; Mapelli, M.; Hueber, A.; et al. The *Drosophila* TNF receptor Grindelwald couples loss of cell polarity and neoplastic growth. *Nature* **2015**, *522*, 482–486. [CrossRef]
49. Chingle, R.; Ratni, S.; Claing, A.; Lubell, W.D. Application of constrained aza-valine analogs for Smac mimicry. *J. Pept. Sci.* **2016**, *106*, 235–244. [CrossRef]
50. Wu, G.; Chai, J.; Suber, T.L.; Wu, J.; Du, C.; Wang, X.; Shi, Y. Structural basis of IAP recognition by Smac/DIABLO. *Nature* **2000**, *408*, 1008–1012. [CrossRef]
51. Liu, Z.; Sun, C.; Olejniczak, E.T.; Meadows, R.P.; Betz, S.F.; Oost, T.; Herrmann, J.; Wu, J.C.; Fesik, S.W. Structural basis for binding of Smac/DIABLO to the XIAP BIR3 domain. *Nature* **2000**, *408*, 1004–1008. [CrossRef] [PubMed]
52. Fadeel, B.; Orrenius, S. Apoptosis: A basic biological phenomenon with wide-ranging implications in human disease. *J. Int. Med.* **2005**, *258*, 479–517. [CrossRef] [PubMed]
53. Sun, H.; Nikolovska-Coleska, Z.; Yang, C.-Y.; Qian, D.; Lu, J.; Qiu, S.; Bai, L.; Peng, Y.; Cai, Q.; Wang, S. Design of small-molecule peptidic and nonpeptidic Smac mimetics. *Acc. Chem. Res.* **2008**, *41*, 1264–1277. [CrossRef] [PubMed]
54. Boeglin, D.; Hamdan, F.F.; Melendez, R.E.; Cluzeau, J.; Laperriere, A.; Heroux, M.; Bouvier, M.; Lubell, W.D. Calcitonin gene-related peptide analogues with aza and indolizidinone amino acid residues reveal conformational requirements for antagonist activity at the human calcitonin gene-related peptide 1 receptor. *J. Med. Chem.* **2007**, *50*, 1401–1408. [CrossRef]
55. Bourguet, C.B.; Goupil, E.; Tassy, D.; Hou, X.; Thouin, E.; Polyak, F.; Hebert, T.E.; Claing, A.; Laporte, S.A.; Chemtob, S.; et al. Targeting the prostaglandin F2α receptor for preventing preterm labor with azapeptide tocolytics. *J. Med. Chem.* **2011**, *54*, 6085–6097. [CrossRef]
56. Mir, F.M.; Atmuri, N.D.P.; Bourguet, C.B.; Fores, J.R.; Hou, X.; Chemtob, S.; Lubell, W.D. Paired utility of aza-amino acyl proline and indolizidinone amino acid residues for peptide mimicry: Conception of prostaglandin F2a receptor allosteric modulators that delay preterm birth. *J. Med. Chem.* **2019**, *62*, 4500–4525. [CrossRef]

57. Bourguet, C.B.; Boulay, P.; Claing, A.; Lubell, W.D. Design and synthesis of novel azapeptide activators of apoptosis mediated by caspase-9 in cancer cells. *Bioorg. Med. Chem. Lett.* **2014**, *24*, 3361–3365. [CrossRef]
58. Chingle, R.; Mulumba, M.; Chung, N.N.; Nguyen, T.M.-D.; Ong, H.; Ballet, S.; Schiller, P.W.; Lubell, W.D. Solid-phase azopeptide Diels-Alder chemistry for aza-pipecolyl residue synthesis to study peptide conformation. *J. Ord. Chem.* **2019**, *84*, 6006–6016. [CrossRef]
59. Chingle, R.; Lubell, W.D. Azopeptides: Synthesis and pericyclic chemistry. *Org. Lett.* **2015**, *17*, 5400–5403. [CrossRef]
60. Oost, T.; Sun, C.; Armstrong, R.C.; Al-Assaad, A.-S.; Betz, S.F.; Deckwerth, T.L.; Ding, H.; Elmore, S.W.; Meadows, R.P.; Olejniczak, E.T.; et al. Discovery of potent antagonists of the antiapoptotic protein XIAP for the treatment of cancer. *J. Med. Chem.* **2004**, *47*, 4417–4426. [CrossRef]
61. Chatterjee, J.; Gilon, C.; Hoffman, A.; Kessler, H. *N*-Methylation of peptides: A new perspective in medicinal chemistry. *Acc. Chem. Res.* **2008**, *41*, 1331–1342. [CrossRef] [PubMed]
62. Chatterjee, J.; Rechenmacher, F.; Kessler, H. *N*-methylation of peptides and proteins: An important element for modulating biological functions. *Angewandte Chemie.* **2013**, *52*, 254–269. [CrossRef] [PubMed]
63. Merlino, F.; Billard, E.; Yousif, A.M.; Di Maro, S.; Brancaccio, D.; Abate, L.; Carotenuto, A.; Bellavita, R.; d'Emmanuele di Villa Bianca, R.; Santicioli, P.; et al. Functional selectivity revealed by *N*-methylation scanning of human urotensin II and related peptides. *J. Med. Chem.* **2019**, *62*, 1455–1467. [CrossRef] [PubMed]
64. Sozen, M.A.; Armstrong, J.D.; Yang, M.; Kaiser, K.; Dow, J.A.T. Functional domains are specified to single-cell resolution in a *Drosophila* epithelium. *Proc. Natl. Acad. Sci. USA* **1997**, *94*, 5207–5212. [CrossRef] [PubMed]
65. Goilav, B. Apoptosis in polycystic kidney disease. *BBA-Mol. Basis Dis.* **2011**, *1812*, 1272–1280. [CrossRef]
66. Ziehm, M.; Kaur, S.; Ivanov, D.K.; Ballester, P.J.; Marcus, D.; Partridge, L.; Thornton, J.M. Drug repurposing for aging research using model organisms. *Aging Cell* **2017**, *16*, 1006–1015. [CrossRef]

EXPERIMENTAL SECTION

General Methods

Chemicals were used as received from commercial sources without further purification unless stated otherwise. All glassware was stored in the oven or flame-dried and let cool under an inert atmosphere prior to use. Anhydrous solvents (DCM, and DMF) were obtained by passage through solvent filtration systems (Glass-Contour, Irvine, CA). Visualization of the developed chromatogram was performed by UV absorbance or staining with ceric ammonium molybdate or potassium permanganate solutions. Silica gel chromatography was performed using 230–400 mesh silica gel (Silicycle), and TLC was on glass-backed silica plates. Nuclear magnetic resonance spectra (^{1}H, ^{13}C) were recorded on Bruker AV 500 spectrometer. ^{1}H NMR spectra were referenced to CD_3OD (3.31 ppm) and ^{13}C NMR spectra were measured in CD_3OD (49.00 ppm) as specified below. Coupling constant, J values were measured in Hertz (Hz) and chemical shift values in parts per million (ppm). Infrared spectra were recorded in the neat on a Perkin Elmer Spectrum One FTIR instrument and are reported in reciprocal centimetres (cm^{-1}). Accurate mass measurements were performed on a liquid chromatography−mass spectrometry (LC−MS) instrument from Agilent Technologies 1200 series in positive electrospray ionization (ESI)-time-of-flight (TOF) mode at the Université de Montréal Mass Spectrometry facility. Sodium and proton adducts ($[M + Na]^+$ and $[M + H]^+$) were used for empirical formula confirmation.

Reagents Used. Aza-Cyclohexaneglycinyl-L-Proline Benzhydrylamide was synthesized according to the literature method (*Biopolymers*, **2016**, *106*, 235-44). *N*-Boc-*N*-methyl-L-alanine and diisopropyl ethyl amine (DIEA) were purchased from Aldrich or Alfa Aesar and used without further purification. Benzotriazol-1-yl-oxytripyrrolidinophosphoniumhexafluorophosphate (PyBop) was purchased from GL Biochem^{TM}, recrystallized prior to use from dry CH_2Cl_2/Et_2O (melting point, 156 °C) and stored in the dark.

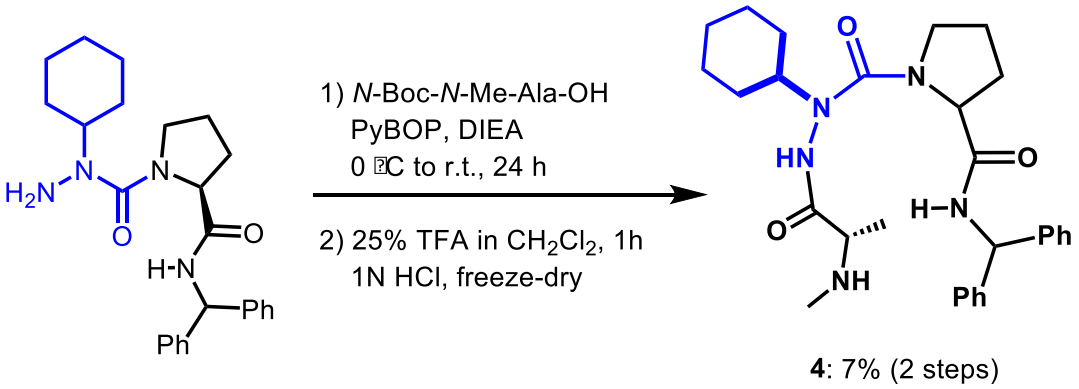

4: 7% (2 steps)

N-methyl Alaninyl-aza-Cyclohexaneglycinyl-L-Proline Benzhydrylamide (**4**). A solution of Aza-Cyclohexaneglycinyl-L-Proline Benzhydrylamide (1 eq., 65 mg, 0.155 mmol) and DIEA (2 eq., 40 mg, 53 μL, 0.309 mmol) was added to a solution of *N*-(tert-butoxycarbonyl)-*N*-methyl-L-alanine (1.2 eq., 38 mg, 0.186 mmol) and PyBOP (1.5 eq., 121 mg, 0.233 mmol) in DMF (3 mL), and stirred overnight. The volatiles were removed under vacuum. The residue was dissolved in EtOAc (10 mL), washed with 5 mL of saturated aqueous $NaHCO_3$, followed by brine (10 mL), dried over Na_2SO_4, filtered, and evaporated. Without further purification, the residue was dissolved in a 25% solution of TFA in dichloromethane (2 mL), and stirred for 2 h. The volatiles were removed under vacuum. The residue was dissolved in CH_2Cl_2 and the solution was evaporated. The residue was suspended in 2 mL of 1N HCl, stirred for 30 min, and freeze-dried to give the hydrochloride salt as off white solid. The crude sample was purified by RP-HPLC on a reverse-phase Gemini® C_{18} column (Phenomenex® Inc., pore size: 110 Å, particle size: 5 μm, 250 x 21.2 mm) using a binary solvent system consisting of a gradient of 5%-60% MeOH (0.1% FA) in water (0.1% FA), with a flow rate of 10.0 mL/min, and UV detection at 214 nm. The desired fractions were combined and freeze-dried to white fluffy powder: azapeptide **2** (5.2 mg, 0.01 mmol, 7%, 2-steps): mp 93-94 °C; ^{1}H NMR (500 MHz, MeOD) δ 8.40 (s, 1H), 7.45 – 7.20 (m, 10H), 6.24 (s, 1H), 4.56 – 4.42 (m, 1H), 4.05 – 3.88 (m, 1H), 3.69 – 3.42 (m, 2H), 2.59 – 2.43 (m, 3H), 2.43 – 2.31 (m, 1H), 2.26 – 2.14 (m, 1H), 2.14 – 2.00 (m, 1H), 2.00 – 1.91 (m, 1H), 1.91 – 1.62 (m, 6H), 1.53 – 1.36 (m, 5H), 1.35 – 1.03 (m, 5H); ^{13}C NMR (125 MHz, MeOD) δ 174.1, 171.2, 161.4, 143.2, 139.1, 129.5 (2C), 129.4 (2C), 129.3 (2C), 128.8 (2C), 128.4, 128.2, 63.6, 57.9, 57.4, 49.6, 31.5, 31.3, 30.8, 26.9, 26.72 (2C), 26.69 (2C), 26.5, 17.5; IR (neat) ν_{max}/cm^{-1} 2929, 1638, 1532, 1495, 1449, 1406, 1344, 1323, 1095; HRMS m/z calculated for $C_{29}H_{40}N_5O_3$ $[M+H]^+$ 506.3126; found 506.3139.

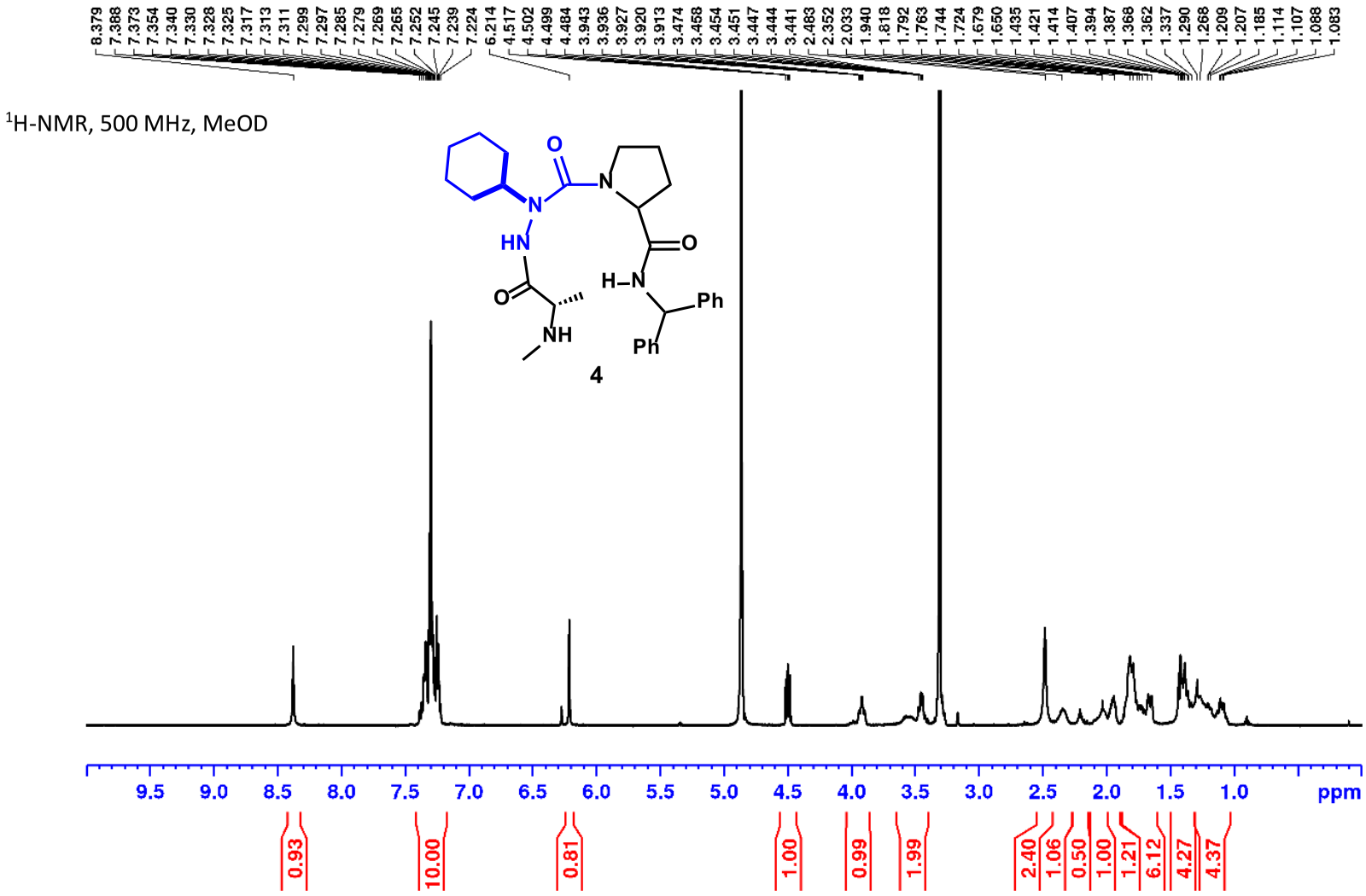
8.379 7.388 7.373 7.354 7.340 7.330 7.328 7.325 7.317 7.313 7.311 7.299 7.297 7.285 7.279 7.269 7.265 7.252 7.245 7.239 7.224 6.214 4.517 4.502 4.499 4.484 3.943 3.936 3.927 3.920 3.913 3.474 3.458 3.454 3.451 3.447 3.444 3.441 2.483 2.352 2.033 1.940 1.818 1.792 1.763 1.744 1.724 1.679 1.650 1.435 1.421 1.414 1.407 1.394 1.387 1.368 1.362 1.337 1.290 1.268 1.209 1.207 1.185 1.114 1.107 1.088 1.083
1H-NMR, 500 MHz, MeOD
O
N
N
HN
O
O
H–N
Ph
Ph
NH
4
9.5 9.0 8.5 8.0 7.5 7.0 6.5 6.0 5.5 5.0 4.5 4.0 3.5 3.0 2.5 2.0 1.5 1.0 ppm
0.93 10.00 0.81 1.00 0.99 1.99 2.40 1.06 0.50 1.00 1.21 6.12 4.27 4.37

^{13}C-NMR, 125 MHz, MeOD

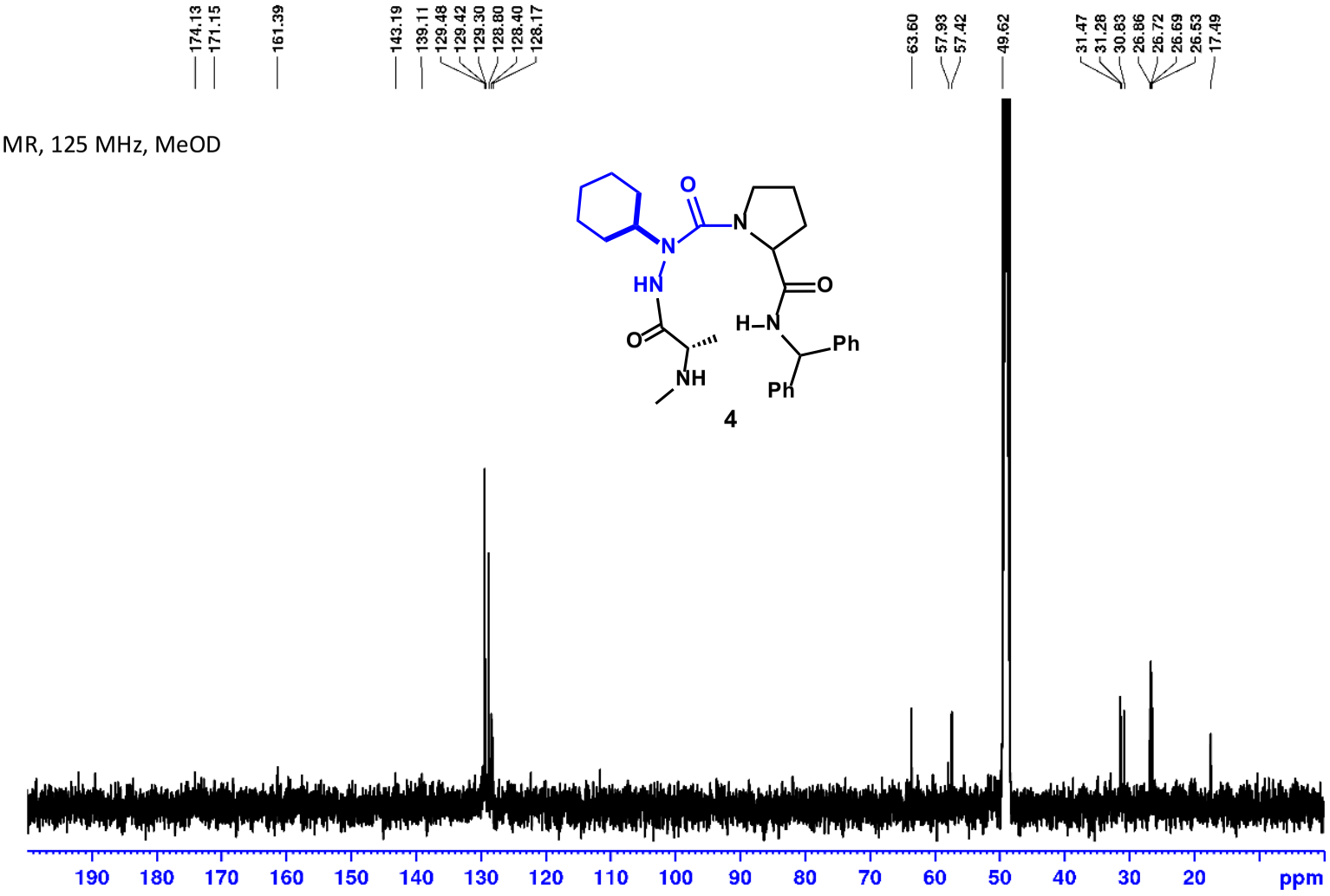

4

Rapport de masse exacte

Data File	WDL-Rc-N-me-chingle 05.d	**Sample Name**	WDL-Rc-N-me-chingle 05
Sample Type	Sample	**Position**	P1-B2
Analysis Date	4/9/2018 9:34:03 AM	**User Name**	KG
Acq Method	ESI_POS_DI.m	**InstrumentName**	TOF 6224
Comment			

MS Spectrum

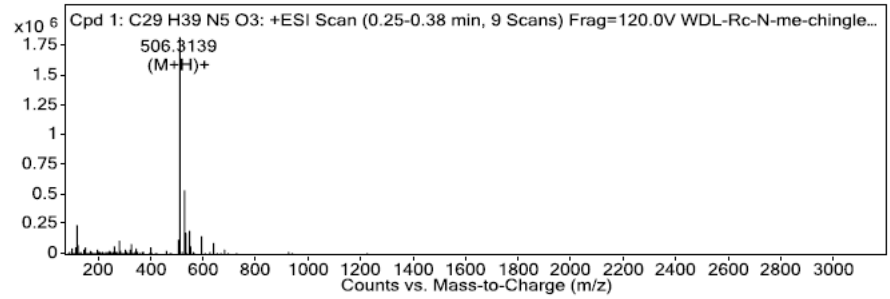

MS Zoomed Spectrum

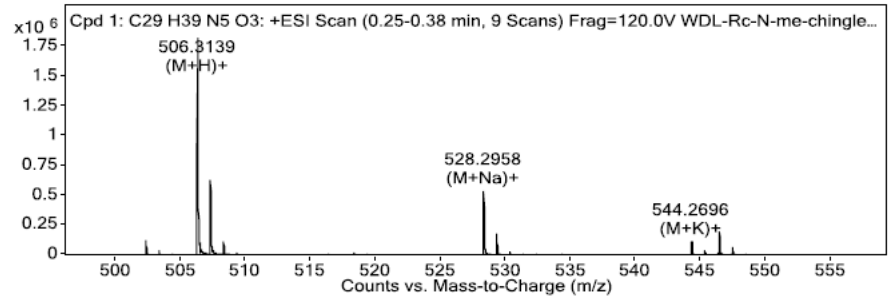

MS Spectrum Peak List

Ion	Formula	Abund	*Expe. m/z*	*Calc. m/z*	Diff(ppm)
(M+H)+	C29H39N5O3	1839043.44	506.3139	506.3126	-2.57
(M+Na)+	C29H39N5O3	545573	528.2958	528.2945	-2.39

Table S2. Scored cyst numbers for each region of the Malpighian tubules as indicated.

Regional cystic index for *BicC$^{\Delta/YC33}$* flies

	Anterior			Posterior		
	Proximal	**Intermediate**	**Terminal**	**Proximal**	**Intermediate**	**Terminal**
Vehicle **1**	2	104	122	59	109	108
Peptide **1**	1	69	57	56	80	84
Vehicle **2**	0	102	114	47	96	101
Mimic **2**	1	97	67	25	68	69
Vehicle **3**	0	96	99	48	90	100
Mimic **3**	0	94	59	38	63	55
Vehicle **4**	0	85	49	8	98	46
Mimic **4**	0	54	39	11	66	47

Regional cystic index for *BicC$^{\Delta/IIF34}$* flies

	Anterior			Posterior		
	Proximal	**Intermediate**	**Terminal**	**Proximal**	**Intermediate**	**Terminal**
Vehicle **1**	8	193	156	86	167	180
Peptide **1**	5	100	94	52	98	122
Vehicle **2**	0	118	115	69	99	134
Mimic **2**	0	70	72	39	72	91
Vehicle **3**	0	53	61	30	50	75
Mimic **3**	0	48	54	18	45	59
Vehicle **4**	1	106	92	40	90	113
Mimic **4**	0	62	57	26	70	55

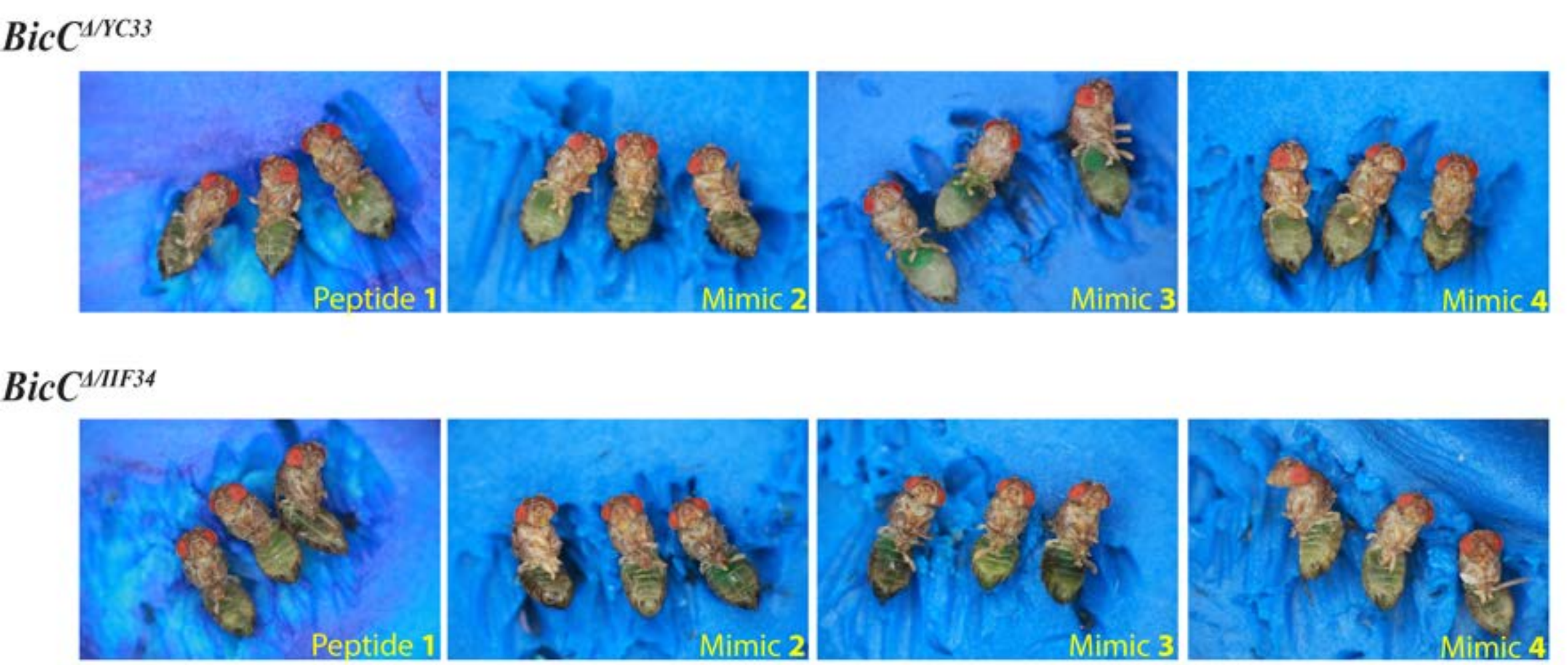

Figure S1. Analog feeding control. *BicC* flies fed Smac mimics mixed with green dye for four days, displayed ingested food contents visible through their semi-transparent abdominal cuticle. Legs were clipped for better visualization.

***BicC* [*delta/YC*] 27-29d** (20 days after treatment)

CONTROL	Anterior Terminal	Anterior Intermediate	Anterior Proximal	Posterior Terminal	Posterior Intermediate	Posterior Proximal	
1	2	0	0	2	2	1	
2	3	5	0	1	3	3	
3	3	4	1	2	2	0	
4	4	5	0	4	4	1	
5	0	0	0	0	0	0	
6	4	1	0	0	3	0	
7	2	2	0	2	2	0	
8	4	5	0	2	3	1	
9	3	2	0	1	3	0	
10	0	2	1	1	3	0	
11	2	0	0	1	4	0	
12	2	2	0	3	3	2	
13	0	0	0	0	0	2	
14	3	4	0	2	3	2	
15	5	6	0	5	7	1	
16	6	3	0	1	3	2	
17	5	6	0	4	3	0	
18	5	1	0	0	5	2	
19	4	3	0	4	2	2	
20	2	5	0	4	0	0	
21	0	3	0	3	2	0	
22	2	2	0	4	2	1	
23	1	1	0	0	0	2	
24	2	3	0	6	4	0	
25	5	1	0	5	2	1	
26	0	0	0	3	3	2	
27	3	0	0	0	2	2	
28	3	3	0	0	0	3	
29	4	3	0	0	0	2	
30	3	5	0	3	5	1	
31	2	2	0	5	5	2	
32	0	0	0	0	0	0	
33	2	1	0	1	1	2	
34	2	2	0	4	1	2	
35	6	4	0	4	2	2	
36	3	2	0	5	2	1	
37	7	2	0	2	2	2	
38	3	2	0	2	2	2	
39	3	2	0	3	1	0	
40	2	1	0	2	2	0	
41	3	0	0	1	4	2	
42	2	0	0	0	0	2	
43	2	0	0	2	0	0	
44	1	3	0	2	3	2	
45	0	2	0	3	2	1	
46	0	0	0	2	3	1	
47	0	0	0	3	0	0	
48	1	3	0	1	1	2	
49	1	0	0	0	1	2	
50	0	1	0	3	2	1	
Total # of cysts	122	104	2	108	109	59	504

Compound 1	Anterior Terminal	Anterior Intermediate	Anterior Proximal	Posterior Terminal	Posterior Intermediate	Posterior Proximal	
1	2	0	0	0	3	2	
2	0	2	0	0	1	1	
3	0	0	0	2	2	2	
4	1	1	0	2	2	0	
5	0	0	0	0	1	0	
6	0	0	0	0	2	0	
7	0	0	0	0	0	0	
8	2	3	0	2	1	2	
9	0	0	0	3	0	1	
10	0	2	0	3	2	2	
11	1	3	0	3	2	2	
12	0	5	0	3	4	4	
13	2	2	0	2	4	1	
14	2	3	0	2	0	1	
15	4	5	0	1	3	1	
16	2	4	0	2	2	2	
17	0	0	0	0	0	0	
18	0	2	0	4	2	2	
19	0	0	0	2	0	0	
20	0	1	0	4	2	2	
21	0	0	0	2	1	2	
22	0	0	0	0	0	2	
23	0	0	0	0	0	0	
24	3	2	0	2	1	2	
25	0	0	0	0	3	0	
26	4	2	0	4	4	2	
27	2	2	0	0	0	1	
28	0	0	0	2	2	0	
29	0	0	0	1	3	1	
30	2	0	0	2	1	1	
31	4	4	0	4	3	0	
32	2	2	0	2	3	1	
33	3	2	0	0	0	0	
34	3	1	0	3	3	1	
35	0	0	0	0	0	2	
36	0	0	0	3	1	1	
37	2	2	0	1	1	0	
38	1	0	0	0	0	2	
39	0	0	0	0	3	0	
40	2	2	1	5	3	2	
41	1	1	0	1	2	0	
42	0	0	0	0	0	0	
43	2	5	0	4	2	1	
44	2	4	0	5	2	0	
45	1	1	0	3	1	1	
46	2	1	0	2	1	1	
47	2	0	0	0	0	2	
48	0	3	0	0	2	3	
49	1	1	0	0	2	1	
50	2	1	0	3	3	2	
Total # of cysts	57	69	1	84	80	56	347

CONTROL	Anterior Terminal	Anterior Intermediate	Anterior Proximal	Posterior Terminal	Posterior Intermediate	Posterior Proximal
1	2	2	0	5	5	2
2	0	0	0	0	0	0
3	2	1	0	1	1	2
4	2	2	0	4	1	2
5	6	4	0	4	2	2
6	3	2	0	5	2	1
7	7	2	0	2	2	2
8	3	2	0	2	2	2
9	3	2	0	3	1	0
10	2	1	0	2	2	0
11	3	0	0	1	4	2
12	4	3	0	2	0	1
13	2	0	0	0	2	0
14	2	3	0	1	2	1
15	0	0	0	0	0	1
16	1	1	0	1	0	1
17	0	5	0	3	5	1
18	1	3	0	3	2	2
19	3	6	0	1	1	0
20	0	0	0	0	0	0
21	3	4	0	3	4	0
22	1	3	0	2	3	1
23	1	2	0	1	0	1
24	2	4	0	2	3	2
25	1	6	0	4	5	0
26	1	4	0	3	2	1
27	3	1	0	2	1	1
28	3	2	0	3	3	0
29	2	4	0	2	3	1
30	0	0	0	3	4	1
31	3	2	0	1	2	1
32	5	2	0	4	2	1
33	4	3	0	1	1	1
34	3	1	0	1	0	1
35	3	2	0	2	2	0
36	2	0	0	3	4	0
37	1	1	0	2	2	0
38	4	2	0	3	1	1
39	2	2	0	1	1	2
40	3	3	0	3	2	2
41	2	3	0	4	4	2
42	2	2	0	2	1	2
43	5	2	0	2	3	2
44	2	0	0	2	1	0
45	2	1	0	2	2	1
46	1	1	0	0	0	0

Compound 2	Anterior Terminal	Anterior Intermediate	Anterior Proximal	Posterior Terminal	Posterior Intermediate	Posterior Proximal
1	1	2	1	2	2	2
2	0	0	0	2	4	2
3	0	0	0	0	3	1
4	1	2	0	1	1	2
5	2	2	0	0	2	2
6	0	2	0	0	0	1
7	0	0	0	1	0	1
8	0	0	0	5	1	2
9	0	0	0	0	0	0
10	0	0	0	0	0	0
11	0	3	0	2	2	1
12	2	2	0	3	3	0
13	1	0	0	3	0	0
14	0	0	0	0	0	0
15	1	0	0	1	0	0
16	3	3	0	2	2	0
17	2	5	0	2	1	0
18	2	4	0	2	0	1
19	0	0	0	0	0	0
20	1	3	0	1	0	0
21	2	1	0	2	0	0
22	2	2	0	0	1	0
23	3	3	0	2	2	0
24	1	0	0	2	2	0
25	2	0	0	0	1	0
26	2	3	0	1	2	0
27	3	1	0	0	1	0
28	4	5	0	1	0	0
29	0	3	0	1	3	0
30	0	3	0	2	3	0
31	1	2	0	4	2	0
32	0	0	0	0	0	0
33	2	1	0	1	1	0
34	2	5	0	2	5	0
35	2	4	0	2	2	0
36	3	2	0	0	1	1
37	1	4	0	1	1	1
38	0	6	0	3	2	0
39	1	4	0	0	2	0
40	3	1	0	1	1	0
41	2	2	0	2	2	1
42	2	0	0	1	2	0
43	2	3	0	1	1	0
44	2	5	0	2	2	2
45	2	0	0	1	0	0
46	3	3	0	2	2	1

47	3	1	0	1	1	1	
48	2	3	0	2	3	0	
49	0	0	0	0	0	0	
50	2	2	0	0	2	0	
Total # of cysts	114	102	0	101	96	47	460

47	1	1	0	3	0	2	
48	0	0	0	0	0	0	
49	2	2	0	3	4	2	
50	1	3	0	2	2	0	
Total # of cysts	67	97	1	69	68	25	327

CONTROL	Anterior Terminal	Anterior Intermediate	Anterior Proximal	Posterior Terminal	Posterior Intermediate	Posterior Proximal	
1	2	2	0	5	5	2	
2	0	0	0	0	0	0	
3	2	1	0	1	1	2	
4	2	2	0	4	1	2	
5	6	4	0	4	2	2	
6	3	2	0	5	2	1	
7	7	2	0	2	2	2	
8	3	2	0	2	2	2	
9	3	2	0	3	1	0	
10	2	1	0	2	2	0	
11	3	0	0	1	4	2	
12	2	0	0	0	0	2	
13	2	0	0	2	0	0	
14	1	3	0	2	3	2	
15	0	2	0	3	2	1	
16	0	0	0	2	3	1	
17	0	0	0	3	0	0	
18	1	3	0	1	1	2	
19	1	0	0	0	1	2	
20	0	1	0	3	2	1	
21	4	3	0	2	0	1	
22	2	0	0	0	2	0	
23	2	3	0	1	2	1	
24	0	0	0	0	0	1	
25	1	1	0	1	0	1	
26	0	5	0	3	5	1	
27	1	3	0	3	2	2	
28	3	6	0	1	1	0	
29	0	0	0	0	0	0	
30	3	4	0	3	4	0	
31	1	3	0	2	3	1	
32	1	2	0	1	0	1	
33	2	4	0	2	3	2	
34	1	6	0	4	5	0	
35	1	4	0	3	2	1	
36	3	1	0	2	1	1	
37	3	2	0	3	3	0	
38	2	4	0	2	3	1	
39	0	0	0	3	4	1	
40	3	2	0	1	2	1	
41	5	2	0	4	2	1	
42	4	3	0	1	1	1	
43	3	1	0	1	0	1	
44	3	2	0	2	2	0	
45	2	0	0	3	4	0	
46	1	1	0	2	2	0	
47	4	2	0	3	1	1	
48	2	2	0	1	1	2	
49	2	3	0	1	1	0	
50	0	0	0	0	0	0	
Total # of cysts	99	96	0	100	90	48	433

Compound 3	Anterior Terminal	Anterior Intermediate	Anterior Proximal	Posterior Terminal	Posterior Intermediate	Posterior Proximal	
1	1	3	0	0	2	2	
2	0	0	0	0	0	2	
3	0	0	0	0	0	2	
4	0	0	0	0	2	1	
5	1	2	0	0	1	0	
6	2	3	0	0	1	2	
7	0	0	0	0	0	0	
8	1	4	0	1	2	0	
9	0	0	0	0	0	0	
10	1	1	0	3	1	0	
11	0	0	0	1	1	2	
12	1	4	0	1	2	2	
13	0	0	0	0	0	2	
14	2	6	0	1	2	1	
15	2	6	0	3	2	2	
16	0	0	0	0	0	2	
17	3	2	0	3	2	1	
18	2	3	0	1	2	1	
19	2	3	0	0	0	2	
20	2	5	0	2	2	1	
21	3	3	0	2	5	0	
22	2	4	0	3	3	3	
23	0	0	0	0	0	0	
24	1	1	0	0	1	0	
25	2	2	0	2	2	1	
26	1	2	0	0	1	1	
27	3	2	0	2	2	0	
28	1	3	0	2	2	0	
29	1	0	0	0	0	0	
30	3	3	0	2	4	0	
31	0	0	0	0	0	0	
32	1	5	0	0	3	0	
33	0	0	0	0	0	0	
34	0	0	0	0	0	0	
35	2	1	0	2	1	1	
36	3	2	0	0	3	1	
37	0	0	0	2	0	0	
38	2	3	0	4	1	0	
39	3	2	0	3	2	0	
40	1	2	0	1	1	1	
41	2	2	0	2	3	0	
42	0	0	0	1	0	0	
43	0	5	0	4	1	1	
44	0	1	0	1	0	0	
45	3	4	0	1	0	0	
46	2	2	0	3	3	1	
47	2	0	0	2	2	3	
48	0	0	0	0	0	0	
49	0	0	0	0	0	0	
50	1	3	0	0	1	0	
Total # of cysts	59	94	0	55	63	38	309

CONTROL	Anterior Terminal	Anterior Intermediate	Anterior Proximal	Posterior Terminal	Posterior Intermediate	Posterior Proximal	
1	0	2	0	0	1	0	
2	0	0	0	0	0	0	
3	0	2	0	2	1	0	
4	1	3	0	0	0	0	
5	0	0	0	3	2	0	
6	0	1	0	0	3	0	
7	0	0	0	0	3	0	
8	1	7	0	2	2	0	
9	0	0	0	0	0	0	
10	2	2	0	2	3	0	
11	0	0	0	1	0	0	
12	0	3	0	0	4	1	
13	4	5	0	3	2	0	
14	0	2	0	0	0	0	
15	1	4	0	2	4	2	
16	0	2	0	1	2	0	
17	1	0	0	1	1	0	
18	2	0	0	0	2	0	
19	2	6	0	0	4	0	
20	0	0	0	0	2	0	
21	2	0	0	1	0	0	
22	0	3	0	1	2	0	
23	2	2	0	1	2	0	
24	2	0	0	1	2	0	
25	0	2	0	1	2	0	
26	0	0	0	0	1	0	
27	0	2	0	2	2	0	
28	1	0	0	0	1	0	
29	1	2	0	2	3	0	
30	3	4	0	3	5	1	
31	3	1	0	2	3	0	
32	2	3	0	2	3	0	
33	1	2	0	1	1	1	
34	2	1	0	3	3	0	
35	2	0	0	1	2	0	
36	3	3	0	1	2	0	
37	3	5	0	0	3	0	
38	1	4	0	1	1	1	
39	0	0	0	1	2	0	
40	1	0	0	0	2	0	
41	1	2	0	0	3	0	

Compound 4	Anterior Terminal	Anterior Intermediate	Anterior Proximal	Posterior Terminal	Posterior Intermediate	Posterior Proximal	
1	0	3	0	0	1	0	
2	0	0	0	0	0	0	
3	0	0	0	0	0	0	
4	0	0	0	0	0	1	
5	2	1	0	2	2	0	
6	1	1	0	1	1	0	
7	0	0	0	0	0	0	
8	0	2	0	0	1	0	
9	1	2	0	1	1	0	
10	0	0	0	0	0	0	
11	0	0	0	0	1	0	
12	0	3	0	2	3	0	
13	1	0	0	1	0	0	
14	0	0	0	1	3	1	
15	2	0	0	0	0	0	
16	2	2	0	0	2	1	
17	1	1	0	2	2	0	
18	0	0	0	1	0	0	
19	0	0	0	2	1	1	
20	0	2	0	1	3	0	
21	2	2	0	1	3	0	
22	0	5	0	2	4	1	
23	0	2	0	2	3	1	
24	2	0	0	0	1	0	
25	2	4	0	1	2	0	
26	1	1	0	2	3	0	
27	0	0	0	0	0	0	
28	1	2	0	1	1	0	
29	0	1	0	0	1	0	
30	0	2	0	2	1	1	
31	1	1	0	1	3	0	
32	0	0	0	0	0	0	
33	3	3	0	3	4	0	
34	3	1	0	3	4	0	
35	0	0	0	0	0	1	
36	2	1	0	1	1	1	
37	0	0	0	0	0	0	
38	2	2	0	1	4	0	
39	0	1	0	0	1	0	
40	0	0	0	0	0	0	
41	0	0	0	0	0	0	

42	0	0	0	0	0	0	
43	1	3	0	1	3	0	
44	1	1	0	1	2	1	
45	1	1	0	1	2	0	
46	0	0	0	0	2	0	
47	1	1	0	1	2	0	
48	0	0	0	0	0	1	
49	1	3	0	1	4	0	
50	0	1	0	0	2	0	
Total # of cysts	49	85	0	46	98	8	286

42	0	1	0	1	2	1	
43	0	0	0	0	0	0	
44	0	2	0	1	1	0	
45	0	0	0	0	0	0	
46	1	1	0	0	1	0	
47	3	0	0	1	0	0	
48	3	1	0	6	2	0	
49	2	4	0	2	2	0	
50	1	0	0	2	1	1	
Total # of cysts	39	54	0	47	66	11	217

BicC [*delta/IIF*] 27-29d (20 days after treatment)

CONTROL	Anterior Terminal	Anterior Intermediate	Anterior Proximal	Posterior Terminal	Posterior Intermediate	Posterior Proximal	
1	0	5	0	3	4	0	
2	3	10	2	4	5	1	
3	3	8	1	4	6	4	
4	4	6	0	4	4	5	
5	5	8	0	4	7	1	
6	5	6	0	4	5	2	
7	9	5	1	7	9	5	
8	7	7	1	7	7	7	
9	4	3	0	5	3	3	
10	5	9	0	3	6	1	
11	0	4	0	4	4	3	
12	3	5	0	5	2	0	
13	3	4	0	4	4	2	
14	2	7	1	6	5	3	
15	7	11	1	5	5	2	
16	4	6	1	6	6	3	
17	5	4	0	5	4	2	
18	6	4	0	4	7	2	
19	4	5	0	5	5	2	
20	4	4	0	3	5	4	
21	3	5	0	6	6	0	
22	0	1	0	2	2	1	
23	0	0	0	2	2	3	
24	0	0	0	0	0	0	
25	1	5	0	0	0	0	
26	1	3	0	2	1	0	
27	5	4	0	4	1	0	
28	4	5	0	4	4	1	
29	2	2	0	4	2	2	
30	2	1	0	5	2	0	
31	2	3	0	4	2	2	
32	9	2	0	9	0	3	
33	6	0	0	3	5	2	
34	4	3	0	3	3	2	
35	0	0	0	0	0	0	
36	0	0	0	0	0	0	
37	2	3	0	3	2	1	
38	2	4	0	3	4	1	
39	5	1	0	6	1	2	
40	7	3	0	5	3	2	
41	2	3	0	4	6	3	
42	2	1	0	2	2	0	
43	2	5	0	3	5	3	
44	2	2	0	3	3	0	
45	0	0	0	2	0	1	
46	1	2	0	2	0	1	
47	4	5	0	1	5	2	
48	1	3	0	2	1	0	
49	0	4	0	1	0	0	
50	4	2	0	3	2	2	
Total # of cysts	156	193	8	180	167	86	790

Compound 1	Anterior Terminal	Anterior Intermediate	Anterior Proximal	Posterior Terminal	Posterior Intermediate	Posterior Proximal	
1	0	3	0	2	2	3	
2	2	5	3	3	6	1	
3	1	4	0	5	5	4	
4	3	5	0	4	3	1	
5	0	0	2	3	0	0	
6	0	0	0	0	0	2	
7	2	3	0	4	2	1	
8	2	5	0	6	3	4	
9	0	0	0	0	0	1	
10	1	2	0	4	5	1	
11	1	3	0	3	2	2	
12	0	0	0	0	0	0	
13	2	3	0	2	4	2	
14	4	6	0	5	3	1	
15	2	2	0	3	4	3	
16	2	3	0	3	4	2	
17	0	0	0	0	2	0	
18	1	0	0	3	1	1	
19	4	3	0	3	3	1	
20	3	3	0	6	2	2	
21	0	0	0	1	1	2	
22	3	3	0	0	0	0	
23	0	2	0	3	2	0	
24	3	3	0	4	2	2	
25	0	0	0	0	0	2	
26	0	0	0	0	0	0	
27	0	0	0	0	0	0	
28	2	3	0	0	3	0	
29	4	2	0	0	2	3	
30	0	2	0	2	2	0	
31	0	0	0	0	0	0	
32	3	3	0	2	4	0	
33	2	3	0	4	3	0	
34	1	1	0	3	3	0	
35	1	2	0	3	3	0	
36	6	2	0	4	0	2	
37	3	0	0	3	3	2	
38	1	1	0	3	1	0	
39	8	1	0	2	1	1	
40	0	0	0	0	0	0	
41	1	3	0	3	2	0	
42	4	0	0	6	4	0	
43	3	4	0	3	1	0	
44	1	1	0	0	0	2	
45	2	4	0	3	1	0	
46	2	0	0	2	2	1	
47	4	1	0	3	1	2	
48	4	4	0	4	3	1	
49	3	3	0	3	1	0	
50	3	2	0	2	2	0	
Total # of cysts	94	100	5	122	98	52	471

CONTROL	Anterior Terminal	Anterior Intermediate	Anterior Proximal	Posterior Terminal	Posterior Intermediate	Posterior Proximal
1	0	1	0	2	2	1
2	0	0	0	2	2	3
3	0	0	0	0	0	0
4	1	5	0	0	0	0
5	1	3	0	2	1	0
6	5	4	0	4	1	0
7	4	5	0	4	4	1
8	2	2	0	4	2	2
9	2	1	0	5	2	0
10	2	3	0	4	2	2
11	9	2	0	9	0	3
12	6	0	0	3	5	2
13	4	3	0	3	3	2
14	0	0	0	0	0	0
15	0	0	0	0	0	0
16	2	3	0	3	2	1
17	2	4	0	3	4	1
18	5	1	0	6	1	2
19	7	3	0	5	3	2
20	2	3	0	4	6	3
21	2	1	0	2	2	0
22	2	5	0	3	5	3
23	2	2	0	3	3	0
24	0	0	0	2	0	1
25	1	2	0	2	0	1
26	4	5	0	1	5	2
27	1	3	0	2	1	0
28	0	4	0	1	0	0
29	4	2	0	3	2	2
30	0	1	0	2	2	1
31	0	0	0	2	2	3
32	0	0	0	0	0	0
33	4	2	0	2	2	3
34	2	6	0	3	4	5
35	3	4	0	4	2	1
36	2	2	0	2	1	0
37	3	0	0	2	1	2
38	0	3	0	2	3	2
39	5	5	0	2	2	2
40	0	3	0	2	2	2
41	3	2	0	1	3	3
42	2	4	0	3	2	2
43	3	3	0	3	2	0
44	2	0	0	2	0	1
45	1	2	0	2	1	2
46	3	4	0	3	3	1

Compound 2	Anterior Terminal	Anterior Intermediate	Anterior Proximal	Posterior Terminal	Posterior Intermediate	Posterior Proximal
1	0	0	0	0	0	0
2	2	4	0	3	0	0
3	0	0	0	0	0	0
4	1	2	0	3	0	0
5	0	0	0	0	0	2
6	0	0	0	4	2	2
7	0	0	0	0	2	0
8	0	3	0	3	1	0
9	0	4	0	0	3	2
10	0	0	0	0	0	0
11	0	0	0	0	0	0
12	3	1	0	1	3	0
13	4	4	0	5	3	2
14	2	1	0	1	0	0
15	2	3	0	3	3	2
16	2	0	0	0	1	0
17	1	0	0	0	0	0
18	1	3	0	1	0	1
19	4	2	0	4	2	0
20	1	0	0	2	2	1
21	4	1	0	4	0	0
22	2	3	0	2	1	1
23	0	0	0	0	0	1
24	1	0	0	1	1	0
25	4	2	0	4	1	1
26	3	1	0	3	3	1
27	0	0	0	0	0	0
28	2	1	0	2	3	1
29	0	1	0	2	0	0
30	3	1	0	2	1	3
31	1	0	0	2	0	2
32	2	1	0	2	2	3
33	0	5	0	2	3	3
34	2	0	0	2	0	0
35	0	0	0	1	0	0
36	2	2	0	2	5	1
37	4	2	0	1	5	1
38	1	1	0	2	3	2
39	0	0	0	0	0	0
40	2	4	0	5	4	0
41	1	5	0	3	3	2
42	3	0	0	2	3	2
43	1	3	0	4	2	3
44	2	2	0	4	1	0
45	1	5	0	3	3	0
46	4	1	0	4	2	0

47	4	4	0	5	2	1	
48	5	3	0	5	3	3	
49	0	0	0	3	2	0	
50	3	3	0	2	2	1	
Total # of cysts	115	118	0	134	99	69	535

47	1	2	0	0	2	0	
48	3	0	0	1	0	0	
49	0	0	0	0	0	0	
50	0	0	0	1	2	0	
Total # of cysts	72	70	0	91	72	39	344

CONTROL	Anterior Terminal	Anterior Intermediate	Anterior Proximal	Posterior Terminal	Posterior Intermediate	Posterior Proximal	
1	0	1	0	2	2	1	
2	0	0	0	2	2	3	
3	0	0	0	0	0	0	
4	1	5	0	0	0	0	
5	1	3	0	2	1	0	
6	5	4	0	4	1	0	
7	4	5	0	4	4	1	
8	2	2	0	4	2	2	
9	2	1	0	5	2	0	
10	2	3	0	4	2	2	
11	9	2	0	9	0	3	
12	6	0	0	3	5	2	
13	4	3	0	3	3	2	
14	0	0	0	0	0	0	
15	0	0	0	0	0	0	
16	2	3	0	3	2	1	
17	2	4	0	3	4	1	
18	5	1	0	6	1	2	
19	7	3	0	5	3	2	
20	2	3	0	4	6	3	
21	2	1	0	2	2	0	
22	2	5	0	3	5	3	
23	2	2	0	3	3	0	
24	0	0	0	2	0	1	
25	1	2	0	2	0	1	
Total # of cysts	61	53	0	75	50	30	269

Compound 3	Anterior Terminal	Anterior Intermediate	Anterior Proximal	Posterior Terminal	Posterior Intermediate	Posterior Proximal	
1	7	2	0	3	2	0	
2	4	1	0	4	0	0	
3	0	0	0	0	0	0	
4	2	2	0	2	2	0	
5	8	4	0	4	4	1	
6	4	3	0	4	3	0	
7	3	0	0	2	3	2	
8	0	0	0	0	0	0	
9	3	3	0	4	2	3	
10	3	6	0	4	4	0	
11	5	6	0	3	4	1	
12	0	0	0	0	0	2	
13	0	0	0	0	0	0	
14	3	6	0	3	7	2	
15	1	3	0	2	0	3	
16	0	0	0	2	0	0	
17	1	1	0	1	0	0	
18	2	0	0	6	4	0	
19	0	0	0	0	0	0	
20	4	0	0	4	2	0	
21	0	3	0	1	1	1	
22	1	5	0	5	4	3	
23	0	1	0	2	2	0	
24	0	0	0	0	0	0	
25	3	2	0	3	1	0	
Total # of cysts	54	48	0	59	45	18	224

CONTROL	Anterior Terminal	Anterior Intermediate	Anterior Proximal	Posterior Terminal	Posterior Intermediate	Posterior Proximal	
1	0	2	0	2	0	0	
2	1	4	0	3	4	0	
3	3	3	0	3	2	0	
4	3	3	0	3	5	0	
5	0	1	0	2	0	0	
6	5	1	0	5	0	0	
7	3	3	1	4	1	0	
8	0	0	0	0	0	0	
9	2	1	0	2	2	0	
10	2	6	0	4	2	0	
11	1	1	0	3	0	0	
12	2	1	0	0	3	1	
13	5	3	0	3	2	0	
14	4	3	0	6	3	2	
15	5	2	0	4	4	0	
16	0	4	0	0	0	2	
17	1	1	0	2	2	0	
18	4	1	0	4	4	0	
19	0	0	0	0	0	0	
20	3	4	0	5	5	2	
21	2	1	0	2	1	2	
22	1	4	0	5	2	2	
23	2	2	0	3	2	2	
24	1	0	0	2	1	2	
25	2	1	0	5	2	0	
26	1	2	0	3	2	0	
27	4	2	0	3	2	2	
28	0	1	0	2	1	1	
29	2	1	0	0	0	1	
30	1	2	0	2	2	2	
31	2	0	0	1	2	0	
32	0	2	0	2	2	0	
33	3	0	0	1	4	2	
34	2	1	0	0	1	0	
35	3	4	0	1	1	0	
36	0	1	0	1	1	2	
37	1	2	0	3	1	0	
38	0	3	0	1	2	1	
39	0	1	0	1	0	0	
40	1	4	0	2	2	0	
41	2	2	0	2	2	1	
42	0	4	0	1	0	0	
43	0	2	0	1	4	1	
44	3	1	0	1	1	0	
45	1	2	0	2	1	1	
46	4	3	0	3	3	2	
47	5	5	0	2	2	2	
48	0	3	0	2	2	2	
49	3	2	0	1	3	3	
50	2	4	0	3	2	2	
Total # of cysts	92	106	1	113	90	40	442

Compound 4	Anterior Terminal	Anterior Intermediate	Anterior Proximal	Posterior Terminal	Posterior Intermediate	Posterior Proximal	
1	2	1	0	3	4	2	
2	3	1	0	3	2	0	
3	3	0	0	2	1	0	
4	0	0	0	0	0	0	
5	6	4	0	0	4	0	
6	2	0	0	0	0	1	
7	3	1	0	0	2	0	
8	2	2	0	3	0	0	
9	0	0	0	0	2	1	
10	2	2	0	2	1	0	
11	0	0	0	1	0	1	
12	1	0	0	1	1	1	
13	1	3	0	1	2	0	
14	5	2	0	3	5	0	
15	0	0	0	0	2	0	
16	0	0	0	0	0	0	
17	0	0	0	0	0	0	
18	0	0	0	1	0	0	
19	2	2	0	1	1	0	
20	3	4	0	3	3	0	
21	1	0	0	1	1	0	
22	2	3	0	1	2	0	
23	0	0	0	0	0	0	
24	0	1	0	1	2	2	
25	1	1	0	1	1	0	
26	2	4	0	0	2	0	
27	0	2	0	1	1	1	
28	1	3	0	0	1	2	
29	1	2	0	0	3	0	
30	0	3	0	0	0	1	
31	0	2	0	0	1	1	
32	1	1	0	2	2	0	
33	0	1	0	2	2	3	
34	1	0	0	2	1	0	
35	1	0	0	3	0	1	
36	3	1	0	2	1	1	
37	0	0	0	0	0	0	
38	2	1	0	0	1	0	
39	0	2	0	1	3	1	
40	0	3	0	2	1	0	
41	0	1	0	2	3	0	
42	0	2	0	2	2	0	
43	0	2	0	0	1	1	
44	1	2	0	3	2	2	
45	2	0	0	1	1	2	
46	1	1	0	2	2	1	
47	0	0	0	0	1	0	
48	0	0	0	0	0	0	
49	0	0	0	1	0	0	
50	2	2	0	1	3	1	
Total # of cysts	57	62	0	55	70	26	270

Appendix II

Introduction to the Appendix II: The following review article on the use of *Drosophila* to model renal disease includes 154 years of scientific literature on Malpighian tubules, dating from 1864 to 2018. This was the first comprehensive and up to date review comparing the *Drosophila* and the human renal systems focusing on the conserved features that could be used to model renal disease. The review especially focused on the Malpighian tubules, which are equivalent to the tubular part of a vertebrate nephron and on selected functional aspects of the nephrocytes, *Drosophila* renal cells which perform similar readsorptive functions to the vertebrate glomerular podocytes and have been recently reviewed elsewhere. Written at the start of my M.Sc., this review enabled me to get acquainted with the field of renal function studies and the intricacies of modeling biological renal pathways in *Drosophila.* This review could be useful for colleagues engaged in comparative and/or fluid transport and renal function studies, as well as those interested in drug screening in *Drosophila*. Finally, similar to human kidneys, the Malpighian tubules are insect detoxification systems implicated in insecticide response. Therefore, improving our understanding of their functions and physiology may be helpful for insect management efforts.

Note: This review paper was published as "Millet-Boureima C., Porras Marroquin J., and Gamberi C. 2018. *BioMed Research International, vol. 2018,* Article ID 5697436" and the entirety of its content is being presented in this thesis. DOI. In the published article, the term Malpighian tubules is abbreviated as MTs.

Contribution of authors:

I wrote the first draft of the manuscript and contributed extensively to the final text.

Jessica Porras Marroquin provided a section on nephrocytes (Section 2.3).

Dr. Chiara Gamberi wrote the sections on PKD (Sections 2.4.2 and 2.4.3).

Dr. Chiara Gamberi and I edited the manuscript.

Hindawi
BioMed Research International
Volume 2018, Article ID 5697436, 13 pages
https://doi.org/10.1155/2018/5697436

Review Article

Modeling Renal Disease "On the Fly"

Cassandra Millet-Boureima, Jessica Porras Marroquin, and Chiara Gamberi

Biology Department, Concordia University, Montreal, QC, Canada

Correspondence should be addressed to Chiara Gamberi; chiara.gamberi@concordia.ca

Received 3 February 2018; Accepted 17 April 2018; Published 31 May 2018

Academic Editor: Daniela Grifoni

Detoxification is a fundamental function for all living organisms that need to excrete catabolites and toxins to maintain homeostasis. Kidneys are major organs of detoxification that maintain water and electrolyte balance to preserve physiological functions of vertebrates. In insects, the renal function is carried out by Malpighian tubules and nephrocytes. Due to differences in their circulation, the renal systems of mammalians and insects differ in their functional modalities, yet carry out similar biochemical and physiological functions and share extensive genetic and molecular similarities. Evolutionary conservation can be leveraged to model specific aspects of the complex mammalian kidney function in the genetic powerhouse *Drosophila melanogaster* to study how genes interact in diseased states. Here, we compare the human and *Drosophila* renal systems and present selected fly disease models.

1. Introduction

Defective kidney function can lead to potentially lethal end-stage renal disease (ESRD) and chronic kidney disease (CKD), for which therapeutic options are limited. ESRD and CKD may be remedied by dialysis and renal replacement therapy (renal transplant), which are both costly [1] and greatly affect the quality of life of both patients and their families. The complexity of the human kidney has posed a formidable challenge to experimental probing for many pathologies. In many cases disease progression is well described; however, the underlying mechanisms at the molecular and cellular levels are incompletely understood, which affects our capacity to design remedial therapeutics. Animal model research on kidney disease has traditionally used rodents for their mammalian-type kidney similar to the human one. However, rodent and human kidneys also share the same complexity, which challenges experimentation. Zebrafish, featuring a streamlined pronephros, has also been used to model renal disease, albeit less frequently, in part because of its adaptation to an aquatic environment. With an open circulatory system, the fly's renal system is aglomerular and urine formation is based on active transport rather than selective readsorption [2]. However, *Drosophila* is a clear evolutionary intermediate towards the glomerular kidney, with recognizable cell types responsible for fulfilling the kidney's main functions: detoxification, filtration, and endocytosis [3, 4]. The small body size and the fastest filtration rate known [5] allow flies to have separate compartments for renal function: the Malpighian Tubules (MTs), which are analogous to the renal tubules [6], and two clusters of nephrocytes within the body cavity, which are analogous to podocytes in the glomerular kidney. Because of extensive functional similarities, the fly has been successfully used to model aspects of mammalian renal function. We will compare the human and *Drosophila* renal systems and discuss the strategic use of fly modeling of human renal disease.

2. The Human Renal Filtration System

The human kidneys, found in the mid to lower back of the trunk on each side of the spine, are bean-shaped organs roughly the size of a person's own fist. Composed of two main layers, the cortex and the medulla, they play a leading role in blood filtration, solute reabsorption, and metabolic waste excretion, which result in urine production. The kidney medulla contains so-called renal pyramids, conical regions collectively holding about one million functional units, which

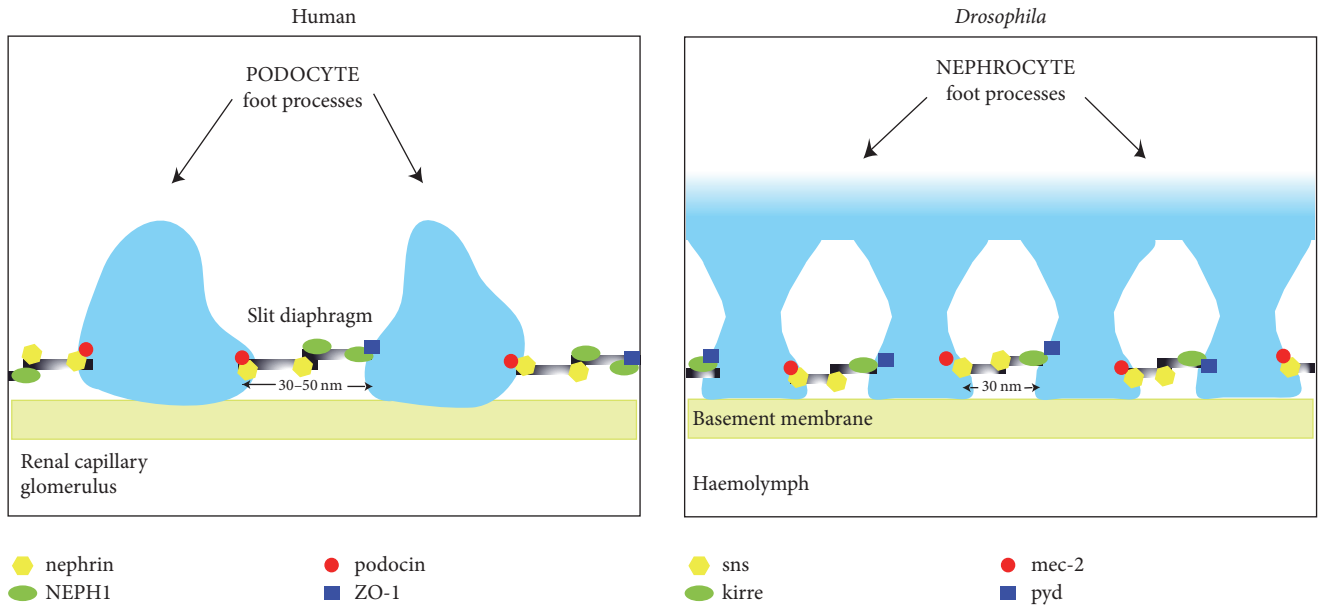

Figure 1: *Comparison of the human podocyte and the Drosophila nephrocyte slit diaphragms.* Selected evolutionary conserved proteins are indicated. The same symbols indicate orthologous proteins between human and *Drosophila*. In the fly, Duf was found to directly interact with Pyd and Sns with podocin ortholog Mec-2 [6].

are called nephrons. The nephrons span both cortex and medulla, starting and ending in the former, with the latter containing variable lengths of the central portion of the tubule. Nephrons modify the filtered fluid and produce urine, which drains into collecting tubules (also called collecting ducts) that in turn fuse into larger ducts that empty into the minor calyx, the ureter and, eventually, the bladder.

Each nephron consists of a tubule closed at one end and enlarged into the cup-like Bowman's capsule, which surrounds a tuft of capillaries called glomerulus. Together, the Bowman's capsule and glomerulus are referred to as renal (or Malpighian) corpuscle. The renal corpuscle filters blood via specialized cells that respond to physiological cues. Glomerular capillaries are fenestrated, that is have pores which allow fluids and small molecules such as ions and sugars to leave the blood and, instead, retain cells and proteins exceeding pore size, complexes of carrier proteins and lipids, as well as calcium ions (Ca^{2+}). Wrapped around the capillaries and with characteristic protrusions called foot processes which contact the capillary's basement membrane are podocytes, specialized epithelial cells integral to the filtration barrier [6–8]. Adjacent foot processes are separated by slit diaphragms about 14 nm wide with 30–50 nm wide pores carrying out filtration [6] (Figure 1). Major components of the slit diaphragm include members of the nephrin protein superfamily and NEPH1, which are coexpressed and form the diaphragm via homotypical and heterotypical interactions [6]. Together, the basement membrane, slit diaphragm, and podocyte processes form a barrier between plasma and filtrate which is essential to glomerular function. Its disruption can lead to kidney disease [9]. Differences in pressure between the glomerulus and Bowman's capsule determine the glomerular filtration rate (GFR, the amount of filtrate produced per minute), which is used to measure kidney function. Because ion and fluid balance depend on flow efficiency, glomerular filtration rate is subject to multiple regulatory mechanisms. The glomerular filtrate is first collected in the Bowman's capsule and directed through the nephron, flowing through the proximal convoluted tubule and the descending and ascending branches of the Loop of Henle, rising through the distal convoluted tubule while being modified, and, finally, arriving to the collecting duct as urine (Figure 2).

2.1. Human Nephron Development. Mammalian nephrons form during the late embryonic and early postnatal stages and display limited cell turnover, resulting in low regeneration rate in the adult [10]. Interactions between two mesoderm-derived tissues, the ureteric bud (UB), and the adjacent metanephric mesenchyme (MM) initiate nephrogenesis [10]. In part driven by developmental regulators Ret, Gfra1, Wnt11, Wnt6, and Pax2 in the UB and Bmp4, Gdnf, Pax2, and Wt1 in the MM, the UB invades the adjacent MM, generating the collecting duct [10–16]. The UB then branches to form a T shape within the MM. The two ends of the T structure then induce formation of the cap mesenchyme, which contains nephron stem cells and progenitors, as well as stromal cells that support kidney ontogenesis by producing signaling molecules, for example retinoic acid, promoting expression of Ret, ERK, MAPK, PI3K, PLC, and WNT [14, 17–20] in the UB. The iteration of this process produces both the branched structure of the ducts and nephron multiplicity. The MM cells then aggregate and, responding to Wnt signaling [21], undergo mesenchymal-to-epithelial transition to produce the renal vesicle or nephron progenitor [10–13]. Vesicle cells polarize, first establishing a proximal-to-distal axis [22] followed by an apical-basal one [23, 24]. After polarization,

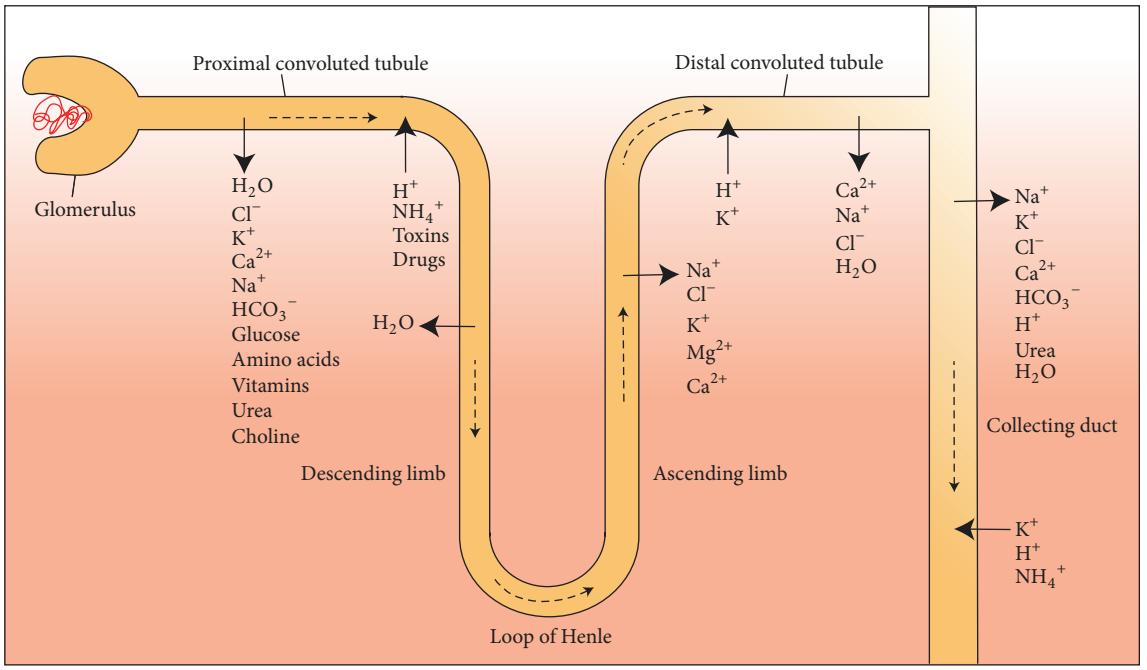

Figure 2: *Schematic features of a generalized human nephron*. The glomerulus, the different regions of the nephron, and corresponding ion and solute transport are indicated. The dashed arrows depict direction of the fluid flow.

the renal vesicle reshapes in the form of a comma, then that of an S, and fuses with the UB, while cells differentiate morphologically [10, 25]. The S-shaped body gives rise to the glomerulus, Bowman's capsule, and both proximal and distal tubules. The intermediate region of the S-shaped body, instead, yields the loop of Henle [26]. Mesangial cells, integral to the glomerulus, derive from the stromal cells [15, 27]. Finally, the vasculature is formed by mesodermal cells that migrate into the developing kidney [28].

3. The *Drosophila* Renal System

In the fly, filtration is carried out by specialized cells called nephrocytes, which display remarkable similarities to the human podocytes [6]. Nephrocytes were originally discovered in the 1800s and found to uptake and store multiple compounds, including silver nitrate, albumin, and dyes [29–34]. Nephrocytes are found in two clusters: one, called pericardial, near the tubular heart and the other, called garland, harboring two nuclei, close to the esophagus [6, 32–36]. *Drosophila* nephrocytes display characteristic in-folding of the plasma membrane which form channels flanked by foot processes [6]. Ultrastructural studies have revealed that nephrocytes form a three-layered filter morphologically similar to that formed by the vertebrate podocytes [6, 32–34, 36, 37]. Like human podocytes, pericardial nephrocytes filter and reabsorb solutes from the *Drosophila* circulating fluid, called haemolymph, via channels regulated by 30 nm wide slit diaphragms [38–40]. Slit diaphragms feature two filaments composed of proteins encoded by genes *sticks and stones* (*sns*) and *dumbfounded* (*duf*, also called *kirre*), a NEPH1 ortholog [6]. Other protein components of the nephrocyte slit diaphragm include the products of genes *mec-2*, a podocin ortholog, and *pyd*, a ZO-1 ortholog [6]. Alike human podocytes, a basement membrane enwraps each nephrocyte. Together, the nephrocyte diaphragm and the basement membrane form the filtration barrier in *Drosophila*, the integrity of which is maintained by protein-protein interactions between orthologs of the human slit diaphragm proteins (Figure 1). The filtrate is actively endocytosed from the sides of the channels, retained in cell vacuoles and either broken down (proteins) or stored (toxins, silver nitrate) [41]. The recent findings that nephrocytes may be apicobasally and basolaterally polarized reinforced their similarity with human podocytes [42, 43]. Moreover, nephrocytes and podocytes appear to respond similarly to pharmacological treatment. Administration of puromycin [44] and protamine sulfate [42] was found to disrupt the filtration barrier. Because of their extensive functional overlap with the necessary podocytes, the discovery that nephrocytes are, instead, dispensable in the adult fly, yet necessary for larval survival [45], was surprising and future studies are being targeted to understand this apparent paradox.

Nephrocytes have been used to model human nephrotic syndromes, in which podocyte processes are effaced as a consequence of mutations in the genes encoding for slit diaphragm proteins. Because these models have been recently reviewed, we refer interested readers to [46].

3.1. Malpighian Tubule Morphology. In *Drosophila* two pairs of MTs are made of a single-layered epithelium and depart from the interface between mid- and hind-gut (Figure 3). With one tubule residing more anteriorly and the other more posteriorly within the abdominal cavity, the MTs are folded

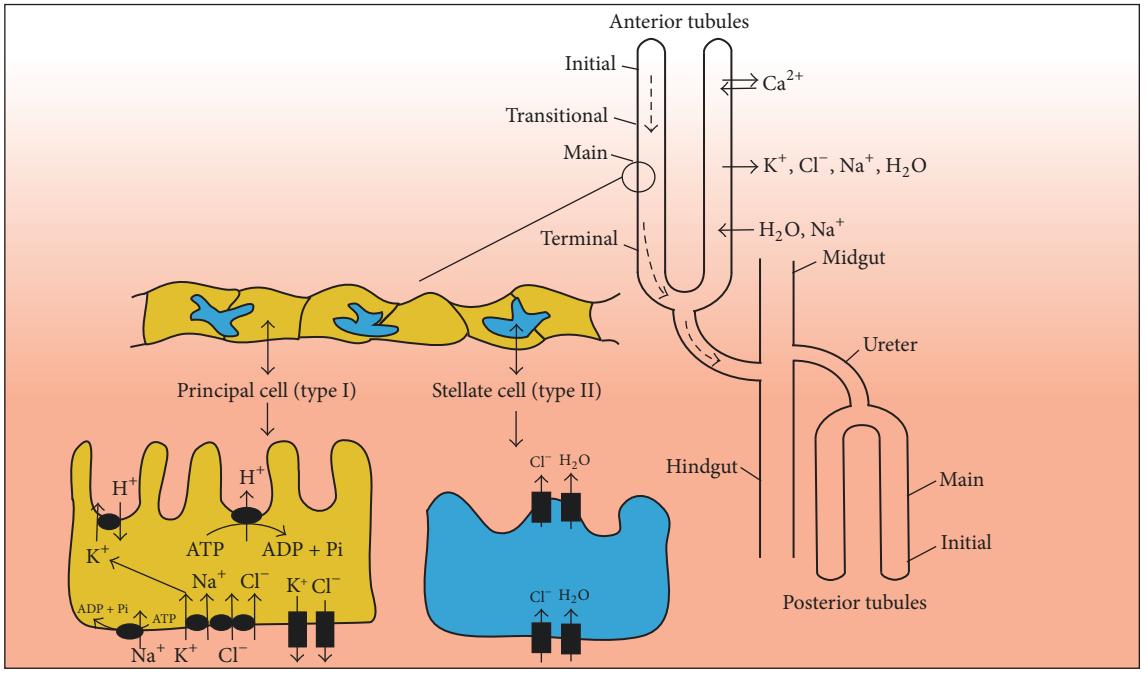

FIGURE 3: *Schematic features of the Drosophila Malpighian tubules*. The anterior and posterior tubules with relative functional segments and ion and water transport are indicated. Dashed arrows depict the direction of the fluid flow. Features and functions of principal and stellate cells are shown (below).

in a stereotypical way, which is thought to ensure efficient metabolic waste removal and osmoregulation in the open circulatory system typical of insects. Unlike the mammalian closed circulatory system in which the circulating fluid is subject to glomerular ultrafiltration, *Drosophila* haemolymph is, instead, filtered. Also different from the mammalian nephrons that are embedded in organ tissues, the two MTs are free inside the fly's body cavity and can be cleanly microdissected. Anterior and posterior MTs can be distinguished both functionally and morphologically, because of their distinct transcriptomes and the anterior tubule being longer [47].

The anterior tubule pair can be divided into four sections: initial, transitional, main, and terminal (Figure 3). These regions contain type I cells, known as principal cells, and type II cells, known as stellate cells (Figure 3). Principal cells arise from a key interaction between the midgut and the hindgut, constitute about ~80% of all tubule cells, and are responsible for the transport of cations and organic solutes [48]. Stellate cells are scattered around the principal cells and are responsible for water and chloride ion (Cl^-) flow [48, 49]. Reducing tubular expression of the vacuolar- (V-) ATPase by using fruit flies heterozygous for a lethal insertion in the gene encoding for the V-ATPase beta subunit revealed that cation transport may solely be performed by principal cells [50]. Stellate cells were only found in secretory regions and were absent from reabsorptive regions, suggesting that they may have secretory roles [50]. The cells in the MT initial segment are thinner and may excrete specifically Ca^{2+} ions at high rates [51]. Cells of the terminal segment appear to regulate ion and water balance via selective readsorption from and secretion into primary urine and by removing nitrogen-containing catabolites from the haemolymph via active transport of uric acid to the tubule lumen and passive diffusion of other molecules through the intercellular spaces. As the primary urine is transported along the tubule, it is sequentially transformed, a process that requires both apicobasal cell polarization of the tubular epithelium and planar cell polarity. Tubular cells were found to be functionally differentiated in a proximal-to-distal fashion and the processed urine is eventually secreted by the more distal cells. Because of their fundamental role in detoxification, the normal development of MTs is essential in the fruit fly.

Just like human nephrons, *Drosophila* MTs exhibit internal marked asymmetry which corresponds to distinct spatial domains of gene expression [50, 51]. Analyses of enhancer trap expression in the MTs revealed that the initial, transitional, and main segment of the anterior tubules and the sole main segment in the posterior tubules correspond to different cell types and distinct physiological functions [50]. The main segment was found to secrete potassium chloride (KCl) and water at high rates [52] and the lower third of the tubule carried out reabsorption [50]. The lower regions of the MTs appeared to modify the travelling fluid from the main segment by reabsorbing potassium ions (K^+) [53] but not water [54], contrary to what was previously reported [50]. Moreover, the lower tubules were found to acidify the fluid and transport Ca^{2+} into the lumen (Figure 3) [53]. Remarkably, in just about 15 seconds, the cells located in the main segment of the *Drosophila* MTs were found to secrete fluid in amounts equal to their own volume, making the MTs the fastest known filtering system [52, 54]. While the observed functional complexity of the MTs was initially

found surprising and in apparent contradiction with its reputation as a simplified epithelial developmental model [50], this same functional complexity turned out to be an asset for modeling human renal disease in combination with the available genetic and technological tools for probing ion transport [52].

3.2. Ion Transport and Fluid Secretion in the Malpighian Tubules. In the MTs, multiple ion transporters regulate ion balance in different sections. An apical V-ATPase generates a primary proton gradient that fuels the activity of sodium/proton (Na^+/H^+) and K^+/H^+ exchangers, also apically localized, which release Na^+ and K^+, respectively, in the lumen [54]. K^+/Cl^- cotransporters localized at the basolateral membrane [55] decrease K^+ concentration in the secreted fluid as it passes through the lower tubule [53]. Channels found in stellate cells transport Cl^- from the haemolymph to the lumen and are under control of the leucokinin peptide-hormone family [49, 54]. Leucokinins are synthesized in response to increased intracellular Ca^{2+} and promote both fluid secretion and epithelial permeability to Cl^- [56].

Cardioacceleratory neuropeptide CAP2b was found to stimulate fluid secretion specifically via cyclic GMP (cGMP) and to activate the nitric oxide (NO) signaling pathway [52, 57] that regulates salt and water balance in the fly MTs [58]. Early studies tested if increased concentration of intracellular Ca^{2+} could stimulate CAP2b and activate the NO/cGMP pathway in different cell types [59]. Producing the first Ca^{2+} reporter system in *Drosophila* MTs, Rosay and collaborators expressed aequorin, a Ca^{2+}-sensitive luminescent protein, in principal cells in the tubule main segment via the GAL4/UAS binary expression system [59, 60]. As aequorin was produced in the tubules in vivo, luminescence indicated both the amount of aequorin and Ca^{2+} amounts. Stimulation of CAP2b-dependent physiological responses caused rapid Ca^{2+} release from internal stores [59]. Because in this system no CAP2b stimulation was observed in stellate cells, principal and stellate cells of the main segment are unlikely to be connected through gap junctions [59].

3.3. Malpighian Tubule Development. The MTs start forming as four primordia derived from the hindgut primordium and visceral mesoderm in the six-hour embryo [4, 61] in a process requiring the gap gene product Krüppel (Kr) and the transcription factor Cut [48, 62, 63]. The specification of future tubule cells is determined via Kr [48] and, similar to mammalian kidney development, the Wnt pathway [10, 48].

Each tubule primordium contains a unique tip cell specified by lateral inhibition via the Notch pathway [4, 48, 64]. The tip cell segregates and activates the Epidermal Growth Factor receptor homolog DER [65] which promotes cell proliferation, tubular growth, and development of the MTs excretory system [64, 65]. As the MTs grow closer to the caudal mesoderm they induce mesenchymal-to-epithelial transition in nearby cells that will insert themselves in the tubules and become stellate cells [4]. The ectoderm-derived tubular epithelium is formed of principal cells [4] and the ureter of ectodermal cells [4]. Cells divide a definite number of times to give rise to 146 principal and 33 stellate cells in each anterior tubule and 105 principal and 22 stellate cells in each posterior tubule in *Drosophila* [50, 66]. Most of tubule ontogenesis is completed during embryogenesis, and the MTs are not histolysed during metamorphosis. Using positively-marked mosaic lineage with GFP-labeled proliferating cells enabled the discovery of multipotent adult stem cells in the lower tubule and ureter [4]. Such cells require JAK-STAT signaling for self-renewal and are analogous to stem cells activated during repair of kidney ischemic injury [4].

3.4. Immune Function of the Malpighian Tubules. The MT epithelium is part of the fly's defenses against pathogens. The MTs display innate immunity with both humoral and cellular responses and no adaptive response, as is typical for insects [67, 68]. Remarkably, studies in *Drosophila* first revealed the immune function of Toll-receptor signaling [69]. In fact, the *Toll* gene, originally identified for its function in embryonic polarity [70], was later found to function in immunity [71] and to have a few homologs in the fly, including *"18-wheeler"* [72] and multiple vertebrate ones dubbed Toll-Like Receptors (TLRs). Unlike other fly organs involved in immunity, the MTs display constitutive production of antimicrobial peptides (AMPs) [73]. Upon sensing infection, the MTs activate distinct pathways when triggered by specific pathogens. The Toll pathway was found to respond to fungal and Gram-positive bacterial infections and the immune deficiency (IMD) pathway to respond to Gram-negative bacterial infections [74, 75]. MTs may also initiate a Toll-independent humoral response [76]. All these eventually trigger release of seven groups of AMPs, either directly from the MTs [73] or indirectly from the fat-body, the latter being the fly liver-equivalent [68, 69, 77]. The groups of AMPs, Drosomycin, Metchnikowin, Defensin, Attacin, Cecropin, Drosocin, and Diptericin, appear to inhibit growth of haemolymph-invading microorganisms [77]. Both the IMD and Toll pathways were found to sense superficial peptidoglycan on the bacterial cell wall via signaling by peptidoglycan-recognition proteins (PGRP) in the MTs principal cells and gut [69, 78, 79]. PGRP function has mainly been studied in the gut [80], yet the pathway appears to function similarly in the MTs. The Toll proteins display homology to the cytoplasmic domain of the vertebrate interleukin 1 receptor and participate into similar intracellular signaling cascades [81]. The IMD pathway is considered to be equivalent to the vertebrate TNF pathway [75]. Both Toll and IMD pathways result in activation of NF-κB-like transcription factor Relish and induce transcriptional changes [82].

The steroid hormone ecdysone that regulates principal and stellate cell fluid secretion [68] also affects MT-dependent immunity. Ecdysone may promote haemocyte proliferation and fast pathogen encapsulation [83]. In S2 cells, ecdysone was also found to induce transcription of the *PGRP-LC* gene encoding the peptidoglycan receptor and, independently, of a subset of AMPs [84]. Ecdysone also triggers histolysis during metamorphosis [83]. However, the MTs are resistant to this process, possibly due to their fundamental role in immunity. Diap2, an antiapoptotic protein, was also found to contribute

to the innate response in the IMD pathway, possibly via regulation of MT ion channels [85]. Diap2 levels increased in the MTs when there was an immune threat; conversely, decreased Diap2 made flies more prone to infections [85].

Finally, upon septic infection, the MT-dependent immune response may alternatively be activated via the NO pathway, which in turn initiates the IMD pathway and leads to increased NO Synthase (dNOS) and improved fly survival [67, 68].

With growing appreciation for the importance of the MT immune function, the ongoing mechanistic studies of gut-mediated immunity will provide resources and paradigms to better define the role of the MTs in the defense from pathogens.

4. Malpighian Tubules to Model Disease

MTs have been utilized to study the physiology of fluid transport because of their anatomical accessibility, streamlined anatomy, and one-cell-thick epithelium. In MTs, the proliferation of the founder cells (anlage), their spatial organization, patterning, and differentiation occur in sequence, rather than concurrently as in other epithelia, enabling studies of separate stages in time course experiments. MTs and mammalian nephrons share functionally distinct regions (Figures 2 and 3), analogous functions, and display remarkable transcriptome conservation [47, 86]. For example, similar to mammalian renal tubules, MTs carry out detoxification thanks to high levels of cytochrome P450 and glutathione transferase [87]. Likewise, mutations in evolutionarily conserved V-ATPase subunits were initially discovered in *Drosophila* because of their renal phenotypes [88, 89]. Three years later, equivalent mutations in the human *ATP6B1* V-ATPase were reported to cause similar defects in patients [90]. As the interest in modeling renal function in the fly continues to grow, we review some of the successful examples below.

4.1. Nephrolithiasis. *Drosophila* has been used to model the most common kind of human kidney stones, namely, calcium oxalate nephrolithiasis [91]. Nephrolithiasis refers to the formation and movement of kidney stones in the urinary tract [91]. There are multiple types of kidney stones that are distinguished for their different composition and origin. Largely dependent on diet and metabolism, kidney stones in the urinary tract are most commonly composed of calcium oxalate (CaOx) and, in lesser quantities, calcium maleate or phosphate. Also dependent on diet and metabolism, cysts composed of uric acid develop when urine is too acidic, for example in severe dehydration, gout, or following chemotherapy. Struvite cysts are caused by kidney infections and may result in urinary obstruction [91]. Finally, cystine stones form as crystals of leaked cystine in rare cystinuria patients. While rats had been the model of choice for CaOx stone formation [92], prohibitive costs of breeding and caring inspired Chen and colleagues [92] to model nephrolithiasis in the fly. Similar to rodents, flies appeared to respond to oral administration of lithogenic agents ethylene glycol, hydroxyl-L-proline, and sodium oxalate, by inducing formation of CaOx crystals in the MTs between two and three weeks after ingestion. Importantly, response severity was dose-dependent [92].

Recently, RNAi-mediated knockdown of the enzyme xanthine dehydrogenase *(Xdh)* in the fly was shown to induce ectopic calcification and accumulation of crystals and stones in the MTs [93]. Well-fed *Xdh*-knockdown flies only survived three days, as opposed to 60 days of the wild type control. Chemical analysis of the stones by micro X-ray fluorescence revealed significant amounts of Ca^{2+} and zinc (Zn). Because the latter had never been involved in kidney stone formation before, genetic confirmation was obtained by RNAi-mediated inhibition of Zn transporters in the fly, which was found to decrease stone formation [93]. Dietary and pharmacologic modulation of Zn levels in the fly and analyses of human kidney stones further confirmed Zn as a bona fide component [93]. In this case, the *Drosophila* model enabled the discovery of a new contributor to nephrolithiasis and indicated Zn-metabolic enzymes as potential therapeutic targets [93]. One issue to be clarified is that dietary Zn intake has been linked to increased risk of kidney stones in the adult (yet not in adolescent) individuals, while inhibiting Zn excretion was found to reduce cyst formation in the fly. One of the possible ways to interpret these apparently contradicting results posits that Zn may promote formation of different crystals depending on concentration [94] and indicates the need to probe additional physiological parameters in future studies to capture the complexity of kidney stone formation.

Flies have been used to study the processes leading to formation of uric acid stones because of their high levels of urate crystals normally accumulating in the tubule. Systematic analyses of the 33 genes encoding for subunits of the V-ATPase, some of which with multiple isoforms, revealed that mutants in the genes encoding core V-ATPase subunits displayed transparent MTs as a result of urine acidification, which decreased uric acid crystallization [89]. Notably, similar acidification defects were also found in patients with mutations in two V-ATPase subunits, which suggests a certain degree of functional conservation [90, 95].

4.2. Polycystic Kidney Disease. Polycystic kidney disease (PKD) is a genetic disease affecting at least 12.5 million people world-wide, regardless of ethnicity [96]. Two forms of PKD exist, one autosomal dominant (AD) and one, rarer and more severe, which is autosomal recessive (AR) [96] and will not be discussed here. ADPKD causes the development and progressive enlargement of fluid-filled cysts in the nephron, that consequently increase kidney size and cause interstitial fibrosis and chronic kidney disease by age 55 [96]. In half of the patients the severe damage results in kidney failure, making dialysis or renal transplant the only treatments [96]. The lack of a cure and dialysis costs that can surpass 150,000$ per patient per year [1] make PKD a global priority.

Genetic Underpinning of PKD. More than 85% of ADPKD patients carry mutations in the *PKD1* gene, which encodes polycystin-1, a G-protein coupled receptor (GPCR) [97]. Complete mutational inactivation of both alleles is rare and lethal pre- or peri-natally [96]; however, incompletely

penetrant *PKD1* alleles have been found in homozygosis [98]. Mutations in another gene, *PKD2*, are found in about 10% of ADPKD cases [97]. *PKD2* encodes polycystin-2, a transmembrane calcium channel of the TRPP family which was found to physically interact with polycystin-1 [99, 100]. The remaining ~5% of ADPKD patients carry unknown mutations other than *PKD1* or *PKD2* [101]. Because of their clear implication in PKD etiology, *PKD1* and *PKD2* genes and corresponding polycystin-1 and polycystin-2 gene products are being studied in much detail. Polycystin-1 and polycystin-2 complexes were found to mediate cell-matrix and cell-cell interactions, planar cell polarity, signal transduction, and cilia-mediated mechanosensation [96]. We have recently reported that cystic tissue from ADPKD patients carrying a *PKD1* mutation exhibited significant reduction of the *Bicaudal C (BICC1)* gene expression [102]. Similarly, $Pkd1^{-/-}$ mice displayed reduced Bicc1 protein specifically in the kidneys [102], placing *BICC1* genetically downstream of *PKD1*. Mutations in the *BicC* gene of many vertebrates, including humans, cause the development of renal cysts [103–110]. *BicC* was originally discovered in the fly during a screen for embryonic polarity determinants in the germline [111].

Cyst formation is complex and unfolds over time. ADPKD patients carrying *PKD1* or *PKD2* mutations already display small renal cysts at birth [96] yet remain asymptomatic until middle age because the renal capacity is in vast excess (in fact, donation of one kidney is compatible with life). After then, kidney function declines rapidly. Because polycystin-1 and polycystin-2 are part of multiple protein complexes with wide cellular distribution, dysregulation of either in the renal tubule affects many pathways, including apicobasal and planar cell polarity, cell proliferation, cell metabolism, fluid secretion, and the extracellular matrix [112–115]. In PKD cysts form in the renal tubular epithelium where some cells reactivate normally quiescent proliferation pathways and begin to divide. In parallel, epithelial polarization is progressively lost, impacting secretion. Fluid accumulation in the cysts, in turn, stimulates further cell division, possibly in response to increased tensional stretch in the tissue [116, 117]. It is currently unclear what triggers cyst formation. As cysts expand, tubular cells display activation of various signal transduction pathways mediated by Ca^{2+} and cAMP, e.g., Raf-MEK-ERK [118, 119], the mammalian Target of Rapamycin (mTOR), PI3-kinase-Akt, JAK-STAT, NF-kB, Wnt, Hippo, and G-proteins [115, 118–130]. In spite of the enumeration of these pathways, the mechanisms of cyst initiation and progressive cystic degeneration remain largely unknown, likely because of the anatomical complexity of the vertebrate kidney and slow disease onset, which hinder experimental probing. The *BicC* fly provided the first account of renal cysts in *Drosophila* [102]. Modeling PKD in the fly may enable biochemical characterization of the cystic tubule and define the genetics of cyst formation and progression due to low genetic redundancy, and may advance our understanding of the core cystic processes. *BicC* encodes a conserved cytoplasmic RNA-binding protein with orthologs in many species [104, 105, 109, 131–133]. BicC can bind to multiple mRNA targets and appeared to reduce their expression posttranscriptionally [134]. The resulting target upregulation in the oocytes from heterozygote *BicC* female flies was found to disrupt anterior-posterior embryonic polarity [7, 115–135], while *BicC* homozygotes displayed oogenesis arrest at stage 10 [136]. Similar to ADPKD patients, *BicC* mutant flies featured fluid-filled cysts in the MTs already at hatching; over time the cysts enlarged and became more numerous [102]. Compared to wild type, *BicC* flies were short-lived, possibly a consequence of their defective renal function [102]. *BicC* MTs also displayed extra branches, indicating underlying developmental and polarity defects. Oocytes from *BicC* mutant flies exhibited abnormal actin structures which prevented secretion of the dorsal fate determinant Gurken [137–141]. Similarly, the BicC protein was required for epithelial polarization via cadherin-mediated cell adhesion in the IMCD murine kidney cell line [142]. Initial molecular analyses of the *BicC* MTs identified the activation of the *myc* and TOR pathways, two hallmarks of vertebrate PKD [102]. Like ADPKD patients, postrenal transplantation (in which diseased kidneys are left in place) and administration of the immune suppressant and TOR inhibitor rapamycin could transiently rescue the *BicC* flies and reduce cysts, relative to untreated controls [102, 126]. Murine PKD models also exhibited mTOR cascade stimulation [143–148] and responded to rapamycin by delaying cystic onset [126, 145, 149]. In sum, the *BicC* cystic flies appeared to recapitulate many of the diseased features of PKD, displayed pharmacological response to rapamycin [102], and may be a valid model to advance our understanding of the molecular bases of renal cyst formation and the formation of extra tubular branches. One interesting aspect is that ciliary (dys)function appears prominent in vertebrate PKD [150]. The absence of ciliated epithelia in *Drosophila* raises the intriguing question of how cysts form and develop in *BicC* MTs versus human nephrons. Considering that other ciliary pathways, e.g., *hedgehog*, were originally discovered in the fly, the striking biochemical similarities between PKD-type cysts and the *BicC*-dependent cysts in the fly may not be as surprising and may suggest new hypotheses on the evolution of ciliary function.

With proper consideration of the differences between flies and humans and of the hierarchical relationship between the *BicC* and *PKD1* genes, the *BicC* cystic fly may offer opportunity to chart conserved pathways that are altered in *BicC* mutation, are relevant for cyst formation and/or progression, may allow to form new hypotheses on *BicC* function and disease mechanism, and contribute to our understanding of the larger functional context of human PKD. Considering that BicC was also found in a protein complex linked to human nephronophthisis, another cystic kidney disease [110, 133], future studies will reveal if *BicC* function may affect multiple pathways of renal cystogenesis.

5. Conclusion

The remarkable conservation of renal functions between fruit flies and humans is suggestive of the presence of strong evolutionary constraints imposed on the detoxification process of all organisms. Emerging evidence of the interplay between renal and immune functions suggests additional

requirements for the renal system. Multiple diseases causing progressive degeneration and loss of function of the kidney result in organ damage that may only be remedied by renal replacement therapy or dialysis, which are costly socially for the health care system and personally to the patients and their families, due to their negative impact on quality of life. Studies aiming at understanding the mechanisms of renal disease have been hindered by the anatomical complexity of the mammalian kidney. *Drosophila* possesses an evolutionary intermediate between glomerular and non-glomerular renal system, consisting of anatomically separated renal tubules and nephrocytes that, together, fulfill the renal functions. Similar developmental origin of the fly MTs and nephrocytes with their human counterparts, the nephron and the glomerular podocytes, respectively, is accompanied by conserved cellular pathways. Making the fruit fly a useful model to study the mechanisms of disease, the structurally streamlined, anatomically isolated, renal structures can be easily microdissected and studied biochemically; moreover, they can be probed genetically utilizing the vast array of *Drosophila* genetic tools. In multiple cases in which human renal disease has been modeled in *Drosophila*, including nephrolithiasis and PKD, the conservation seemed to extend to pharmacological responses, echoing similar examples in other fly disease models. Considering that many drug binding sites were found to be conserved in the fly [151], development of proper pharmacological screen protocols in the fly may in future provide a rapid and effective alternative strategy for drug discovery.

Conflicts of Interest

The authors declare that they have no conflicts of interest.

Authors' Contributions

Cassandra Millet-Boureima contributed sections on MT and nephron function, development and disease modeling, made the figures, and edited the manuscript. Jessica Porras Marroquin wrote text on nephrocytes and podocytes and conducted a literature search that contributed to the manuscript in its current format. Chiara Gamberi contributed sections on PKD, MT, nephron function and development, planned contents, and edited the manuscript.

Acknowledgments

The authors are grateful to C. Charbonneau (Institut de Recherche en Immunologie et Cancerologie) for help with the graphics and to Professor W. D. Lubell for discussion. This research was funded in part by a CUPFA Professional Development Award to Chiara Gamberi.

References

[1] K. L. Lentine, H. Xiao, G. Machnicki, A. Gheorghian, and M. A. Schnitzler, "Renal function and healthcare costs in patients with polycystic kidney disease," *Clinical Journal of the American Society of Nephrology*, vol. 5, no. 8, pp. 1471–1479, 2010.

[2] K. W. Beyenbach and P. L.-F. Liu, "Mechanism of fluid secretion common to aglomerular and glomerular kidneys," *Kidney International*, vol. 49, no. 6, pp. 1543–1548, 1996.

[3] J. A. T. Dow and M. F. Romero, "*Drosophila* provides rapid modeling of renal development, function, and disease," *American Journal of Physiology-Renal Physiology*, vol. 299, no. 6, pp. F1237–F1244, 2010.

[4] S. R. Singh, W. Liu, and S. X. Hou, "The adult *Drosophila* Malpighian tubules are maintained by multipotent stem cells," *Cell Stem Cell*, vol. 1, no. 2, pp. 191–203, 2007.

[5] S. H. P. Maddrell, "The fastest fluid-secreting cell known: The upper Malpighian tubule of *Rhodnius*," *BioEssays*, vol. 13, no. 7, pp. 357–362, 1991.

[6] H. Weavers, S. Prieto-Sánchez, F. Grawe et al., "The insect nephrocyte is a podocyte-like cell with a filtration slit diaphragm," *Nature*, vol. 457, no. 7227, pp. 322–326, 2008.

[7] R. Rodewald and M. J. Karnovsky, "Porous substructure of the glomerular slit diaphragm in the rat and mouse," *The Journal of Cell Biology*, vol. 60, no. 2, pp. 423–433, 1974.

[8] H. Pavenstädt, W. Kriz, and M. Kretzler, "Cell biology of the glomerular podocyte," *Physiological Reviews*, vol. 83, no. 1, pp. 253–307, 2003.

[9] R. G. Spiro, "Studies on the renal glomerular basement membrane. Preparation and chemical composition," *The Journal of Biological Chemistry*, vol. 242, no. 8, pp. 1915–1922, 1967.

[10] N. Barker, M. B. Rookmaaker, P. Kujala et al., "Lgr5+ve stem/progenitor cells contribute to nephron formation during kidney development," *Cell Reports*, vol. 2, no. 3, pp. 540–552, 2012.

[11] A. T. Dudley, K. M. Lyons, and E. J. Robertson, "A requirement for bone morphogenetic protein-7 during development of the mammalian kidney and eye," *Genes & Development*, vol. 9, no. 22, pp. 2795–2807, 1995.

[12] T. J. Carroll, J. S. Park, S. Hayashi, A. Majumdar, and A. P. McMahon, "Wnt9b plays a central role in the regulation of mesenchymal to epithelial transitions underlying organogenesis of the mammalian urogenital system," *Developmental Cell*, vol. 9, no. 2, pp. 283–292, 2005.

[13] K. Stark, S. Vainio, G. Vassileva, and A. P. McMahon, "Epithelial transformation metanephric mesenchyme in the developing kidney regulated by Wnt-4," *Nature*, vol. 372, no. 6507, pp. 679–683, 1994.

[14] S. Jain, "The many faces of RET dysfunction in kidney," *Organogenesis*, vol. 5, no. 4, pp. 177–190, 2014.

[15] A. Kobayashi, M. T. Valerius, J. W. Mugford et al., "Six2 defines and regulates a multipotent self-renewing nephron progenitor population throughout mammalian kidney development," *Cell Stem Cell*, vol. 3, no. 2, pp. 169–181, 2008.

[16] A. J. Murphy, J. Pierce, C. De Caestecker et al., "SIX2 and CITED1, markers of nephronic progenitor self-renewal, remain active in primitive elements of Wilms' tumor," *Journal of Pediatric Surgery*, vol. 47, no. 6, pp. 1239–1248, 2012.

[17] E. Batourina, S. Gim, N. Bello et al., "Vitamin A controls epithelial/mesenchymal interactions through *Ret* expression," *Nature Genetics*, vol. 27, no. 1, pp. 74–78, 2001.

[18] B. D. Humphreys, S.-L. Lin, A. Kobayashi et al., "Fate tracing reveals the pericyte and not epithelial origin of myofibroblasts in kidney fibrosis," *The American Journal of Pathology*, vol. 176, no. 1, pp. 85–97, 2010.

[19] A. Tufro, J. Teichman, N. Banu, and G. Villegas, "Crosstalk between VEGF-A/VEGFR2 and GDNF/RET signaling pathways," *Biochemical and Biophysical Research Communications*, vol. 358, no. 2, pp. 410–416, 2007.

[20] I. V. Yosypiv, M. Schroeder, and S. S. El-Dahr, "Angiotensin II type 1 receptor-EGF receptor cross-talk regulates ureteric bud branching morphogenesis," *Journal of the American Society of Nephrology*, vol. 17, no. 4, pp. 1005–1014, 2006.

[21] J.-K. Guo and L. G. Cantley, "Cellular maintenance and repair of the kidney," *Annual Review of Physiology*, vol. 72, pp. 357–376, 2009.

[22] R. Kopan, H.-T. Cheng, and K. Surendran, "Molecular insights into segmentation along the proximal-distal axis of the nephron," *Journal of the American Society of Nephrology*, vol. 18, no. 7, pp. 2014–2020, 2007.

[23] K. Georgas, B. Rumballe, M. T. Valerius et al., "Analysis of early nephron patterning reveals a role for distal RV proliferation in fusion to the ureteric tip via a cap mesenchyme-derived connecting segment," *Developmental Biology*, vol. 332, no. 2, pp. 273–286, 2009.

[24] C. Heliot, A. Desgrange, I. Buisson et al., "HNF1B controls proximal-intermediate nephron segment identity in vertebrates by regulating Notch signalling components and Irx1/2," *Development*, vol. 140, no. 4, pp. 873–885, 2013.

[25] M. Takemoto, L. He, J. Norlin et al., "Large-scale identification of genes implicated in kidney glomerulus development and function," *EMBO Journal*, vol. 25, no. 5, pp. 1160–1174, 2006.

[26] K. Reidy and A. Tufro, "Semaphorins in kidney development and disease: Modulators of ureteric bud branching, vascular morphogenesis, and podocyte-endothelial crosstalk," *Pediatric Nephrology*, vol. 26, no. 9, pp. 1407–1412, 2011.

[27] H. Hölthofer, K. Sainio, and A. Miettinen, "The glomerular mesangium: studies of its developmental origin and markers in vivo and in vitro," *APMIS-Acta Pathologica, Microbiologica et Immunologica Scandinavica*, vol. 103, no. 1-6, pp. 354–366, 1995.

[28] J. W. Mugford, P. Sipilä, J. A. McMahon, and A. P. McMahon, "Osr1 expression demarcates a multi-potent population of intermediate mesoderm that undergoes progressive restriction to an Osr1-dependent nephron progenitor compartment within the mammalian kidney," *Developmental Biology*, vol. 324, no. 1, pp. 88–98, 2008.

[29] A. Weismann, "Die nachembryonale Entwicklung der Musciden nach Beobachtungen an *Musca vomitoria* und *Sarcophaga carnaria*," *Zeitschrift für wissenschaftliche Zoologie*, vol. 14, pp. 187–336, 1864.

[30] A. O. Kowalevsky, "Zum Verhalten des Rückengefäßes und des guirlandenförmigen Zellstranges der Musciden während der Metamorphose," *Biologisches Centralblatt*, vol. 6, pp. 74–79, 1886.

[31] A. C. Hollande, "La cellule péricardiale des insectes: Cytologie, histochemie, role physiologique," *Archives D'anatomie Microscopique*, vol. 18, pp. 85–307, 1922.

[32] R. P. Mills and R. C. King, "The pericardial cells of *Drosophila melanogaster*," *Journal of Cell Science*, vol. 106, pp. 261–268, 1965.

[33] S. K. Aggarwal and R. C. King, "The ultrastructure of the wreath cells of *Drosophila melanogaster* larvae," *Protoplasma*, vol. 63, no. 4, pp. 343–352, 1967.

[34] A. C. Crossley, "The ultrastructure and function of pericardial cells and other nephrocytes in an insect: *Calliphora erythrocephala*," *Tissue & Cell*, vol. 4, no. 3, pp. 529–560, 1972.

[35] J. Miller, T. Chi, P. Kapahi et al., "*Drosophila melanogaster* as an emerging translational model of human nephrolithiasis," *The Journal of Urology*, vol. 190, no. 5, pp. 1648–1656, 2013.

[36] S. Zhuang, H. Shao, F. Guo, R. Trimble, E. Pearce, and S. M. Abmayr, "Sns and Kirre, the *Drosophila* orthologs of Nephrin and Neph1, direct adhesion, fusion and formation of a slit diaphragm-like structure in insect nephrocytes," *Development*, vol. 136, no. 14, pp. 2335–2344, 2009.

[37] M. Kestilä, U. Lenkkeri, M. Männikkö et al., "Positionally cloned gene for a novel glomerular protein—nephrin—is mutated in congenital nephrotic syndrome," *Molecular Cell*, vol. 1, no. 4, pp. 575–582, 1998.

[38] M. Simons and T. B. Huber, "Flying podocytes," *Kidney International*, vol. 75, no. 5, pp. 455–457, 2009.

[39] J. Na and R. Cagan, "The *Drosophila* nephrocyte: Back on stage," *Journal of the American Society of Nephrology*, vol. 24, no. 2, pp. 161–163, 2013.

[40] F. Zhang, Y. Zhao, Y. Chao, K. Muir, and Z. Han, "Cubilin and amnionless mediate protein reabsorption in *Drosophila* nephrocytes," *Journal of the American Society of Nephrology*, vol. 24, no. 2, pp. 209–216, 2013.

[41] R. L. Cagan, "The *Drosophila* nephrocyte," *Current Opinion in Nephrology and Hypertension*, vol. 20, no. 4, pp. 409–415, 2011.

[42] T. Hermle, D. A. Braun, M. Helmstädter, T. B. Huber, and F. Hildebrandt, "Modeling monogenic human nephrotic syndrome in the *Drosophila* garland cell nephrocyte," *Journal of the American Society of Nephrology*, vol. 28, no. 5, pp. 1521–1533, 2017.

[43] F. Hochapfel, L. Denk, G. Mendl et al., "Distinct functions of Crumbs regulating slit diaphragms and endocytosis in *Drosophila* nephrocytes," *Cellular and Molecular Life Sciences*, vol. 74, no. 24, pp. 4573–4586, 2017.

[44] A. S. Tutor, S. Prieto-Sánchez, and M. Ruiz-Gómez, "Src64B phosphorylates Dumbfounded and regulates slit diaphragm dynamics: *Drosophila* as a model to study nephropathies," *Development*, vol. 141, no. 2, pp. 367–376, 2014.

[45] J. R. Ivy, M. Drechsler, J. H. Catterson et al., "Klf15 is critical for the development and differentiation of *Drosophila* nephrocytes," *PLoS ONE*, vol. 10, no. 8, Article ID e0134620, 2015.

[46] M. Helmstädter, T. B. Huber, and T. Hermle, "Using the *Drosophila* nephrocyte to model podocyte function and disease," *Frontiers in Pediatrics*, vol. 5, 2017.

[47] J. Wang, L. Kean, J. Yang et al., "Function-informed transcriptome analysis of *Drosophila* renal tubule," *Genome Biology*, vol. 5, no. 9, p. R69, 2004.

[48] A. C. Jung, B. Denholm, H. Skaer, and M. Affolter, "Renal tubule development in *Drosophila*: A closer look at the cellular level," *Journal of the American Society of Nephrology*, vol. 16, no. 2, pp. 322–328, 2005.

[49] M. J. O'Donnell, M. R. Rheault, S. A. Davies et al., "Hormonally controlled chloride movement across *Drosophila* tubules is via ion channels in stellate cells," *American Journal of Physiology-Regulatory, Integrative and Comparative Physiology*, vol. 274, no. 4, pp. R1039–R1049, 1998.

[50] M. A. Sözen, J. D. Armstrong, M. Yang, K. Kaiser, and J. A. T. Dow, "Functional domains are specified to single-cell resolution in a *Drosophila* epithelium," *Proceedings of the National Academy of Sciences of the United States of America*, vol. 94, no. 10, pp. 5207–5212, 1997.

[51] V. R. Chintapalli, S. Terhzaz, J. Wang et al., "Functional correlates of positional and gender-specific renal asymmetry in *Drosophila*," *PLoS ONE*, vol. 7, no. 4, Article ID e32577, 2012.

[52] J. A. T. Dow, S. H. P. Maddrell, S.-A. Davies, N. J. V. Skaer, and K. Kaiser, "A novel role for the nitric oxide-cGMP signaling pathway: The control of epithelial function in *Drosophila*," *American Journal of Physiology-Regulatory, Integrative and Comparative Physiology*, vol. 266, no. 5, pp. R1716–R1719, 1994.

[53] M. J. O'Donnell and S. H. Maddrell, "Fluid reabsorption and ion transport by the lower Malpighian tubules of adult female *Drosophila*," *Journal of Experimental Biology*, vol. 198, no. 8, pp. 1647–1653, 1995.

[54] M. R. Rheault and M. J. O'Donnell, "Analysis of epithelial k+ transport in Malpighian tubules of *Drosophila melanogaster*: Evidence for spatial and temporal heterogeneity," *Journal of Experimental Biology*, vol. 204, no. 13, pp. 2289–2299, 2001.

[55] S. M. Linton and M. J. O'Donnell, "Contributions of K+:Cl- cotransport and Na+/K+-ATPase to basolateral ion transport in Malpighian tubules of *Drosophila melanogaster*," *Journal of Experimental Biology*, vol. 202, no. 11, pp. 1561–1570, 1999.

[56] M. J. O'Donnell, J. A. T. Dow, G. R. Huesmann, N. J. Tublitz, and S. H. P. Maddrell, "Separate control of anion and cation transport in Malpighian tubules of *Drosophila melanogaster*," *Journal of Experimental Biology*, vol. 199, no. 5, pp. 1163–1175, 1996.

[57] S. A. Davies, G. R. Huesmann, S. H. P. Maddrell et al., "CAP(2b), a cardioacceleratory peptide, is present in *Drosophila* and stimulates tubule fluid secretion via cGMP," *American Journal of Physiology-Regulatory, Integrative and Comparative Physiology*, vol. 269, no. 6, pp. R1321–R1326, 1995.

[58] A. Martínez, "Nitric oxide synthase in invertebrates," *The Histochemical Journal*, vol. 27, no. 10, pp. 770–776, 1995.

[59] C. Dani, A. G. Smith, S. Dessolin et al., "Differentiation of embryonic stem cells into adipocytes in vitro," *Journal of Cell Science*, vol. 110, no. 11, pp. 1279–1285, 1997.

[60] A. H. Brand and N. Perrimon, "Targeted gene expression as a means of altering cell fates and generating dominant phenotypes," *Development*, vol. 118, no. 2, pp. 401–415, 1993.

[61] P. Baumann and H. Skaer, "The *Drosophila* EGF receptor homologue (DER) is required for Malpighian tubule development," *Development*, vol. 119, pp. 65–75, 1993.

[62] R. Harbecke and W. Janning, "The segmentation gene Krüppel of *Drosophila melanogaster* has homeotic properties," *Genes & Development*, vol. 3, no. 1, pp. 114–122, 1989.

[63] B. Denholm, V. Sudarsan, S. Pasalodos-Sanchez et al., "Dual origin of the renal tubules in *Drosophila*: Mesodermal cells integrate and polarize to establish secretory function," *Current Biology*, vol. 13, no. 12, pp. 1052–1057, 2003.

[64] S. Wan, A.-M. Cato, and H. Skaer, "Multiple signalling pathways establish cell fate and cell number in *Drosophila* Malpighian tubules," *Developmental Biology*, vol. 217, no. 1, pp. 153–165, 2000.

[65] E. Livneh, L. Glazer, D. Segal, J. Schlessinger, and B.-Z. Shilo, "The *Drosophila* EGF receptor gene homolog: Conservation of both hormone binding and kinase domains," *Cell*, vol. 40, no. 3, pp. 599–607, 1985.

[66] W. Janning, A. Lutz, and D. Wissen, "Clonal analysis of the blastoderm anlage of the Malpighian tubules in *Drosophila melanogaster*," *Roux's Archives of Developmental Biology*, vol. 195, no. 1, pp. 22–32, 1986.

[67] J. McGettigan, R. K. J. McLennan, K. E. Broderick et al., "Insect renal tubules constitute a cell-autonomous immune system that protects the organism against bacterial infection," *Insect Biochemistry and Molecular Biology*, vol. 35, no. 7, pp. 741–754, 2005.

[68] N. K. Gautam, P. Verma, and M. G. Tapadia, "*Drosophila* Malpighian tubules: A model for understanding kidney development, function, and disease," *Results and Problems in Cell Differentiation*, vol. 60, pp. 3–25, 2017.

[69] S.-A. Davies, G. Overend, S. Sebastian et al., "Immune and stress response "cross-talk" in the *Drosophila* Malpighian tubule," *Journal of Insect Physiology*, vol. 58, no. 4, pp. 488–497, 2012.

[70] K. V. Anderson, "Pinning down positional information: Dorsal-ventral polarity in the *Drosophila* embryo," *Cell*, vol. 95, no. 4, pp. 439–442, 1998.

[71] B. Lemaitre, E. Nicolas, L. Michaut, J. Reichhart, and J. A. Hoffmann, "The dorsoventral regulatory gene cassette spatzle/Toll/Cactus controls the potent antifungal response in *Drosophila* adults," *Cell*, vol. 86, no. 6, pp. 973–983, 1996.

[72] M. J. Williams, A. Rodriguez, D. A. Kimbrell, and E. D. Eldon, "The 18-wheeler mutation reveals complex antibacterial gene regulation in *Drosophila* host defense," *EMBO Journal*, vol. 16, no. 20, pp. 6120–6130, 1997.

[73] P. Verma, M. G. Tapadia, and M. Kango-Singh, "Correction: Immune response and anti-microbial peptides expression in Malpighian tubules of *Drosophila melanogaster* is under developmental regulation," *PLoS ONE*, vol. 7, no. 8, Article ID e40714, 2012.

[74] N. Silverman and T. Maniatis, "NF-κB signaling pathways in mammalian and insect innate immunity," *Genes & Development*, vol. 15, no. 18, pp. 2321–2342, 2001.

[75] T. Tanji and Y. T. Ip, "Regulators of the Toll and Imd pathways in the *Drosophila* innate immune response," *Trends in Immunology*, vol. 26, no. 4, pp. 193–198, 2005.

[76] D. Ferrandon, A. C. Jung, M.-C. Criqui et al., "A drosomycin-GFP reporter transgene reveals a local immune response in *Drosophila* that is not dependent on the Toll pathway," *EMBO Journal*, vol. 17, no. 5, pp. 1217–1227, 1998.

[77] J. A. Hoffmann, "The immune response of *Drosophila*," *Nature*, vol. 426, no. 6962, pp. 33–38, 2003.

[78] T. Kaneko, T. Yano, K. Aggarwal et al., "PGRP-LC and PGRP-LE have essential yet distinct functions in the *Drosophila* immune response to monomeric DAP-type peptidoglycan," *Nature Immunology*, vol. 7, no. 7, pp. 715–723, 2006.

[79] C. Neyen, M. Poidevin, A. Roussel, and B. Lemaitre, "Tissue- and ligand-specific sensing of gram-negative infection in *Drosophila* by PGRP-LC isoforms and PGRP-LE," *The Journal of Immunology*, vol. 189, no. 4, pp. 1886–1897, 2012.

[80] J. D. Molkentin, J. R. Lu, C. L. Antos et al., "A calcineurin-dependent transcriptional pathway for cardiac hypertrophy," *Cell*, vol. 93, no. 2, pp. 215–228, 1998.

[81] S. D. Wright, "Toll, a new piece in the puzzle of innate immunity," *The Journal of Experimental Medicine*, vol. 189, no. 4, pp. 605–609, 1999.

[82] D. Ferrandon, J.-L. Imler, C. Hetru, and J. A. Hoffmann, "The *Drosophila* systemic immune response: sensing and signalling during bacterial and fungal infections," *Nature Reviews Immunology*, vol. 7, no. 11, pp. 862–874, 2007.

[83] N. K. Gautam, P. Verma, and M. G. Tapadia, "Ecdysone regulates morphogenesis and function of Malpighian tubules in *Drosophila melanogaster* through EcR-B2 isoform," *Developmental Biology*, vol. 398, no. 2, pp. 163–176, 2015.

[84] F. Rus, T. Flatt, M. Tong et al., "Ecdysone triggered PGRP-LC expression controls *Drosophila* innate immunity," *EMBO Journal*, vol. 32, no. 11, pp. 1626–1638, 2013.

[85] P. Verma and M. G. Tapadia, "Epithelial immune response in *Drosophila* Malpighian tubules: Interplay between diap2 and ion channels," *Journal of Cellular Physiology*, vol. 229, no. 8, pp. 1078–1095, 2014.

[86] J. A. T. Dow and S. A. Davies, "The Malpighian tubule: Rapid insights from post-genomic biology," *Journal of Insect Physiology*, vol. 52, no. 4, pp. 365–378, 2006.

[87] J. Yang, C. McCart, D. J. Woods et al., "A *Drosophila* systems approach to xenobiotic metabolism," *Physiological Genomics*, vol. 30, no. 3, pp. 223–231, 2007.

[88] R. L. Davis, "Physiology and biochemistry of *Drosophila* learning mutants," *Physiological Reviews*, vol. 76, no. 2, pp. 299–317, 1996.

[89] A. K. Allan, J. Du, S. A. Davies, and J. A. T. Dow, "Genome-wide survey of V-ATPase genes in *Drosophila* reveals a conserved renal phenotype for lethal alleles," *Physiological Genomics*, vol. 22, pp. 128–138, 2005.

[90] F. E. Karet, K. E. Finberg, R. D. Nelson et al., "Mutations in the gene encoding B1 subunit of H^+-ATPase cause renal tubular acidosis with sensorineural deafness," *Nature Genetics*, vol. 21, no. 1, pp. 84–90, 1999.

[91] A. Ramello, C. Vitale, and M. Marangella, "Epidemiology of nephrolithiasis," *Journal of Nephrology*, vol. 13, supplement 3, pp. S45–S50, 2000.

[92] Y. Chen, H. Liu, H. Chen et al., "Ethylene glycol induces calcium oxalate crystal deposition in Malpighian tubules: a *Drosophila* model for nephrolithiasis/urolithiasis," *Kidney International*, vol. 80, no. 4, pp. 369–377, 2011.

[93] T. Chi, M. S. Kim, S. Lang et al., "A *Drosophila* model identifies a critical role for zinc in mineralization for kidney stone disease," *PLoS ONE*, vol. 10, no. 5, Article ID e0124150, 2015.

[94] A. L. Negri, "The role of zinc in urinary stone disease," *International Urology and Nephrology*, pp. 1–5, 2018, https://doi.org/10.1007/s11255-017-1784-7.

[95] A. N. Smith, J. Skaug, K. A. Choate et al., "Mutations in ATP6N1B, encoding a new kidney vacuolar proton pump 116-kD subunit, cause recessive distal renal tubular acidosis with preserved hearing," *Nature Genetics*, vol. 26, no. 1, pp. 71–75, 2000.

[96] P. C. Harris and V. E. Torres, "Polycystic kidney disease," *Annual Review of Medicine*, vol. 60, Article ID 125712, pp. 321–337, 2009.

[97] S. Rossetti, M. B. Consugar, A. B. Chapman et al., "Comprehensive molecular diagnostics in autosomal dominant polycystic kidney disease," *Journal of the American Society of Nephrology*, vol. 18, no. 7, pp. 2143–2160, 2007.

[98] S. Rossetti, V. J. Kubly, M. B. Consugar et al., "Incompletely penetrant *PKD1* alleles suggest a role for gene dosage in cyst initiation in polycystic kidney disease," *Kidney International*, vol. 75, no. 8, pp. 848–855, 2009.

[99] F. Qian, F. J. Germino, Y. Cai, X. Zhang, S. Somlo, and G. G. Germino, "PKD1 interacts with PKD2 through a probable coiled-coil domain," *Nature Genetics*, vol. 16, no. 2, pp. 179–183, 1997.

[100] L. Tsiokas, E. Kim, T. Arnould, V. P. Sukhatme, and G. Walz, "Homo- and heterodimeric interactions between the gene products of *PKD1* and *PKD2*," *Proceedings of the National Academy of Sciences of the United States of America*, vol. 94, no. 13, pp. 6965–6970, 1997.

[101] P. D. Wilson, "Polycystin: New aspects of structure, function, and regulation," *Journal of the American Society of Nephrology*, vol. 12, no. 4, pp. 834–845, 2001.

[102] C. Gamberi, D. R. Hipfner, M. Trudel, and W. D. Lubell, "*Bicaudal C* mutation causes *myc* and TOR pathway up-regulation and polycystic kidney disease-like phenotypes in *Drosophila*," *PLoS Genetics*, vol. 13, no. 4, Article ID e1006694, 2017.

[103] D. J. Bouvrette, V. Sittaramane, J. R. Heidel, A. Chandrasekhar, and E. C. Bryda, "Knockdown of bicaudal C in zebrafish (*Danio rerio*) causes cystic kidneys: A nonmammalian model of polycystic kidney disease," *Comparative Medicine*, vol. 60, no. 2, pp. 96–106, 2010.

[104] C. Maisonneuve, I. Guilleret, P. Vick et al., "Bicaudal C, a novel regulator of Dvl signaling abutting RNA-processing bodies, controls cilia orientation and leftward flow," *Development*, vol. 136, no. 17, pp. 3019–3030, 2009.

[105] U. Tran, L. Zakin, A. Schweickert et al., "The RNA-binding protein Bicaudal C regulates polycystin 2 in the kidney by antagonizing miR-17 activity," *Development*, vol. 137, no. 7, pp. 1107–1116, 2010.

[106] M. R.-C. Kraus, S. Clauin, Y. Pfister et al., "Two mutations in human *BICC1* resulting in wnt pathway hyperactivity associated with cystic renal dysplasia," *Human Mutation*, vol. 33, no. 1, pp. 86–90, 2012.

[107] O. Wessely and E. M. De Robertis, "The *Xenopus* homologue of Bicaudal-C is a localized maternal mRNA that can induce endoderm formation," *Development*, vol. 127, no. 10, pp. 2053–2062, 2000.

[108] O. Wessely, U. Tran, L. Zakin, and E. M. De Robertis, "Identification and expression of the mammalian homologue of Bicaudal-C," *Mechanisms of Development*, vol. 101, no. 1-2, pp. 267–270, 2001.

[109] C. Gamberi and P. Lasko, "The Bic-C family of developmental translational regulators," *Comparative and Functional Genomics*, vol. 2012, Article ID 141386, 2012.

[110] E. E. Stagner, D. J. Bouvrette, J. Cheng, and E. C. Bryda, "The polycystic kidney disease-related proteins Bicc1 and SamCystin interact," *Biochemical and Biophysical Research Communications*, vol. 383, no. 1, pp. 16–21, 2009.

[111] J. Mohler and E. F. Wieschaus, "Bicaudal mutations of *Drosophila melanogaster*: alteration of blastoderm cell fate," *Cold Spring Harbor Symposium on Quantitative Biology*, vol. 50, pp. 105–111, 1985.

[112] I. A. Drummond, "Polycystins, focal adhesions and extracellular matrix interactions," *Biochimica et Biophysica Acta (BBA) - Molecular Basis of Disease*, vol. 1812, no. 10, pp. 1322–1326, 2011.

[113] H. Happé, E. de Heer, and D. J. M. Peters, "Polycystic kidney disease: the complexity of planar cell polarity and signaling during tissue regeneration and cyst formation," *Biochimica et Biophysica Acta (BBA) - Molecular Basis of Disease*, vol. 1812, no. 10, pp. 1249–1255, 2011.

[114] K. Lee, L. Battini, and G. L. Gusella, "Cilium, centrosome and cell cycle regulation in polycystic kidney disease," *Biochimica et Biophysica Acta (BBA) - Molecular Basis of Disease*, vol. 1812, no. 10, pp. 1263–1271, 2011.

[115] I. Rowe, M. Chiaravalli, V. Mannella et al., "Defective glucose metabolism in polycystic kidney disease identifies a new therapeutic strategy," *Nature Medicine*, vol. 19, no. 4, pp. 488–493, 2013.

[116] H. Happé and D. J. M. Peters, "Translational research in ADPKD: Lessons from animal models," *Nature Reviews Nephrology*, vol. 10, no. 10, pp. 587–601, 2014.

[117] H. Happé, A. M. Van Der Wal, D. C. F. Salvatori et al., "Cyst expansion and regression in a mouse model of polycystic kidney disease," *Kidney International*, vol. 83, no. 6, pp. 1099–1108, 2013.

[118] T. Arnould, E. Kim, L. Tsiokas et al., "The polycystic kidney disease 1 gene product mediates protein kinase C α-dependent and c-Jun N-terminal kinase-dependent activation of the transcription factor AP-1," *The Journal of Biological Chemistry*, vol. 273, no. 11, pp. 6013–6018, 1998.

[119] T. Yamaguchi, S. Nagao, D. P. Wallace et al., "Cyclic AMP activates B-Raf and ERK in cyst epithelial cells from autosomal-dominant polycystic kidneys," *Kidney International*, vol. 63, no. 6, pp. 1983–1994, 2003.

[120] H. Happé, W. N. Leonhard, A. van der Wal et al., "Toxic tubular injury in kidneys from Pkd1-deletion mice accelerates cystogenesis accompanied by dysregulated planar cell polarity and canonical Wnt signaling pathways," *Human Molecular Genetics*, vol. 18, no. 14, pp. 2532–2542, 2009.

[121] A. K. Bhunia, K. Piontek, A. Boletta et al., "PKD1 induces p21waf1 and regulation of the cell cycle via direct activation of the JAK-STAT signaling pathway in a process requiring PKD2," *Cell*, vol. 109, no. 2, pp. 157–168, 2002.

[122] H. Happé, A. M. van der Wal, W. N. Leonhard et al., "Altered Hippo signalling in polycystic kidney disease," *The Journal of Pathology*, vol. 224, no. 1, pp. 133–142, 2011.

[123] T. Weimbs, "Polycystic kidney disease and renal injury repair: Common pathways, fluid flow, and the function of polycystin-1," *American Journal of Physiology-Renal Physiology*, vol. 293, no. 5, pp. F1423–F1432, 2007.

[124] S. C. Parnell, B. S. Magenheimer, R. L. Maser et al., "The polycystic kidney disease-1 protein, polycystin-1, binds and activates heterotrimeric G-proteins in vitro," *Biochemical and Biophysical Research Communications*, vol. 251, no. 2, pp. 625–631, 1998.

[125] M. Boca, G. Distefano, F. Qian, A. K. Bhunia, G. G. Germino, and A. Boletta, "Polycystin-1 induces resistance to apoptosis through the phosphatidylinositol 3-kinase/Akt signaling pathway," *Journal of the American Society of Nephrology*, vol. 17, no. 3, pp. 637–647, 2006.

[126] J. M. Shillingford, N. S. Murcia, C. H. Larson et al., "The mTOR pathway is regulated by polycystin-1, and its inhibition reverses renal cystogenesis in polycystic kidney disease," *Proceedings of the National Academy of Sciences of the United States of America*, vol. 103, no. 14, pp. 5466–5471, 2006.

[127] C. Renken, D.-C. Fischer, G. Kundt, N. Gretz, and D. Haffner, "Inhibition of mTOR with sirolimus does not attenuate progression of liver and kidney disease in PCK rats," *Nephrology Dialysis Transplantation* , vol. 26, no. 1, pp. 92–100, 2011.

[128] W. N. Leonhard, A. van der Wal, Z. Novalic et al., "Curcumin inhibits cystogenesis by simultaneous interference of multiple signaling pathways: In vivo evidence from a *Pkd1*-deletion model," *American Journal of Physiology-Renal Physiology*, vol. 300, no. 5, pp. 1193–1202, 2011.

[129] X. Song, V. Di Giovanni, N. He et al., "Systems biology of autosomal dominant polycystic kidney disease (ADPKD): Computational identification of gene expression pathways and integrated regulatory networks," *Human Molecular Genetics*, vol. 18, no. 13, pp. 2328–2343, 2009.

[130] M. Lal, X. Song, J. L. Pluznick et al., "Polycystin-1 C-terminal tail associates with β-catenin and inhibits canonical Wnt signaling," *Human Molecular Genetics*, vol. 17, no. 20, pp. 3105–3117, 2008.

[131] N. Piazzon, C. Maisonneuve, I. Guilleret, S. Rotman, and D. B. Constam, "Bicc1 links the regulation of cAMP signaling in polycystic kidneys to microRNA-induced gene silencing," *Journal of Molecular Cell Biology*, vol. 4, no. 6, pp. 398–408, 2012.

[132] U. Tran, L. M. Pickney, B. D. Özpolat, and O. Wessely, "Xenopus Bicaudal-C is required for the differentiation of the amphibian pronephros," *Developmental Biology*, vol. 307, no. 1, pp. 152–164, 2007.

[133] T. A. Yakulov, T. Yasunaga, H. Ramachandran et al., "Anks3 interacts with nephronophthisis proteins and is required for normal renal development," *Kidney International*, vol. 87, no. 6, pp. 1191–1200, 2015.

[134] J. Chicoine, P. Benoit, C. Gamberi, M. Paliouras, M. Simonelig, and P. Lasko, "Bicaudal-C recruits CCR4-NOT deadenylase to target mRNAs and regulates oogenesis, cytoskeletal organization, and its own expression," *Developmental Cell*, vol. 13, no. 5, pp. 691–704, 2007.

[135] E. E. Saffman, S. Styhler, K. Rother, W. Li, S. Richard, and P. Lasko, "Premature translation of oskar in oocytes lacking the RNA-binding protein Bicaudal-C," *Molecular and Cellular Biology*, vol. 18, no. 8, pp. 4855–4862, 1998.

[136] M. Mahone, E. E. Saffman, and P. F. Lasko, "Localized Bicaudal-C RNA encodes a protein containing a KH domain, the RNA binding motif of FMR1," *EMBO Journal*, vol. 14, no. 9, pp. 2043–2055, 1995.

[137] F. S. Neuman-Silberberg and T. Schüpbach, "The *Drosophila* dorsoventral patterning gene gurken produces a dorsally localized RNA and encodes a TGFα-like protein," *Cell*, vol. 75, no. 1, pp. 165–174, 1993.

[138] R. P. Ray and T. Schüpbach, "Intercellular signaling and the polarization of body axes during *Drosophila* oogenesis," *Genes & Development*, vol. 10, no. 14, pp. 1711–1723, 1996.

[139] J. E. Wilhelm, M. Buszczak, and S. Sayles, "Efficient protein trafficking requires trailer hitch, a component of a ribonucleoprotein complex localized to the ER in *Drosophila*," *Developmental Cell*, vol. 9, no. 5, pp. 675–685, 2005.

[140] J.-M. Kugler, J. Chicoine, and P. Lasko, "Bicaudal-C associates with a Trailer Hitch/Me31B complex and is required for efficient Gurken secretion," *Developmental Biology*, vol. 328, no. 1, pp. 160–172, 2009.

[141] M. J. Snee and P. M. Macdonald, "Bicaudal C and trailer hitch have similar roles in *gurken* mRNA localization and cytoskeletal organization," *Developmental Biology*, vol. 328, no. 2, pp. 434–444, 2009.

[142] Y. Fu, I. Kim, P. Lian et al., "Loss of Bicc1 impairs tubulomorphogenesis of cultured IMCD cells by disrupting E-cadherin-based cell-cell adhesion," *European Journal of Cell Biology*, vol. 89, no. 6, pp. 428–436, 2010.

[143] G. Distefano, M. Boca, I. Rowe et al., "Polycystin-1 regulates extracellular signal-regulated kinase-dependent phosphorylation of tuberin to control cell size through mTOR and its downstream effectors S6K and 4EBP1," *Molecular and Cellular Biology*, vol. 29, no. 9, pp. 2359–2371, 2009.

[144] V. H. Gattone II, R. M. Sinders, T. A. Hornberger, and A. G. Robling, "Late progression of renal pathology and cyst enlargement is reduced by rapamycin in a mouse model of nephronophthisis," *Kidney International*, vol. 76, no. 2, pp. 178–182, 2009.

[145] Z. Novalic, A. M. van der Wal, W. N. Leonhard et al., "Dose-dependent effects of sirolimus on mTOR signaling and polycystic kidney disease," *Journal of the American Society of Nephrology*, vol. 23, no. 5, pp. 842–853, 2012.

[146] J. M. Shillingford, K. B. Piontek, G. G. Germino, and T. Weimbs, "Rapamycin ameliorates PKD resulting from conditional inactivation of Pkd1," *Journal of the American Society of Nephrology*, vol. 21, no. 3, pp. 489–497, 2010.

[147] Y. Tao, J. Kim, R. W. Schrier, and C. L. Edelstein, "Rapamycin markedly slows disease progression in a rat model of polycystic kidney disease," *Journal of the American Society of Nephrology*, vol. 16, no. 1, pp. 46–51, 2005.

[148] P. R. Wahl, A. L. Serra, M. Le Hir, K. D. Molle, M. N. Hall, and R. P. Wüthrich, "Inhibition of mTOR with sirolimus slows disease progression in Han:SPRD rats with autosomal dominant polycystic kidney disease (ADPKD)," *Nephrology Dialysis Transplantation*, vol. 21, no. 3, pp. 598–604, 2006.

[149] V. H. Gattone II, N. X. Chen, R. M. Sinders et al., "Calcimimetic inhibits late-stage cyst growth in ADPKD," *Journal of the American Society of Nephrology*, vol. 20, no. 7, pp. 1527–1532, 2009.

[150] F. Hildebrandt, T. Benzing, and N. Katsanis, "Ciliopathies," *The New England Journal of Medicine*, vol. 364, no. 16, pp. 1533–1543, 2011.

[151] J. R. Pinto, J. Muller-Delp, and P. B. Chase, "Will you still need me (Ca^{2+}, TnT, and DHPR), will you still cleave me (calpain), when I'm 64?" *Aging Cell*, vol. 16, no. 2, pp. 202–204, 2017.